Plant Cytogenetics and Molecular Biology Group
Institute of Biology, Biotechnology and Environmental Protection
Faculty of Natural Sciences
University of Silesia in Katowice

Serhii Mykhailyk

Evolution of 35S rRNA gene loci in selected genotypes of allotetraploid model grass *Brachypodium hybridum*

Doctoral thesis

Supervisor: Prof. dr hab. Robert Hasterok
Auxiliary supervisor: Dr Natalia Borowska-Zuchowska

Katowice 2023

Some of the results presented in this dissertation have been published in the following papers:

Borowska-Zuchowska, N., Robaszkiewicz, E., **Mykhailyk, S.**, Wartini, J., Pinski, A., Kovarik, A., and Hasterok, R. (2021). To be or not to be expressed: the first evidence of a nucleolar dominance tissue-specificity in *Brachypodium hybridum*. *Frontiers in Plant Science* 12:768347, doi: 10.3389/fpls.2021.768347

Borowska-Zuchowska, N., **Mykhailyk, S.**, Robaszkiewicz, E., Matysiak, N., Mielanczyk, L., Wojnicz, R., Kovarik, A., and Hasterok, R. (2023). Switch them off or not: selective rRNA gene repression in grasses. *Trends in Plant Science* 28:661-672, doi: 10.1016/j.tplants.2023.01.002

The following grant supported this study:

OPUS research project "*Cytogenomic analysis of key aspects of nuclear genome organisation in the polyploid model grass Brachypodium hybridum and its evolutionary ancestors"* (PI prof. dr hab. Robert Hasterok); funded by the National Science Centre Poland (project no. 2018/31/B/NZ3/01761)

TABLE OF CONTENT

1. INTRODUCTION

1.1. Biodiversity and economic significance of the grass family.

Approximately one-fourth of the Earth's land area consists of grasslands. Grasses comprise the majority (up to 80%) of agricultural land and have been essential to human life for centuries, providing food for the population, livestock pastures, and raw materials for producing biofuels and energy from biomass (Boval and Dixon, 2012; Hodkinson et al., 2015; Jones et al., 2015; Hodkinson, 2018; Odintsova et al., 2020). They are one of the most abundant plant groups, with around 11 000–12 000 species divided into about 750–770 genera that had branched off from an ancestral progenitor 50-70 million years ago (Levy and Feldman, 2002; Hodkinson, 2018). Grasses demonstrate a very successful lineage in the evolution of angiosperms, with a wide range of species, making them the fifth most abundant family of flowering plants since they are only surpassed in numbers by the Asteraceae (daisies), Orchidaceae (orchids), Fabaceae (beans), and Rubiaceae (coffee family) (Hodkinson and Parnell, 2006).

Important cereals grown in temperate climates include wheat (*Triticum aestivum* L., *Triticum turgidum* subsp. *durum* (Desf.), barley (*Hordeum vulgare* L.), oats (*Avena sativa* L.), rye (*Secale cereale* L.) and millet (*Panicum miliaceum* L.). From the tropics, the most important cereals are rice (*Oryza sativa* L.), maize (*Zea mays* L.), sorghum (*Sorghum bicolor* (L.) Moench., *S. vulgare* Pers.) and sugar cane (*Saccharum officinarum* L.). Additionally, many grasses are used as fodder species, such as foxtail (*Alopecurus*), cocksfoot (*Dactylis*), fescue (*Festuca*), ryegrass (*Lolium*), timothy (*Phleum*) and meadow grass (*Poa*). They are also a valuable raw material for the production of biofuels and obtaining energy from biomass, including giant cane (*Arundo donax* L.), miscanthus (*Miscanthus*) and sugar cane (*Saccharum officinarum* L.) (Hodkinson, 2018; Mohapatra et al., 2019). Furthermore, grasses are used in the construction industry, in paper making, and in perfumery needs by producing scented oils; moreover, some species are used medicinally, and others are grown as ornamental lawns (Odintsova et al., 2020).

1.2. Characteristics of the *Brachypodium* genus.

Brachypodium is a genus of temperate grasses, which consists of ~20 species distributed worldwide (Hasterok et al., 2022; Sancho et al., 2022). Its wide geographic range and small number of species suggest that the genus is characterised by a long evolutionary

history (Gordon et al., 2020). *Brachypodium* systematic position has been debated for many years, as it has been classified into tribes such as Poeae, Bromeae and Triticeae (Catalán and Olmstead, 2000). Early cytological, physiological and anatomical analyses led to the creation of a separate tribe Brachypodieae, which was later confirmed by the intergenic spacer (IGS) and internal transcribed spacer 1 (ITS1) sequence analyses (Shi et al., 1993; Catalán and Olmstead, 2000), polymorphism of RFLP and RAPD markers (Catalán et al., 1995) and variation of the 3' ends of the chloroplast *ndh*F gene (Catalán and Olmstead, 2000). It was observed that, unlike in species from the Triticeae tribe, there is no significant variation in the length of the rDNA sequence in the perennial *Brachypodium* representatives. In addition, a unique *Brachypodium* restriction site for the *Eco*RI enzyme was demonstrated at the 3' end of the IGS intergenic region. These findings, combined with the differences in the structure of ribosomal 35S rRNA genes observed by Shi et al. (1993) and the results of comparative analyses of the chloroplast *ndh*F gene (Catalán and Olmstead, 2000), proved that the genus *Brachypodium* should be classified in a separate tribe Brachypodeiae and is more closely related to the agronomically important Triticeae grasses (wheat, barley, rye) than to rice.

Although most of the species in the genus are perennial, there are three *Brachypodium* annuals: *B. distachyon, B. stacei,* and *B. hybridum*. It was initially thought that *Brachypodium distachyon* (L.) P. Beauv was the only annual species in the genus. The early karyological analysis showed the presence of three different *B. distachyon* cytotypes with 2n = 10, 20 and 30 (Robertson, 1981) and, at that time, the cytotypes with 2n = 20 and 2n = 30 were suggested to be autotetraploid and autohexaploid ecotypes of *B. distachyon*, respectively. Further studies using molecular cytogenetic approaches such as genomic *in situ* hybridisation (GISH) (Hasterok et al., 2004) and fluorescence *in situ* hybridisation (FISH) with bacterial artificial chromosome (BAC) clones as probes (Hasterok et al., 2006) revealed that the cytotype with 2n = 30 was an allotetraploid, most likely resulting from the natural cross of two diploid progenitors with 2n = 10 and 2n = 20. The cytotype with 2n = 20 was identified as a separate diploid species that belongs to the genus *Brachypodium*. After detailed morphological, phylogenetic and cytogenetic analyses, the 2n = 20 and 2n = 30 cytotypes were postulated as independent species and named *B. stacei* Catalan, Joch. Mull., Mur & Langdon and *B. hybridum* Catalan, Joch. Mull., Hasterok & Jenkins, respectively (Catalán et al., 2012). The characteristics of *Brachypodium* annuals are shown in Table 1.

Table 1. Characteristics of *B. distachyon*, *B. stacei* and *B. hybridum* (according to Catalán et al. (2012).

Taxon	Geographical distribution	Chromosome Number	Ploidy	Basic chromosome number	Genome size
B.distachyon	Native to the Mediterranean region. Probably spread in southern Europe, south-west Asia and North Africa.	2n = 10	diploid	x = 5	0.316 pg/1C
B. stacei	Native to the western Mediterranean region. Also cited from Sardinia, Sicily, southern Spain, southern Italy and Morocco.	2n = 20	diploid	x = 10	0.282 pg/1C
B. hybridum	Native to the Mediterranean region. Introduced in central and western Europe, Australia, North and South America, and South Africa.	2n = 30	allotetraploid	x = 5 + 10	0.633 pg/1C

In 2001, Draper et al. proposed *B. distachyon* as an amenable model system for functional genomics in temperate grasses. *B. distachyon,* with its small and compact genome with low repetitive content, a short life cycle, and small size of individual plants, appeared to be a good model when compared with other grass species that possess large and complex genomes (Draper et al., 2001; Scholthof et al., 2018). Its usefulness in the functional genomics of grasses has been proven. The annotated *B. distachyon* reference genome (IBI, 2010) was used to map and clone many important genes from the large and complex wheat genome (Consortium et al., 2014; Gatti et al., 2018; Ma et al., 2018). Also, the *B. distachyon* reference genome constituted a scaffold for the accurate genome

assembly of many Triticeae species, including barley (Mayer et al., 2012), hexaploid wheat (Consortium et al., 2018), *Triticum urartu* (AA) (Ling et al., 2018), *Aegilops tauschii* (DD) (Luo et al., 2017), and *Triticum durum* (AABB) (Maccaferri et al., 2019).

The creation of pangenomes (i.e., a combination of genomes from different genotypes of the given species) for the three annual plants, *B. distachyon*, *B. stacei*, and their resulting allotetraploid *B. hybridum*, has yielded a precious asset for better understanding the origins and implications of plant polyploidy (Catalán and Vogel, 2020; Hasterok et al., 2022).

1.3. Ribosomal RNA genes.

1.3.1. Structure and function of rDNA.

It is widely accepted that the current DNA-based world was preceded by an RNA world, likely due to the ability of RNA to store genetic information and catalyse the chemical reactions in primitive cells (Gilbert, 1986; Robertson and Joyce, 2012). Even though the details of the transition from RNA to a DNA-based world are still unknown (Nelson and Breaker, 2017; Le Vay and Mutschler, 2019), evidence, such as the role of RNA in translation and its capacity to replicate itself, support this theory. Moreover, ribozymes (RNA enzymes) remain in modern cells, acting as living fossils. Ribosomal RNA (rRNA) comprises approximately 80% of the total RNA found in a cell. Eukaryotes have four types of rRNA genes – the 18S, 5.8S, and 25-28S ribosomal DNA, transcribed as a single operon called 35-48S pre-rRNA, and the 5S rRNA gene that is usually located outside this operon (Hori et al., 2023). The rDNAs are typically placed in a head-to-tail array in the genome, with only a few exceptions (Ironside, 2013), and the number of 35-48S rDNA units in the array can range from hundreds to tens of thousands, depending on the species. 35-48S rDNA loci, which are transcribed, are called nucleolus organiser regions (NORs). At the cytological level, during the interphase, transcribed rDNA units are located in the nucleolus (Ritossa and Spiegelman, 1965). At the level of mitotic chromosomes, the 35-48S rRNA genes expressed during the previous interphase can be seen as secondary constrictions (SC).

In eukaryotes, the 18S, 5.8S, and 25-28S rRNA genes are transcribed by RNA polymerase I (Pol I), while the 5S rRNA genes are transcribed by RNA polymerase III (Pol III). A 35-45S rDNA transcription unit is commonly found in plants (depending on the size of ETS), 35S rDNA in yeast, and 48S rDNA in mammals (Borowska-Zuchowska

et al., 2023). Each 35-48S rDNA unit is composed of: (i) the coding 18S, 5.8S, and 25-28S rDNAs sequences; (ii) IGS consisting of a non-transcribed spacer (NTS) and external transcribed spacer (ETS); and (iii) two internal transcribed spacers (ITS1 and ITS2; Figure 1). The IGS contains essential regulatory elements, including the transcription initiation site (TIS) and transcription termination site (TTS) (Volkov et al., 2007) (see Figure 1). The 35S rDNA unit is 8-20 kb long; meanwhile, the 5S rDNA unit is substantially shorter and comprises a 120-bp conserved genic region and a 100-1000 bp long spacer region (5S rDNA SR) (Volkov et al., 2007; Garcia et al., 2016).

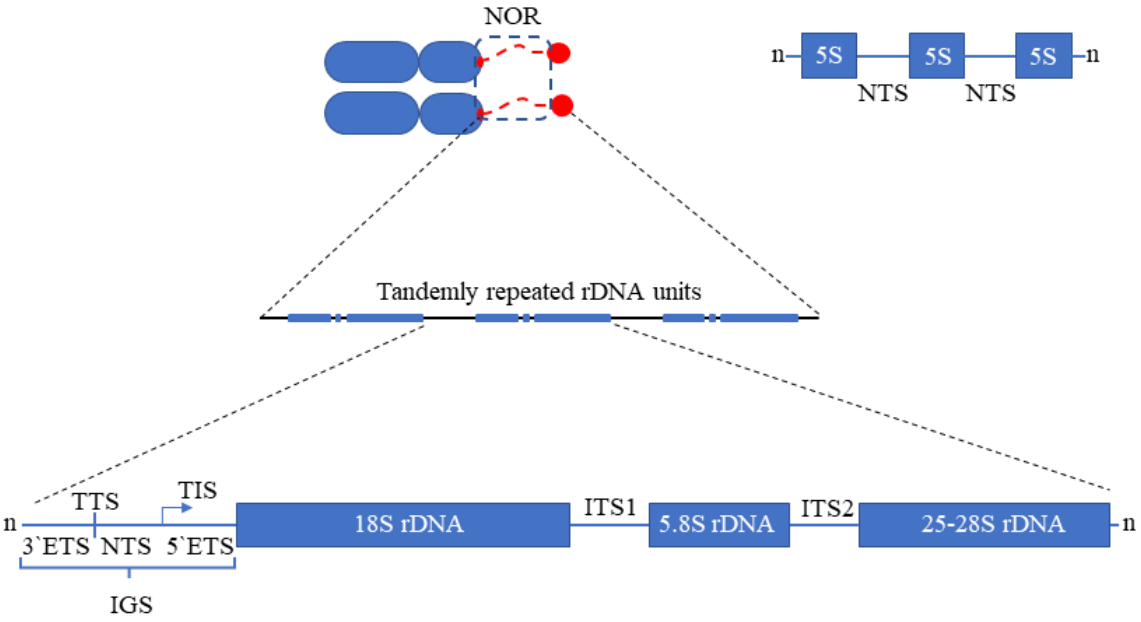

Figure 1. The structure of 5S and 35S rDNA single repeat.

As a non-coding element, the IGS is less conserved than rDNA coding regions, leading to its significant sequence and size differences between closely related species. It is also possible for the same genome to contain different length variants of rDNA due to the IGS length polymorphism (Hemleben et al., 2004). For example, in *Arabidopsis thaliana*, a length variant of the IGS was identified among 35S rDNA repeats at NOR2 on chromosome 2. In contrast, NOR4 on chromosome 4 contained three length variants not interlaced but clustered. This suggests that the concerted evolution of rDNA leads to the homogenisation of the rDNA variants due to the local propagation of new ones (Copenhaver and Pikaard, 1996). However, the variations in the IGS length between closely related species and even individuals of the same population may serve as evidence

that these sequences can escape from concerted evolution mechanisms. The variations in the length of the IGS are primarily due to the amplification of various subrepeats present within the spacer. Usually, several classes of short subrepeated elements are located upstream of the TIS, while downstream of the TIS subrepeats are rarely present (Borisjuk et al., 1997). The amplification/deletion of subrepeats in the IGS is a continuous process throughout evolution. Such differentiation in the IGS regions makes them useful for phylogenetic studies (Krawczyk et al., 2017).

The 18S-5.8S-25S rDNA coding regions were shown to belong to one of the most evolutionary conserved sequences (Hemleben et al., 2004). They show little or no intragenomic sequence variability due to the homogenisation process that leads to the concerted evolution of 35S rDNA repeats. It was proposed that unequal crossing-over and gene conversion drive rDNA homogenisation processes (Dover, 1982). In the 35S rDNA context, rDNA units within the same locus are more alike than those from different NORs, suggesting that intralocus homogenisation is more effective than interlocus one (Wang et al., 2016).

1.3.2. L-type and S-type organisation of rRNA genes.

The 35-48S and 5S rRNA genes are usually arranged in distinct loci in most eukaryotic organisms. The transcription by two different RNA polymerases, Pol I (DNA-dependent RNA polymerase I) in the case of 35-48S rDNA and Pol III (DNA-dependent RNA polymerase III) in the case of 5S rDNA, is likely the reason for the physical separation of 35-48S and 5S rDNA loci. The separated arrangement of the 35-48S rDNA and 5S rDNA that occupy distinct loci is known as the S-type rDNA organisation. The S-type arrangement appears as the most common type of rDNA organisation among angiosperms and gymnosperms (Garcia and Kovařík, 2013). However, there are some exceptions to this rule. For instance, 5S rRNA genes are linked with 35S rDNA in some organisms, e.g., in some mosses (Sone et al., 1999), gymnosperms (Garcia and Kovařík, 2013) and even angiosperms (Garcia et al., 2012). This suggests that linked rDNA arrangement in some plants may represent a transitional stage between linked (prokaryotic) and unlinked (present in most eukaryotes studied so far) arrangements.

The 5S and 35S rRNA gene organisation in plants was investigated by Garcia et al. (2016) in the representatives of *Artemisia* (family Asteraceae), where a linked arrangement of rDNA was discovered for the first time in angiosperms. This L-type arrangement refers to the 5S rRNA gene located in an inverted orientation within the large

IGS of the 35S rDNA. This type of rDNA molecular organisation is not common in angiosperms studied so far; however, it can be found in certain algae, bryophytes, and ferns (Sone et al., 1999; Garcia et al., 2016). In *Artemisia*, there are two 5S rDNA units inserted into the 35S rDNA IGS: (i) the first one is positioned close to the end of the 25S rRNA gene, and (ii) the second insertion (pseudogenised with a deletion in a promoter region) located further toward the 3' end of the IGS (Garcia et al., 2016). Such unit structure suggests that different versions of a unit are being mixed, and none of them has been established as the standard or most common type (although no separate units were observed in *Artemisia*) (Garcia et al., 2016).

Studies conducted on different genera, such as *Tragopogon*, *Centaurea*, *Helianthus* and *Hipochaeris* (Cuellar et al., 1996; Weiss-Schneeweiss et al., 2003; Kovarik et al., 2005; Ruas et al., 2005; Dydak et al., 2009), have revealed S-type of rRNA genes arrangement, which is different from the one that was found in *Artemisia*. To further explore the rDNA structure and organisation in approximately 200 representatives of the Asteraceae family, additional research was conducted using molecular (PCR, Southern blot, IGS sequencing, quantitative PCR) and cytogenetic (FISH) approaches (Garcia et al., 2010). The L-type rDNA arrangement was shown in three major subsections of the Asteroideae subfamily: (i) the Anthemideae tribe (93% of the studied species); (ii) the Gnaphalieae tribe (100%); and (iii) the "Heliantheae alliance" clade (23% of the studied species). The other five tribes of the Asteroideae in the Asteraceae family had an S-type arrangement of rDNA (Garcia et al., 2016).

Thus, Asteraceae representatives seem to have two distinct types of rDNA organisation. The 'L-type genera' are distributed in the phylogeny in a way that suggests the linked arrangement has arisen independently multiple times in the largest subfamily, Asteroideae (Garcia et al., 2010; Garcia et al., 2016). This indicates that the L-type arrangement may be more prevalent than previously thought. Understanding the pattern of 35S and 5S rDNA loci organisation may shed light on their expression and regulation features.

1.4. Polyploidy in grasses.

Polyploidy is when more than two haploid chromosome sets are present within a single nucleus. There are two distinct classes of polyploids: (i) autopolyploids (e.g., autotetraploid cytotype of *Hordeum bulbosum*), (ii) allopolyploids (e.g., *Triticum aestivum*) (Levy and Feldman, 2002; Svačina et al., 2020; Levy and Feldman, 2022). An

autopolyploid formation is accompanied by a genome doubling within one species. For example, a species with the genome composition AA doubles to become an autotetraploid AAAA. During meiosis in autopolyploids, the chromosomes may form multivalents and exhibit a multisomic inheritance, usually associated with sterility. This can be why so many autopolyploids are perennials propagating vegetatively (Levy and Feldman, 2002). Allopolyploids (or amphiploids) are created when two different species with diverged genomes hybridise, followed by chromosome doubling. The hybrids are generally sterile, but WGD can occasionally restore fertility. Forming bivalents, full fertility, and disomic inheritance define a stable allopolyploid. Many allopolyploid grasses (e.g., *T. aestivum*) are annuals, where hybridisation permanently maintains heterozygosity between homoeoalleles, even in the self-pollinating species. (Levy and Feldman, 2002).

The fact that polyploidy is so common and still occurring today implies that plants are pre-adapted to handle the challenges of polyploidy. For the new polyploid to survive, there must be mechanisms to manage the genomic stress of chromosome doubling (Baduel et al., 2018). In addition to its evolutionary purpose, interspecific hybridisation followed by whole genome duplication (WGD) has been practically utilised in various breeding initiatives.

The introduction of genomic approaches has shed more light on the role of polyploidy in the evolution of angiosperms. It was shown that WGDs occurred before the divergence of gymnosperms and angiosperms (also known as the ζ event) (Jiao et al., 2011). Plants that experienced WGD in the distant past and now have a disomic inheritance are called paleopolyploids. Their ancestors cannot be identified through cytological tools or DNA markers, but they can be identified through bioinformatic analysis (Levy and Feldman, 2002).

An increasing number of research on the evolution of allopolyploids showed that one of the ancestral genomes might become dominant and the other the under-dominant one in successive generations. This advantage of one genome over another is called "genome dominance" (Rapp et al., 2009).

1.4.1. Genome dominance in plants.

The phenomenon of "genome dominance" in allopolyploids (also known as "subgenome dominance" (Thomas et al., 2006)) has become increasingly evident in the past decades. The genome dominance may involve (i) global epigenetic alterations; (ii) an increase in the size of the dominant genome and/or under-dominant genome size decreasing; (iii) the

elimination of chromosomes from the under-dominant genome; (iv) the elimination or epigenetic silencing of alleles from the under-dominant genome leading to homoeologous expression bias and expression level dominance; and (v) preferential activation of mobile elements (Glombik et al., 2020). An example of genome dominance, particularly chromosome elimination from the under-dominant genome, can be chromosome elimination in *Hordeum vulgare* × *H. bulbosum* hybrids (Thomas and Pickering, 1983). The hybrids resulting from the cross between *H. vulgar*e and *H. bulbosum* manifest chromosomal instability throughout their growth, typically resulting in the loss of *H. bulbosum* chromosomes in subsequent generations. Nonetheless, a distinct scenario arises in an allotetraploid variant featuring the 'Vada' cultivar, where the preservation of *H. bulbosum* chromosomes endures across successive sexual cycles, making the *H. bulbosum*-originated genome "dominant" (Thomas and Pickering, 1983).

An allopolyploidisation event leads to a "transcriptomic shock" in which the gene expression patterns are altered (Rapp et al., 2009). This shock can cause unequal parental contribution and change the expression patterns of the genes (Grover et al., 2012). In the long term, several evolutionary scenarios are possible for the homoeologous genes in allopolyploids: (i) genetic or epigenetic alterations can cause the inactivation/repression of one homoeologue (the process known as non-functionalisation); (ii) one copy develops a new, usually advantageous purpose, while the other retains the original function (neo-functionalisation); or (iii) the two copies can split functions (sub-functionalisation) (Ma and Gustafson, 2005; Glombik et al., 2020). An illustrative instance of an "evolutionary transcriptomic shock" can be found in the work of Feldman et al. (1986) conducted on hexaploid wheat. In this study, a notable case of non-functionalisation emerges, with the genes coding for high molecular weight glutenin within the A-genome being suppressed while their counterparts originating from the B- and D-subgenomes maintain their expression activity (Feldman et al., 1986).

The dominance of one parental genome over the other at the expression level is known as biased fractionation, bringing instability in the genome maintenance and causing functional conflicts between interacting genes. It has been found that dominance is usually established in the first generations after polyploidisation and is transmitted over the generations (Guo and Han, 2014) or multiple rounds of polyploidy (Woodhouse et al., 2014). Genome dominance has been shown to affect the expression of various genes, such as rRNA genes and genes encoding for centromeric proteins. Exemplary, Talbert et al. (2002) used an antibody raised against the *A. thaliana*-like CENH3 in *A. suecica*

(allotetraploid that came from a cross between *A. thaliana* and *A. arenosa*) to test the presence of *A. thaliana* centromeric H3 histone (CENH3) in the *A. arenosa*-like centromeres. Interestingly, the antibody identified the epitope in both synthetic and natural allopolyploids derived from the two species, demonstrating the dominant nature of the *A. thaliana* CENH3 gene and its product incorporated into the centromeres of chromosomes of *A. suecica* regardless of their diploid ancestor origin (Talbert et al., 2002).

The event of genome dominance can usually be displayed by changing the gene regulation – by either increasing the dominant allele's activity or decreasing the under-dominant allele's activity (Zhu et al., 2017). Usually, gene expression can be modified by epigenetic regulation, which can be mediated by TEs and small interfering RNAs (siRNA) (Wang and Chekanova, 2016; Hirsch and Springer, 2017). Specifically, siRNAs play a crucial role in guiding methyltransferases to establish DNA methylation at CG, CHG, and CHH sites (H = A, T, or C). For example, Zhu et al. (2017), in their work on *A. thaliana* and *A. lyrata* interspecific hybrid, demonstrate that the methylation levels at CHH, CHG and CG sites are frequently altered (either increased or decreased) following hybridisation events (Zhu et al., 2017).

However, not only DNA methylation plays a role in genome dominance maintenance. The study on hexaploid wheat and one of its putative progenitors – *Aegilops tauschii* – showed that alterations in gene expression patterns caused by changes in their DNA methylation level concern as little as 11% of genes from chromosome 3DL. A decrease in gene expression level appears to be more closely linked to a higher level of chromatin compaction and reduced accessibility of the wheat chromosome arm (Lu et al., 2020). Therefore, it is thought that the competition between parental genomes in hybrids for TEs regulation, chromatin condensation and the overall amount of siRNAs are essential for hybrid vigour and the expression changes of hybrids (Groszmann et al., 2013). One of the manifestations of genome dominance is another phenomenon called nucleolar dominance (ND).

1.5. Nucleolar dominance in plants.

Navashin (1934) was the first to discover ND in *Crepis* hybrids. Later, this phenomenon was found among the consequences of genome dominance in many plant hybrids, allopolyploids, and some interspecific animal hybrids (Pikaard, 2000). A common characteristic of ND is that the 35S rRNA genes from one progenitor (the dominant one)

are expressed, while those from the other progenitor are transcriptionally silenced (Pikaard, 2000; Borowska-Zuchowska et al., 2023).

The phenomenon of ND has been documented in interspecific hybrids and allopolyploids across various plant genera, including *Salix* (Wilkinson, 1944), *Ribes* (Keep, 1962), *Solanum* (Komarova et al., 2004), *Hordeum* (Nicoloff et al., 1979), *Triticum* (Thomas and Kaltsikes, 1983), *Agropyron* (Heneen, 1962), *Brassica* (Chen and Pikaard, 1997b), *Arabidopsis* (Earley et al., 2006), *Brachypodium* (Idziak and Hasterok, 2008) and others (Pikaard, 2000; Borowska-Zuchowska et al., 2023). It was shown that epigenetic mechanisms are responsible for the repression of the under-dominant rDNA loci. Since epigenetic silencing is a reversible process, thus ND can be abolished at different developmental stages. An illustrative example of ND regulation during development is the progressive repression of rRNA genes originating from *A. thaliana*, occurring during the early stages of postembryonic development in allotetraploid *A. suecica* (Pontes et al., 2007). A similar establishment of ND has also been observed in rapeseed, where both ancestral 35S rDNA sets are transcriptionally active in seedlings that are 2-3 days old (Hasterok and Maluszynska, 2000), while stable ND towards the rRNA genes derived from *Brassica rapa* exists in the leaves of mature plants (Sochorova et al., 2017).

One possible mechanism of ND maintenance can be the rRNA dosage control, which is well-studied in diploid organisms. It was shown in two different yeast strains that a dosage control system regulates the amount of transcriptionally active rDNA. Even though the two strains have considerable differences in the number of 35S rDNA copies, the level of rDNA expression is still the same. This dosage control of rRNA genes occurs due to a higher occupancy of Pol I per single 35S rDNA unit (French et al., 2003). A dosage control effect was also observed in *A. thaliana* mutant created through Cas9-mediated genome editing at 45S rDNA loci. Despite a significant decrease (up to 90%) in the number of 45S rDNA units, the transcriptional rates and steady-state levels of rRNA transcripts were similar to those in the wild-type plants (Lopez et al., 2021). However, it is yet to be determined how ND is established in plant hybrids/allopolyploids, whether a given parental rDNA is always dominant, or whether other factors, such as the neighbouring regulatory sequences within the IGSs, chromosomal positioning, and/or chromatin organisation during interphase, affect this phenomenon (Pikaard, 2000; Mohannath et al., 2016). Moreover, ND appears to be independent of maternal or paternal effects (Chen and Pikaard, 1997b).

1.5.1. The role of chromosomal positioning in ND.

Some studies have suggested that the chromosomal position of 35S rDNA loci may play a role in the 35S rDNA expression patterns. Until now, the impact of the rDNA chromosomal positioning on the expression of 35S rDNA was studied in three species: barley, *A. thaliana*, and wheat.

The role of chromosome position in the 35S rRNA gene expression patterns was observed for the first time in a barley translocation line, where both 35S rDNA loci were located on different arms of a single chromosome (in the wild-type barley, there are two 35S rDNA loci per genome and they are located on two distinct chromosomes; both are transcriptionally active). Using a *H. vulgare* translocation line with NOR region translocated from $5H^v$ to $6H^v$, Nicoloff et al. (1979) showed an example of a chromosomal position-dependent 35S rRNA gene expression. The 35S rDNA units that had been translocated were not transcribed (Nicoloff et al., 1979). Later Schubert and Künzel (1990) showed that such suppression was caused neither by the 35S rDNA loss nor the change in the DNA methylation patterns (Schubert and Künzel, 1990).

In *A. thaliana*, the 45S rRNA genes are located in two distinct loci known as nucleolus organiser regions (NORs). These NORs, NOR2 on chromosome 2 (under-dominant) and NOR4 on chromosome 4 (dominant), are positioned at the ends of their respective chromosomes (Mohannath et al., 2016). In *A. thaliana* mutants lacking histone H3 lysine 27 monomethylase activity, usually silenced rDNA units from NOR2 were translocated to NOR4. At the new chromosomal location, the NOR2 35S rRNA genes were expressed. Such a process of activation suggests that the neighbouring pericentromeric sequences may be involved in silencing the 35S rDNA units in their original position of NOR2 of *A. thaliana* (Mohannath et al., 2016).

Studies on wheat conducted by Handa et al. (2018) suggested the possible impact of transposons and highly methylated regions surrounding major wheat NORs 1B and 6B on their activity (Handa et al., 2018). These areas may not only control the expression of nearby NORs but could also affect minor wheat rDNA sites. The mechanism by which chromosomal position affects 35S rRNA gene expression is still unknown. This is probably because the ND phenomenon is complex and involves the interactions of multiple factors, such as the expression of genes, epigenetic patterns, and other factors that have not been identified yet. Further research is needed in dicot and monocot allopolyploid systems to understand how and why chromosomal position affects ND.

1.5.2. The role of epigenetics in ND.

In plants, ND is driven and maintained through epigenetic mechanisms involving both DNA methylation and repressive histone modifications. Early experiments using the inhibitors of cytosine methyltransferases and histone deacetylases (5-azacytidine or 5-aza-deoxycytidine and trichostatin A, respectively) revealed that the under-dominant 35S rRNA genes could be reactivated in both monocot and dicot representatives that exhibit ND (Vieira et al., 1990b; Neves et al., 1995; Amado et al., 1997; Chen and Pikaard, 1997a; Earley et al., 2006). For example, the treatment of seeds of wheat × rye hybrids and Triticale with 5-azacytidine (5-aza-C) leads to the appearance of a higher number of nucleoli in interphase nuclei, supporting the role of DNA methylation in ND maintenance (Vieira et al., 1990b; Carvalho et al., 2013). Moreover, experiments performed on different triticale cultivars along with several wheat aneuploid lines crossed with rye demonstrated the reactivation of 1R NOR region after treatment with 5-aza-C, implying the role of DNA methylation in the suppression of rye 35S rDNA in the wheat background (Vieira et al., 1990b; Neves et al., 1995; Amado et al., 1997; Castilho et al., 1999). The same picture was obtained in two dicot species, *B. napus* and *A. suecica,* where 5-aza-deoxycytidine treatment led to the reactivation of the under-dominant 35S rRNA genes (Chen and Pikaard, 1997a; Chen et al., 1998). Also, a reduction of CG and CHG DNA methylation likely contributed to the reactivation of 35S rDNA loci of the *Tragopogon porrifolius* origin (the under-dominant rDNA locus) in the allotetraploid *T. mirus*, where it was shown that deletion of the 96% of the NOR region does not significantly affect rDNA expression (Dobesova et al., 2015). Thus, ND appeared to be a fully reversible epigenetic process.

The RNA-directed DNA methylation pathway (RdDM) is thought to be among the mechanisms responsible for the transcriptional silencing of under-dominant 35S rRNA genes via ND (Costa-Nunes et al., 2010; Singh et al., 2019). RdDM is an epigenetic process that involves the production of small RNA molecules. These molecules guide DNA methyltransferases to specific DNA sequences, resulting in DNA methylation and gene silencing (Matzke and Mosher, 2014). RdDM plays a crucial role in regulating gene expression and maintaining genome stability. This plant-specific pathway is mainly controlled by 24-nt-long siRNAs that direct the addition of DNA methylation to specific DNA sequences. Studies on *A. suecica* revealed that the essential RdDM proteins involved in the preferential silencing of the *A. thaliana*-inherited rRNA genes are: (i)

domains rearranged methyltransferase 2 (DRM2), which is responsible for catalysing *de novo* DNA methylation; (ii) RNA-dependent RNA polymerase 2 (RDR2), which physically associates with Pol IV, to produce dsRNAs; (iii) dicer-like 3 protein (DCL3) involved in long dsRNAs processing into siRNAs; and (iv) methylcytosine binding domain protein 6 (MBD6) that is recruited to chromatin by recognition of CG methylation, and redundantly repress a subset of genes and transposons without affecting DNA methylation levels (Preuss et al., 2008; Ichino et al., 2021).

Besides the crucial DRM2, RDR2 and DLC3, several proteins have also been proven to be involved in ND enforcement. These include the histone deacetylase 6 (HDA6), which is involved in the deacetylation of histones and the subsequent repression of gene transcription, and histone H3K9 methyltransferase (SUVR4) (Pontvianne et al., 2012), which methylates histones and promotes gene silencing (Earley et al., 2006; Costa-Nunes et al., 2010). Epigenetic modifications such as the dimethylation of lysine 9 of histone H3 (H3K9me2) resulted in the repression of the *A. thaliana*-derived NORs in allotetraploid *A. suecica* (Lawrence et al., 2004). In the synthetic hexaploid wheat, the under-dominant A-genome 35S rDNA loci were enriched in H3K27me3 and H3K9me2 histone marks and methylated at CHG and CHH sequence contexts in promoters. These resulted in their transcriptional silencing and elimination in later generations (Guo and Han, 2014). In contrast, acetylation of histones H3 and H4, e.g., H4K5ac, H4K16ac and H3K9ac, appeared to be associated with the active 35S rDNA loci as was shown in *B. hybridum* (Borowska-Zuchowska and Hasterok, 2017).

Overall, the studies on ND in dicot and monocot plants have identified several key proteins, mechanisms and pathways involved in the epigenetic regulation of rRNA gene expression. These findings broadly expand our understanding of the genetic mechanisms that underlie complex traits in plants and other organisms. However, the question of how one ancestral/parental set of 35S rRNA genes is selected to be suppressed in the allopolyploid/hybrid organisms still needs to be answered.

1.6. ND studies in monocots.

While ND has been extensively studied in dicots, the Poaceae family has also been subjected to ND research. Many grasses, including allopolyploids and recombinant inbred lines, have been analysed in this context. Around 200 species showed the variable occurrence of ND, ranging from partial to strong dominance of one genome's 35S rRNA genes over another. The ND has also been observed in some economically important

cereals, e.g., in bread wheat (*T. aestivum*), and hexaploid and octoploid triticale (× *Triticosecale* Wittmack; a hybrid of wheat and rye) (Shkutina and Khvostova, 1971; Thomas and Kaltsikes, 1983). The experiments on Triticale and Triticale × rye hybrids demonstrated the dominance of wheat NORs over the rye ones (Appels et al., 1986; Capesius and Appels, 1989).

In *Hordeum* and *Secale*, dominance patterns were observed in experiments involving different hybrids. The suppression hierarchy in *Hordeum* hybrids was established, with *H. parodii* and *H. procerum* showing dominance over other species (Santos et al., 1984; Cabrera and Martín, 1991). Rye NORs were weakly expressed in hybrid genomes, and barley NORs showed dominance over rye NORs (Thomas and Pickering, 1985; Schwarzacher-Robinson et al., 1987; Linde-Laursen and Bothmer, 1989; Linde-Laursen et al., 1993). Similar dominance patterns were observed in Triticale × *Tritordeum* hybrids (Lima-Brito et al., 1998).

The ND investigation in the *Triticum* genus focused mainly on bread wheat (genome composition AABBDD) with at least four chromosome pairs that bear 35S rDNA loci. Chromosomes 1B and 6B were found to carry the major (able to form nucleoli) rDNA loci, while chromosomes 5D and 1A were characterised by the presence of minor loci that produced smaller nucleoli or none, respectively (Flavell and O'Dell, 1976; Vieira et al., 1990a). The number of rDNA units varied among these loci (Tulpová et al., 2022), but there was no correlation between the number of genes per locus and nucleoli formation. Wheat NORs located on B genome chromosomes also showed dominance in some hexaploid and tetraploid wheat varieties (Hutchinson and Miller, 1982; Frankel et al., 1987).

Studies on the 35S rDNA locus structure are often challenging due to the repetitive nature of 35S rDNA. Thus, rDNA arrays that span millions of nucleotides usually heavily hamper genome investigation by providing gaps in the sequencing assemblies. The situation is even more complicated if there is more than one 35S rDNA locus per genome in the allopolyploid species. The allohexaploid bread wheat is among grasses that exhibit ND; however, the studies on its molecular basis are challenging mainly due to its large and complex genome of over 16.5 Gbp and numerous 35S rDNA loci. To overcome these challenges in wheat, Tulpová et al. (2022) used a complex approach that involved (i) RepeatExplorer pipeline to reconstruct the consensus sequences of the major and minor wheat loci; (ii) the BioNano optical mapping to reveal the major and minor 35S rDNA loci structure; (iii) RNA-seq to verify whether 35S rRNA genes expression is locus- and

tissue-specific; and (iv) bisulphite sequencing to verify the DNA methylation patterns of these loci. Interestingly, using RNA-seq, Tulpová et al. (2022) discovered that the 1BS rRNA variants were more abundant than the 6BS variants in all tissues, with a ratio of approximately 2:1, although this ratio slightly differed across tissues. The coleoptile exhibited the highest frequency of 6BS-specific variants, whereas the mature leaf had the highest 1BS-specific variants (Tulpová et al., 2022).

To reveal the structure of wheat rDNA loci, Tulpová et al. (2022) used bread wheat genome short-read data along with highly accurate HiFi PacBio reads (Sato et al., 2021) and created *in silico* pseudomolecules of wheat NOR-bearing chromosome regions (Tulpová et al., 2022). Further analysis revealed the main limitation of assemblies – the lack of NORs core regions in 1BS, 6BS, and 5DS pseudomolecules. However, the fine structure of the degenerated rDNA locus in the 1AS pseudomolecule was preserved. Simultaneously, the Bionano Genomics platform reinforced bioinformatical results and created optical maps (OM) of 1AS, 1BS, 6BS, and 5DS chromosome arms (Tulpová et al., 2022). OM provides a subsequent physical structure of a single DNA molecule based on a restriction pattern, serving as an excellent tool for studying complex repetitive regions, including rDNA loci. Using OMs, positions of rDNA units missing in pseudomolecule assemblies were accurately located. Such discrepancies between OMs and pseudomolecules were considerably lower in PacBio HiFi assemblies, indicating that highly accurate long-read sequencing outperformed other technologies in rDNA loci assemblies; however, it is still unable to provide clear and comprehensive insight into rDNA loci structure.

1.6.1. *Brachypodium hybridum* as a model in ND studies.

Brachypodium hybridum (2n = 30; subgenome composition DDSS) is an allotetraploid grass that arose from a cross between two diploid ancestors, which resembled *B. distachyon* (2n = 10; DD) and *B. stacei* (2n = 20; SS). It was shown that in most of the studied genotypes of *B. hybridum,* two chromosomal pairs bear the 35S rDNA loci: (i) the first one derived from the D-subgenome, in which the 35S rDNA locus is localised distally on the short arm of chromosome Bd5; and (ii) the second one that originated from the S-subgenome, in which the 35S rDNA locus is distributed proximally on chromosome Bs6 (Hasterok et al., 2004; Lusinska et al., 2018; Borowska-Zuchowska et al., 2020; Gordon et al., 2020). In 2008, Idziak and Hasterok performed sequential silver staining and fluorescence *in situ* hybridisation with 25S rDNA as a probe to verify the

transcriptional activity of 35S rDNA loci in the root-tip cells of six genotypes of *B. hybridum*. They revealed that only two out of four 35S rDNA sites were silver-stained and thus considered transcriptionally active during the previous interphase. Since the two active rDNA sites were terminally located on the chromosomes, it was concluded that they belonged to the D-subgenome. Studies conducted by Borowska-Zuchowska et al. (2016) showed that the 35S rDNA loci inherited from *B. stacei* were located at the nuclear periphery in interphase nuclei and were not associated with the nucleolus. In contrast, the hybridisation signals corresponding with the 35S rDNA loci inherited from the *B. distachyon* were often found within the nucleolus or in the chromocenters located adjacent to the nucleolus.

Further studies on the ND in *B. hybridum* were performed to verify: (i) the structure of both the dominant and under-dominant 35S rDNA loci; (ii) the role of epigenetic modifications in the selective repression of rDNA loci of *B. stacei* origin; and (iii) the developmental regulation of ND in this allotetraploid. As part of the study of the structure of dominant and under-dominant 35S rDNA loci, the IGSs from both the putative ancestors, *B. distachyon* and *B. stacei*, and the allotetraploid were sequenced and analysed, and the putative transcription initiation sites were predicted (Borowska-Zuchowska et al., 2016). In several *B. hybridum* genotypes, an apparent reduction of the *B. stacei* rDNA loci size, accompanied by their inactive transcriptional status, was revealed. Moreover, genotype ABR117 showed the elimination of 35S rDNA loci originating from the S-subgenome, as shown by FISH (Hasterok et al., 2004; Borowska-Zuchowska et al., 2020). However, the presence of one S-genome 35S rDNA family in ABR117 was shown by Southern blot hybridisation, suggesting that even in this genotype, the elimination of *B. stacei*-inherited rDNA units is still in progress (Borowska-Zuchowska et al., 2020).

It is well known that ND has an epigenetic origin (Costa-Nunes et al., 2010). Thus, the immunostaining approach was used to verify the epigenetic state of dominant and the under-dominant 35S rDNA loci in different *B. hybridum* genotypes. It was shown that a high level of DNA methylation characterised the repressed *B. stacei*-inherited rDNA loci. However, global hypomethylation induced by 5-azacytidine did not lead to transcriptional reactivation of these loci, indicating that other factors besides DNA methylation may be involved in their suppression. These findings suggest that the preferential silencing of *B. stacei*-originated rDNA loci may result from structural changes in the sequence rather than solely from epigenetic silencing (Borowska-Zuchowska and Hasterok, 2017). In

contrast, the D-subgenome 35S rDNA loci were characterised by significantly lower DNA methylation levels and were enriched in euchromatic histone modifications, e.g., acetylated histones H3 (K9) and H4 (K5 and K16) (Borowska-Zuchowska and Hasterok, 2017).

Additionally, the presence of ND during different stages of development in the reference *B. hybridum* genotype ABR113 was investigated by Borowska-Zuchowska et al. (2019). It was shown that ND is present not only in root meristematic and differentiated cells but also in: (i) male meiocytes at prophase I; (ii) tetrads of microspores; and (iii) different tissues of embryos. Silver staining confirmed the inactive state of *B. stacei*-originated rDNA loci (Borowska-Zuchowska et al., 2019). ND's developmental regulation and stability in *B. hybridum* were further investigated by comparing two genotypes, ABR113 and 3-7-2 (Borowska-Zuchowska et al., 2021). While in the ABR113, the ND was stable in the primary and adventitious roots, leaves, and spikes, in the 3-7-2 genotype, a strong upregulation of the *B. stacei* rDNA loci was observed in adventitious roots. Thus, it was shown that ND in *B. hybridum* may be a fully reversible and developmentally regulated process, depending on the genotype.

These studies contribute to a better understanding of ND in *B. hybridum* and highlight the complex interplay between genetic and epigenetic factors that regulate this intriguing phenomenon. As more research is conducted, *B. hybridum*, with its wide range of genetic resources, comprehensive sequencing data, and relatively simple genome to be analysed, emerges as an up-and-coming model for exploring ND. Notably, this small-genome grass shares a close relationship with key cereals, further enhancing its potential as a valuable model organism in ND studies. The regulation of ND in *B. hybridum* is influenced by specific genotypes and intricate epigenetic modifications. Considering the unique characteristics of its rDNA loci (only one locus per each ancestral genome), *B. hybridum* becomes an exceptionally appealing candidate for unravelling the mechanisms underlying ND, particularly in grasses.

2. AIMS OF THE THESIS

This work aimed to shed more light on the evolutionary patterns of 35S rDNA in *B. hybridum* and verify whether the molecular mechanisms responsible for the ND establishment and maintenance are the same in *B. hybridum* as in the much better-studied dicot allopolyploids. The specific goals were as follows:

- Determination of 35S rDNA loci number and chromosomal localisation in different *B. hybridum* genotypes by FISH;
- Determination of the ancestral 35S rDNA contributions in selected *B. hybridum* genotypes by Southern hybridisation and based on the bioinformatic analysis of raw Illumina reads;
- Analysis of the expression patterns of *B. hybridum* 35S rRNA genes by RT-CAPS (Reverse Transcription-Cleaved Amplified Polymorphic Sequence) and RT-qPCR (Reverse Transcription-quantitative Polymerase Chain Reaction);
- Identification of *B. hybridum* genotypes in which ND is developmentally regulated;
- Identification of the maternal parent in different *B. hybridum* genotypes based on the chloroplast *trn*LF gene barcoding.

The following hypotheses have been verified:

1. The under-dominant S-subgenome 35S rDNA units undergo gradual elimination from the *B. hybridum* genome.
2. ND is regulated developmentally in *B. hybridum.*
3. There is no maternal effect on the S-subgenome 35S rDNA silencing in *B. hybridum*.

3. MATERIALS AND METHODS

3.1. Origin of the plant material.

Three species were used in this study: *B. hybridum* (2n = 30; subgenome composition DDSS), *B. distachyon* (2n = 10; genome DD) and *B. stacei* (2n = 20; genome SS). Seeds of different genotypes were sourced from the University of Aberystwyth in Great Britain (ABR genotypes) and the US Department of Agriculture – National Plant Germplasm System (Bd21). Dr Shira Penner kindly provided the seeds of genotypes from the natural populations in Israel (Penner et al., 2020). The information on the plant material origin, including the GPS coordinates of the genotypes collected in Israel, is shown in Table 2.

Table 2. Origin and GPS coordinates of the plant material.

No.	Genotype name	2n	Species	GPS coordinates
				Latitude/longitude or country of origin
1	1.12.1	30	*B. hybridum*	33°16'53.36"N/35°44'2.72"E
2	1.24.1	30	*B. hybridum*	33°16'53.36"N/35°44'2.72"E
3	2.2.2	30	*B. hybridum*	33°16'41.59"N/35°46'26.71"E
4	2.6.1	30	*B. hybridum*	33°16'41.59"N/35°46'26.71"E
5	3.4.2	30	*B. hybridum*	33°15'56.32"N/35°44'31.35"E
6	3.16.1	30	*B. hybridum*	33°15'56.32"N/35°44'31.35"E
7	4.5.2	30	*B. hybridum*	33°15'10.89"N/35°43'4.42"E
8	5.6.5	30	*B. hybridum*	33°14'40.74"N/35°41'49.12"E
9	5.8.3	30	*B. hybridum*	33°14'40.74"N/35°41'49.12"E
10	6.5.1	30	*B. hybridum*	33°14'11.97"N/35°34'31.35"E
11	7.19.2	30	*B. hybridum*	33° 5'4.70"N/35°18'26.59"E
12	7.27.1	30	*B. hybridum*	33° 5'4.70"N/35°18'26.59"E
13	8.5.4	30	*B. hybridum*	32°59'39.98"N/35°24'57.25"E
14	8.8.2	30	*B. hybridum*	32°59'39.98"N/35°24'57.25"E
15	9.1.3	30	*B. hybridum*	32°55'40.06"N/35°18'2.56"E
16	9.7.6	30	*B. hybridum*	32°55'40.06"N/35°18'2.56"E
17	10.11.2	30	*B. hybridum*	32°44'38.02"N/35° 2'33.75"E

18	10.19.5	30	*B. hybridum*	32°44'38.02"N/35° 2'33.75"E
19	11.17.6	20	*B. stacei*	32°43'40.29"N/35° 0'52.85"E
20	11.24.1	30	*B. hybridum*	32°43'40.29"N/35° 0'52.85"E
21	12.5.3	30	*B. hybridum*	32°42'52.05"N/34°58'23.23"E
22	12.23.2	30	*B. hybridum*	32°42'52.05"N/34°58'23.23"E
23	13.3.5	30	*B. hybridum*	31°53'45.27"N/34°57'30.09"E
24	13.19.2	30	*B. hybridum*	31°53'45.27"N/34°57'30.09"E
25	14.2.2	30	*B. hybridum*	31°48'46.63"N/35° 6'47.53"E
26	15.3.1	30	*B. hybridum*	31°48'43.27"N/35° 0'45.39"E
27	16.2.5	30	*B. hybridum*	31°42'58.81"N/34°58'36.90"E
28	16.18.3	20	*B. stacei*	31°42'58.81"N/34°58'36.90"E
29	17.10.1	20	*B. stacei*	31°38'49.23"N/34°55'06"E
30	18.5.2	30	*B. hybridum*	31°31'30.30"N/34°53'58.49"E
31	18.6.1	30	*B. hybridum*	31°31'30.30"N/34°53'58.49"E
32	19.16.5	30	*B. hybridum*	31°23'31.72"N/34°51'42.90"E
33	21.7.2	30	*B. hybridum*	30° 4'21.36"N/34°49'41.88"E
34	21.11.1	30	*B. hybridum*	30° 4'21.36"N/34°49'41.88"E
35	23.101	n/a	*B. hybridum*	30°36'39.76"N/34°51'25.29"E
36	24.1	30	*B. hybridum*	30°52'2.80"N/34°46'7.18"E
37	24.3	30	*B. hybridum*	30°52'2.80"N/34°46'7.18"E
38	26.12	30	*B. hybridum*	31°20'55.49"N/34°51'27.91"E
39	26.24	30	*B. hybridum*	31°20'55.49"N/34°51'27.91"E
40	28.28	30	*B. hybridum*	31°16'1.78"N/34°49'10.70"E
41	28.29	30	*B. hybridum*	31°16'1.78"N/34°49'10.70"E
42	29.3	30	*B. hybridum*	31°15'41.49"N/35° 1'5.29"E
43	29.5	30	*B. hybridum*	31°15'41.49"N/ 35° 1'5.29"E
44	30.20	20	*B. stacei*	31°15'42.92"N/35°14'18.86"E
45	31.8	30	*B. hybridum*	31°8'42.88"N/34°59'5.04"E
46	ABR 103	30	*B. hybridum*	Nr. Carmel, Israel
47	ABR 113	30	*B. hybridum*	Lisbon, Portugal
48	ABR 114	20	*B. stacei*	Formentera, Spain
49	ABR 116	30	*B. hybridum*	Afghanistan
50	ABR 117	30	*B. hybridum*	Afghanistan

51	ABR 118	30	*B. hybridum*	Afghanistan
52	ABR 119	30	*B. hybridum*	Afghanistan
53	ABR 121	30	*B. hybridum*	Iran
54	ABR 123	30	*B. hybridum*	Iran
55	ABR 124	30	*B. hybridum*	Israel
56	ABR 127	30	*B. hybridum*	Iran
57	ABR 129	30	*B. hybridum*	Pakistan
58	ABR 130	30	*B. hybridum*	Morocco
59	ABR 132	30	*B. hybridum*	Spain
60	ABR 134	30	*B. hybridum*	Israel
61	ABR 135	30	*B. hybridum*	Uruguay
62	ABR 136	30	*B. hybridum*	Germany
63	ABR 137	30	*B. hybridum*	W. Australia
64	ABR 138	30	*B. hybridum*	Quinta da Pacheca, Portugal
65	3-7-2	30	*B. hybridum*	38°17'40.2"N/27°24'13.9"E
66	ABR101	30	*B. hybridum*	South Africa
67	ABR100	30	*B. hybridum*	Iran
68	ABR115	30	*B. hybridum*	South Africa
69	Bd21	10	*B. distachyon*	Iraq

3.2. Material cultivation and preparation.

For cytogenetic analysis, seeds were grown on Petri dishes on a filter paper moistened with distilled water for 3-4 days in a dark at room temperature. The 1-1.5 cm-long roots were cut and immersed in ice-cold water for 24 h, fixed in 3:1 v/v methanol:glacial acetic acid at 4 °C overnight and stored at -20 °C.

The remaining seeds were sown in pots containing soil mixed with vermiculite (3:1 w/w) and grown at 22 °C, 16 h light/8 h night photoperiod in a greenhouse. The plants used in the study were not subjected to vernalisation.

3.3. Cytomolecular analysis.

3.3.1. Root meristem preparations.

Cytogenetic preparations were made from fixed primary and adventitious roots (collected from 6-week-old plants), as described by Jenkins and Hasterok (2007). Roots were washed in 0.01 M citrate buffer (pH 4.8) for 15 min, with three buffer changes at room temperature. After washing, the roots were digested enzymatically for 1-1.5 h at 37 °C in a mixture of 6% (v/v) pectinase (Sigma-Aldrich, St. Louis, MO, USA) and cellulase: (i) 0.5% w/v cellulase (Sigma-Aldrich); and (ii) 0.5% w/v "Onozuka R-10" cellulase (Serva, Heidelberg, Germany). After digestion, the meristems were washed in citrate buffer for 10 min on ice. The meristems were dissected from the root tips and squashed in 45% acetic acid. After freezing on dry ice, the coverslips were removed using a razor blade, and the slides were air-dried. The quality of the preparations was assessed using a phase-contrast microscope, and only the slides with a high number of metaphase plates and a small amount of cytoplasm were taken for further analysis.

3.3.2. Preparation of DNA probes for FISH.

Two types of probes were used in the study:

(i) a 410-bp-long clone pTa794 from *Triticum aestivum* (Gerlach and Dyer, 1980) was used to detect the 5S rDNA loci.

(ii) a 2.3 kb fragment of the 25S rRNA gene from *A. thaliana* (Unfried and Gruendler, 1990) was used to visualise the 35S rDNA loci.

The rDNA sequences were labelled either with tetramethylrhodamine-5-dUTP (TAMRA-dUTP, Roche, Basel, Switzerland) or digoxigenin-11-dUTP (DIG-dUTP, Roche) using the Nick Translation Mix labelling kit (Roche). The composition of the mixture used for the nick-translation reaction is provided in Table 3.

Table 3. The composition of the nick-translation reaction.

Name of the component	**Volume**
dATP (0.4 mM)	2.5 µl
dTTP (0.4 mM)	1.67 µl
dCTP (0.4 mM)	2.5 µl
dGTP (0.4 mM)	2.5 µl
25S rDNA or 5S rDNA (100 ng/µl)	6 µl
Tetramethylrhodamine-5-dUTP or digoxigenin-11-dUTP	0.83 µl
10x reaction buffer and nick-translation enzymes	4 µl
Total volume	**20 µl**

The nick-translation reaction was conducted in the thermocycler under the following conditions: 95 min at 15 °C and 10 min at 60 °C to stop the reaction. The probes were precipitated by adding 2 µl of 3 M ice-cold sodium acetate and 50 µl of chilled 100% ethanol and incubated at either -80 °C for 1 h or -20 °C overnight. The tubes were then centrifuged at 14,000 rpm for 30 min at 4 °C, and the supernatant was removed. The pellet was washed twice with 70% ethanol and centrifuged at 14,000 rpm for 5 min at 4 °C. After drying, the pellet was dissolved in 10 µl of sterile distilled water. The probes were stored at -20 °C or used immediately in FISH.

3.3.3. Fluorescence *in situ* hybridisation.

The slides were incubated with RNase (100 µg/ml) in 2× SSC in a moist chamber for 1 h at 37 °C. Then, the slides were washed three times with 2× SSC buffer for 5 min each and fixed in 1% formaldehyde in 1× PBS for 10 min at 37 °C. Then, the slides were washed three times in 2× SSC, dehydrated in ethanol series (70%, 90%, and 99%), and air-dried. The hybridisation mixture was prepared by mixing the reagents listed in Table 4.

Table 4. Composition of the hybridisation mix.

Name of the component	**Volume**
100% deionised formamide	20 µl
50% (w/v) dextran sulphate (heated before adding)	8 µl
20× SSC (sterile)	4 µl
10% (w/v) SDS	2 µl
25S rDNA or 5S rDNA probe (75-200 ng/slide)	1-6 µl
Sterile distilled water	0-5 µl
Total volume	**40 µl**

The hybridisation mixture was incubated for 10 min at 75 °C and stabilised on ice for 10 min. Then, 40 µl of the hybridisation mixture was applied to each slide and covered with plastic coverslips from autoclavable plastic bags. The probe and chromosomes were denatured for 4.5 min at 75 °C using an *in situ* Hybaid OmniSlide Thermal Cycler System (Fischer Thermo Scientific, Waltham, MA, USA). After denaturation, the slides were placed in a humid chamber and incubated at 37 °C for approximately 16-24 h.

After hybridisation, the coverslips were removed by incubating slides in a staining jar with 2× SSC at 42 °C. Then, stringent washes were performed. The slides were incubated twice in 15% formamide in 0.1× SSC at 42 °C for 5 min (corresponding to a stringency of 82%). The slides were washed three times in 2× SSC at 37 °C, followed by three washes in 2× SSC at room temperature.

The slides were washed in 4× SSC with 0.2% Tween20 for 5 min at room temperature. Then, 200 µl of blocking reagent (5% solution of skimmed powder milk in 4× SSC) was applied on each slide and covered with plastic coverslips. After 20 min of incubation at room temperature, 40 µl of FITC fluorochrome-conjugated anti-DIG antibody (fluorescein isothiocyanate, Roche) was applied on each slide. The plastic coverslips were applied, and the slides were incubated in a humid chamber for 1-2 h at 37 °C. Then, the slides were washed in 4× SSC with 0.2% Tween20 for 10 min at 37 °C. This step was repeated three times. Then, slides were dehydrated in ethanol series (70%, 90%, and 99%) and air-dried. The dried slides were sealed in Vectashield buffer (Vector Laboratories, Newark, CA, USA) with DAPI (4',6-diamidino-2-phenylindole, Serva) at a concentration of 2.5 µg/ml and stored in the dark at 4 °C until use.

3.3.4. Image acquisition and processing.

Photomicrographs were acquired using AxioImager.Z.2 (Zeiss, Oberkochen, Germany) wide-field epifluorescence microscope equipped with a monochromatic AxioCam HRm (Zeiss) camera. All images were processed with Photoshop CS3 (Adobe, San Jose, CA, USA) and ZEN Lite (Zeiss).

3.4. Molecular analyses.

3.4.1. DNA isolation.

Total genomic DNA (gDNA) from the leaves of 4-week-, 6-week- and 8-week-old plants, adventitious roots from 6-week-old plants and young spikes containing meiocytes was extracted with chloroform:isoamyl alcohol (24:1) and precipitated with isopropanol according to the CTAB method as described by Doyle (1991). 100 mg of tissue was collected, frozen in liquid nitrogen, and ground into a fine powder with a mortar and pestle. Then, the fine powder was transferred into a 2 ml sterile tube containing 750 µl of CTAB buffer, 2 µl of β-mercaptoethanol and 3 µl of RNase (100 mg/ml) and mixed well by vortexing. The tube was incubated for 60 min at 60 °C, occasionally mixed by inverting the tube. Then, 800 µl of chloroform:isoamyl alcohol (24:1) was added to the tube, mixed by inverting the tube, and incubated for 3 min at room temperature. The tube was centrifuged at 14,000 rpm for 10 min at room temperature. The upper aqueous phase was transferred to a new sterile 1.5 ml tube. 600 µl of ice-cold isopropanol was added to the tube and gently mixed. The tube was then centrifuged at 14,000 rpm for 15 min at 4 °C. The supernatant was discarded, and the DNA pellet was washed with ice-cold 70% ethanol. The tube was centrifuged at 14,000 rpm for 10 min at 4 °C. The supernatant was discarded, and the DNA pellet was dried for 20 min at 37 °C. Subsequently, the DNA pellet was resuspended in 100-200 µl of sterile DNase/RNase-free water. To remove RNA contamination, RNase A was added to a final concentration of 0.1 mg/ml, and the tube was incubated at 37 °C for 60 min. The quality of the isolated DNA was verified by gel electrophoresis.

The isolated gDNAs from 36 *B. hybridum* genotypes were sent to the U.S. Department of Energy (DOE) Joint Genome Institute (JGI) at Lawrence Berkeley National Laboratory (Berkeley, CA, USA) for Illumina sequencing. The list of genotypes is presented in Table 5.

Table 5. List of the *B. hybridum* genotypes sequenced by Illumina.

Genotype names			
9.7.6	16.2.5	ABR 132	3-7-2
2.2.2	10.11.2	18.6.1	ABR 134
3-4-2	2.6.1	10.19.5	19.16.5
ABR 135	20-15	3.4.2	12.5.3
24.1	ABR 137	19-6-2	7.19.2
12.23.2	28.28	ABR 138	18-19
7.27.1	13.3.5	ABR 103	ABR101
11-8	9.1.3	13.19.2	ABR 116
ABR115	14.2.2	ABR 127	ABR107

3.4.2. RNA isolation and reverse transcription.

The total RNA was isolated from the leaves of 4-week-, 6-week- or 8-week-old plants, pulled primary roots, adventitious roots from 6-week-old plants (washed with tap water from soil residues) and young spikes that contained meiocytes. Isolation was carried out as described by Muoki et al. (2012) with additional purification. Approximately 50-100 mg of the tissue was ground into a fine powder using a sterile pestle and mortar in liquid nitrogen. Then, the powder was transferred into a 2 ml tube containing 950 ml of the pre-heated (65 °C) extraction buffer I (see the Reagent setup). The tube was vortexed briefly and incubated at 65 °C for 15 min, with occasional shaking. Then, 1 ml of chloroform:isoamyl alcohol (24:1) was added to the tube, vortexed briefly, and centrifuged at 14,000 rpm for 10 min at room temperature. The supernatant was transferred to a fresh tube, and washing with chloroform:isoamyl alcohol (24:1) was repeated. The supernatant was transferred to a new 2 ml tube, 950 ml of extraction buffer II (see the Reagent setup) was added, and the tube was vortexed briefly. Then, 200 µl of chloroform was added to the tube, vortexed, and incubated for 10 min at room temperature. After incubation, the tube was centrifuged at 14,000 rpm for 10 min at 4 °C. The upper aqueous phase was transferred to a fresh sterile 1.5 ml tube without interphase contamination. 600 µl of chilled isopropanol was added, and the tube was mixed by inverting. After 10 min of incubation at room temperature, the tube was centrifuged at 14,000 rpm for 10 min at 4 °C. The supernatant was discarded, and the RNA pellet was washed twice with 1 ml of 70% ice-cold ethanol, followed by centrifugation at 14,000

rpm for 10 min at 4 °C. The pellet was dried at 37 °C until the complete ethanol evaporation. Finally, the pellet was resuspended in 87.5 µl of DEPC-treated water, 2.5 µl of TURBO™DNase I, and 10 µl of RNase-free buffer were added (Ambion, Austin, TX, USA). After 10 min of incubation at room temperature, the RNA was purified as follows: 10 µl of cold 3 M sodium acetate was added to the RNA sample, followed by 330 µl of ice-cold 100% ethanol. The tube was mixed by inverting and incubated at -20 °C for 30 min. After incubation, the tube was centrifuged at 14,000 rpm for 15 min at 4 °C. The supernatant was discarded, and the pellet was washed with 500 µl of ice-cold 70% ethanol. The tube was then gently mixed by inverting and centrifuged for 5 min at 4 °C at 14,000 g. The supernatant was carefully discarded (avoiding losing the pellet), and the pellet was dried at 37 °C until the ethanol evaporated. The RNA pellet was dissolved in 50-200 µl RNA-free water and stored at -80 °C until use.

Before the reverse transcription, the RNA was verified for DNA contamination by PCR amplification with 18Sfor and 5.8Srev primers (Kovarik et al., 2005). The lack of a PCR product serves as evidence that no DNA resides. The reverse transcription mixture (20 µl) contained 1 µg of total RNA, 100 pmol of random hexamer primer, 0.5 mM of dNTP, and 1 µl of Maxima H Minus Enzyme Mix with reverse transcriptase (Thermo Scientific). Before adding reverse transcriptase and buffer, the mix was incubated at 65 °C for 5 min. After adding the enzyme and buffer, the reaction was performed in the following conditions: 10 min at 25 °C followed by 30 min at 65 °C. The reaction was terminated by heating at 85 °C for 5 min. The obtained cDNA was stored at -80 °C.

3.4.3. gCAPS and RT-CAPS analysis.

Genomic-Cleaved Amplified Polymorphic Sequence (gCAPS) analysis is based on the polymorphisms in the ITS1 region in *B. hybridum* – ITS1 region of *B. distachyon* has a single *Mlu*I restriction site, while the ITS1 region of *B. stacei* is not cut by *Mlu*I enzyme. The expected pattern of *Mlu*I restriction is presented in Figure 2.

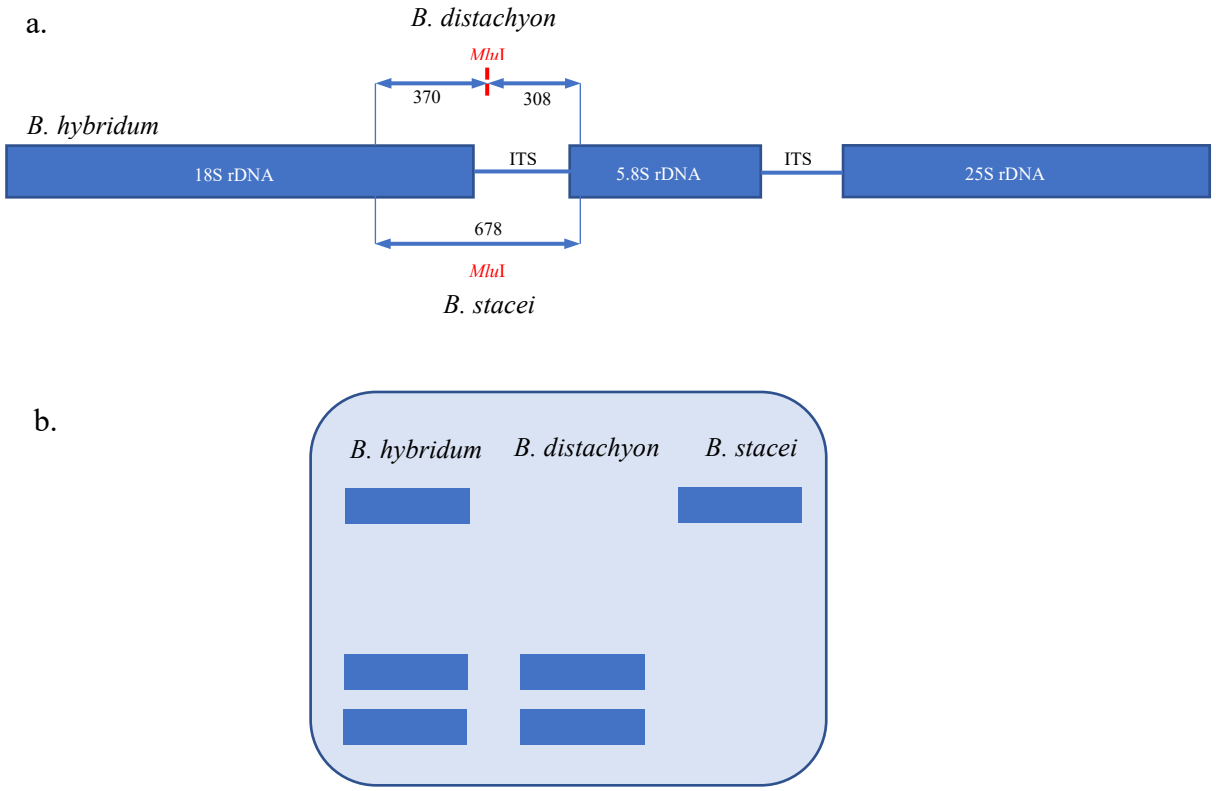

Figure 2. The *Mlu*I restriction profile of the D-subgenome and S-subgenome ITS1 amplification products (a) and the expected sizes of the bands after digestion (b).

For the gCAPS method, 50 ng of genomic DNA was used as a template in the PCR reaction to amplify the fragment of the 18 rDNA and the ITS1 region (Figure 2a). The 18Sfor and 5.8Srev primers designed by Kovarik et al. (2005) were used. PCR conditions were as follows: 95 °C (180 sec); 35 cycles of: 95 °C (20 sec), 60 °C (20 sec) and 72 °C (80 sec); followed by a final 72 °C extension (10 min). The 5 µl amplification mixture was digested with 5 U of *Mlu*I restriction enzyme (2 h at 37 °C) and visualised on 1% (w/v) agarose gel. *B. stacei* ABR114 and *B. distachyon* Bd21 PCR products subjected for *Mlu*I digestion were used as a reference to control digestion efficiency.

To study the expression pattern of parental 35S rDNA in *B. hybridum,* the Reverse Transcription-Cleaved Amplified Polymorphic Sequence (RT-CAPS) method was used according to Sochorova et al. (2017). ITS1 region was amplified by PCR as in the case of gCAPS; however, the cDNA was used as a template. gDNA from *B. stacei* ABR114 and *B. distachyon* Bd21 was used as a reference to control digestion efficiency.

3.4.4. RT-qPCR.

The *B. stacei*-originated and *B. distachyon*-originated 35S pre-rRNA transcript ratios were determined using the reverse transcription quantitative PCR (RT-qPCR) on a LightCycler® 480 Real-Time PCR System (Roche) with the use of LightCycler® 480 SYBR Green I Master Mix (Roche). Three different *B. hybridum* genotypes were analysed by RT-qPCR: the reference genotype ABR113, 2.2.2 (Israel) and 3-7-2 (Turkey).

A total RNAs from (i) primary roots; (ii) fresh and greenish leaves from 4-week-old, 6-week-old and 8-week-old plants; (iii) adventitious roots from 6-week-old plants; and (iv) +8-week-old spikes containing meiocytes were isolated. Isolated RNA was used for reverse transcription. cDNA was diluted 50-fold, and 2 µl of the diluted one was used in the RT-qPCR reaction with the following conditions: an initial step at 95 °C (5 min), 45 cycles of 95 °C (10 sec), 60 °C (20 sec), and 72 °C (10 sec) with the signal acquisition. Ubiquitin and S-adenosylmethionine decarboxylase genes were used as the reference genes. All reactions were performed in two technical replicates and three biological replicates, except for the 6-week-old leaves of genotype 2.2.2, where ten biological replicates were performed. The primers were designed to selectively amplify either the *B. distachyon*-like rRNA genes or the *B. stacei*-like ones (Table 6). To ensure the efficiency of each primer set, a four-fold serial dilution of template cDNA over six points was performed, and amplification efficiency was calculated based on the results of RT-qPCR. All primer pairs displayed a reaction efficiency between 90-110% and a linear correlation coefficient (R^2) greater than 0.99, as outlined in the study by Taylor et al. (2010).

Table 6. Primers used in RT-qPCR experiment.

Primer name	Sequence
18Sfor	5`-GCGCTACACTGATGTATTCAACGAG-3`
5.8Srev	5`-CGCAACTTGCGTTCAAAGACTCGA-3`
C	5`-CGAAATCGGTAGACGCTACG-3`
F	5`-ATTTGAACTGGTGACACGAG-3`
M13F	5′-GCCAGGGTTTTCCCAGTCACGA-3′
M13R	5′-CAGGAAACAGCTATGAC-3′
ITS1 Bd F1	5′-CGCACGCGTCATCCATCCTG-3′
ITS1 Bd R1	5′-TCTTTTGCCCCATGCACCAG-3′
ITS1 Bs F1	5′-CGCACGTGTCATCCATCCCA-3′
ITS1 Bs R2	5′-GGGGGCAGCAAGCAGGCGA-3′
BdSamDC_F	5′-TGTGCTAAGGAGATGACAA-3′
BdSamDC_R	5′-GATGGCGTTCATGGAGTAG-3′
Ubi10F	5′-TCCACACTCCACTTGGTGCT-3′
Ubi10R	5′-GAGGGTGGACTCCTTTTGGA-3′

3.4.5. Southern hybridisation.

Southern hybridisation was carried out according to the procedure described by Kovarik et al. (2005). Approximately 1 μg of gDNA from selected genotypes was subjected to restriction with *Bgl*II (a methylation-insensitive enzyme that recognises AGATCT motif) or *Pst*I (a methylation-sensitive enzyme that cuts the CTGCAG motif, and the cleavage is blocked by the C methylation) for 2 h at 37 °C. The *Bgl*II restriction maps of the 35S rDNA units of *B. distachyon* and *B. stacei* are shown in Figure 3. *Pst*I restriction maps of the 35S rDNA units of *B. distachyon* and *B. stacei* are presented in Figure 4. The gDNA that underwent restriction was loaded on a 1% (w/v) agarose gel and separated by gel electrophoresis overnight. The gel was washed in 0.4 M NaOH solution for 30 min and transferred onto a nylon membrane (Amersham Hybond, GE Healthcare, USA). Constant pressure was applied to the gel using a 0.4 M NaOH buffer to transfer the DNA onto the membrane. This solution was drawn upward through the gel by capillary action using filter paper, which moved the DNA from a high 0.4 M NaOH potential to an area of low buffer potential. Afterwards, the membrane was washed in 2× SSC and hybridised with

a fragment of 25S rDNA labelled with ^{32}P as a probe. The probe was labelled by random priming using the *Nicotiana tabacum* 25S rDNA as a template. After overnight hybridisation, the membrane was washed in 2× SSC buffer, dried out, and the signal was detected using a phosphoimager (Typhoon 9500; GE Healthcare, USA). The intensity of the 35S rDNA signal was calculated using ImageQuant (GE Healthcare) and Image Lab (Bio-Rad Laboratories, Hercules, CA, USA) software. All Southern blots were repeated twice to ensure the experiment's accuracy.

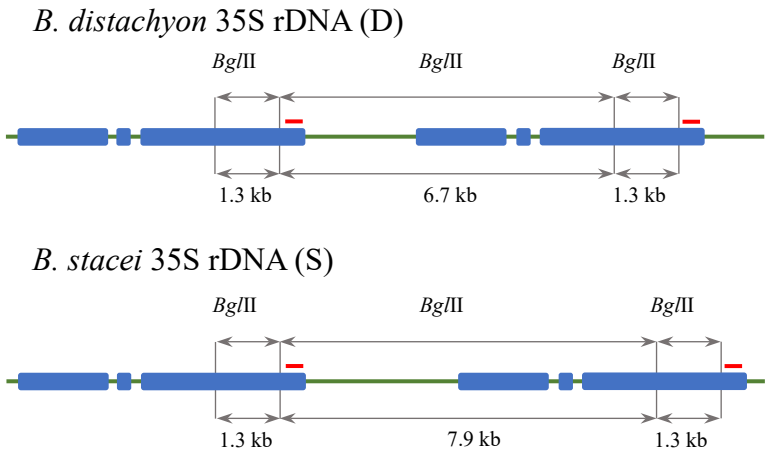

Figure 3. Schematic representation of *Bgl*II restriction map on *B. distachyon* and *B. stacei* 35S rDNA units. Red bar – probe.

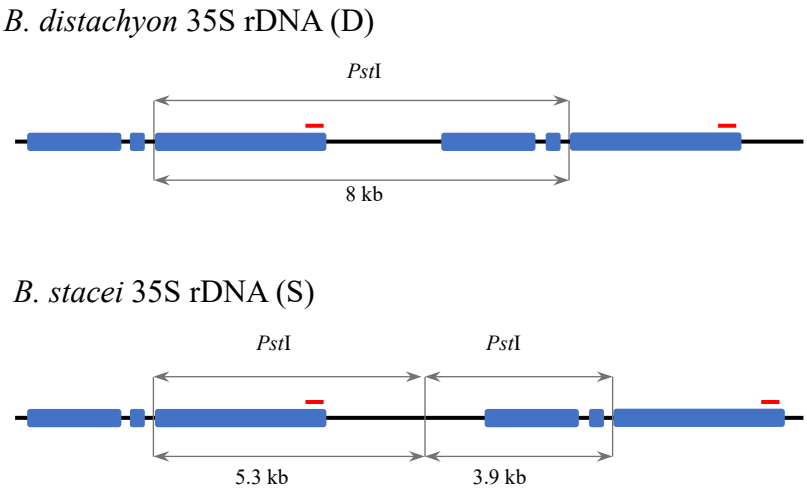

Figure 4. Schematic representation of *Pst*I restriction map on *B. distachyon* and *B. stacei* 35S rDNA units. Red bar – probe.

3.4.6. Bioinformatic analysis of raw Illumina reads.

Eight *B. hybridum* genotypes were analysed to estimate the D- and S-subgenome 35S rDNA homoeologous content: 3-7-2, 2.2.2, 12.23.2, 3.4.2, 10.11.2, 10.19.5, 24.1 and ABR132. Bioinformatic analysis of raw Illumina reads was used to determine 35S rDNA copy number by reads count, according to Borowska-Zuchowska et al. (2020). All bioinformatic analyses were done using CLC GENOMICS WORKBENCH (Qiagen, Hilden, Germany) software. The Illumina reads from each genotype were subjected to quality control (QC) and trimmed – the "TRIM" command was used to eliminate reads that were shorter than 150 bp, contained ambiguous nucleotides or failed to pass a quality score limit of P = 0.05. 10% of the trimmed Illumina reads from each library were randomly sampled using the "Subsample Sequence List" command. Local BLAST libraries from the sampled reads were created.

A short 50-bp-long ITS1 fragment that showed a 10% sequence variation between the *B. distachyon*- and *B. stacei*-like 35S rDNA consensus sequences were selected for the haplotypic analysis based on Borowska-Zuchowska et al. (2020). The S-subgenome ITS1 fragment was then BLASTed against the local BLAST libraries of the selected *B. hybridum* genotypes. The hit sequences were: (i) trimmed for length (≥ 50 bp); (ii) trimmed for quality (no ambiguous nucleotides allowed; quality score limit P = 0.05); (iii) sampled at random for approximately 10% of the reads. The sampled reads were aligned using the "Multiple Alignment" tools with the following parameters: gap open cost, 10; gap extension cost, 1; end gap cost, as any other; and alignment mode, very accurate.

Neighbour-joining phylogenetic trees were constructed using the Jukes-Cantor distance algorithm and a bootstrap of 500 replicates. Finally, the D- and S-subgenome-specific reads ratio was quantified by dividing the number of specific haplotypes by the total number of sequences. The circular phylogenetic trees were constructed, and colours were designated in Geneious Prime software (v2021.01.1, Biomatters Ltd.).

To extract a 35S rDNA unit consensus sequence in selected *B. hybridum* genotypes, trimmed Illumina reads were mapped to the *B. distachyon*-like and *B. stacei*-like 35S rDNA consensus sequences that were published previously by Borowska-Zuchowska et al. (2020). The "Map Reads to Reference" tool was used with the following parameters: mismatch cost of 2, insertion cost of 3, deletion cost of 3, length fraction of 0.5, and a similarity fraction of 0.8. The resulting mapped reads were used to extract the initial subgenome consensus sequences D1 and S1 (for *B. distachyon*-like and *B. stacei*-

like rDNA) through the "Extract Consensus" tool. Then, the raw Illumina reads were remapped to the initial subgenome consensuses D1 and S1 using the same parameters as before. The resulting reads were then used to extract the consensus D2 and S2 through the "Extract Consensus" tool. Finally, read coverage maps were created using the "Create Mapping Graph" tool.

3.4.7. *trn*LF region analysis.

The fragment of the *trn*LF gene was sequenced to determine the maternal parent of different *B. hybridum* genotypes. The fragment of the *trn*LF gene was amplified by PCR with C forward and F reverse primers (see Table 6) (Lopez-Alvarez et al., 2012). The gDNAs from all 63 *B. hybridum* genotypes were used as templates for PCR. The PCR temperature profile was as follows: 95 °C (180 sec); 35 cycles of 95 °C (20 sec), 60 °C (20 sec) and 72 °C (80 sec), followed by a 72 °C of final extension (10 min). The PCR product was assessed for its mass and integrity by running it on an agarose gel and purified using the NucleoSpin™ Gel and PCR clean-up kit (Macherey-Nagel, Düren, Germany). The resulting amplicons were sequenced by Sanger sequencing (Macrogen Europe, Amsterdam, Netherlands), using either the C or F primer. The chromatograms were then checked for quality, and the sequences were trimmed and aligned using the Clustal Omega 1.2.2 algorithm in Geneious Prime software version v2021.01.1 (Biomatters Ltd).

To construct the phylogenetic tree, the *trn*LF gene from *Brachypodium boissieri* (GenBank ID JN187655) was used as the root using Mesquite v3.7 software (Maddison and Maddison, 2009). The *trn*LF regions from *B. stacei* (GenBank ID JX666003) and *B. distachyon* (GenBank ID JN187665) were used as references. The phylogenetic tree was created using the IQ-TREE web server, with an ultrafast bootstrap analysis option, according to Trifinopoulos et al. (2016). Based on the Bayesian information criterion, the best-fit model was determined to be F81+F+I.

3.4.8. SNP analysis of the ITS1 region.

Three *B. hybridum* genotypes (ABR113, ABR101 and 2.2.2) and *B. stacei* genotype (ABR114) were used to analyse the homogeneity of the ITS1 region and fragment of the 18S rRNA gene. The amplified fragment of the 18S rDNA and ITS1 (as described in section 3.4.3) were separated by gel electrophoresis, isolated from the agarose gel and re-

amplified by an additional PCR run with conditions described for gCAPS in section 3.4.3. In brief, the whole PCR product was loaded on the 1% (w/v) agarose gel and ran for mass checking. The bands were excised from the gel with a sterile scalpel and purified by NucleoSpin™ Gel and PCR clean-up kit (Macherey-Nagel) with subsequent ligation into a pGEM-T vector (Promega, Madison, WI, USA). The ligation reaction was performed as follows: 2.5 µl of reaction buffer, 0.5 µl of vector, 1.5 µl of isolated PCR product and 0.5 µl of T4 DNA ligase were added to a 0.5 ml tube and incubated overnight at 4 °C.

The transformation was done according to Hus et al. (2020). In detail, 2 µl of the ligation product was added to the competent One Shot TOP10 Chemically Competent *Escherichia coli* cells (Thermo Scientific) and incubated on ice for 30 min. The sample was subjected to heat shock by incubating in a water bath at 42 °C for 30 seconds and then immediately transferred to ice for 2 min. 250 µl of pre-warmed SOC medium (Thermo Scientific) was added to the sample and incubated for 1 h at 37 °C with shaking at 250 rpm. After that, 100 µl of the bacterial culture was plated on solid LB Agar (Sigma-Aldrich) containing ampicillin (100 µg/ml, Duchefa Biochemie, Haarlem, Netherlands) on Petri dishes and incubated for 16-17 h at 37 °C. Single colonies (several for each genotype) were selected using a micropipette with a sterile tip and transferred to new sterile tubes containing 5 ml of LB liquid medium (Sigma-Aldrich) with ampicillin (100 mg/ml). The liquid culture was then carried out in an incubator for 16-17 h at 37 °C at 250 rpm.

Plasmids were isolated from bacterial cultures using a NucleoSpin® Plasmid kit from Qiagen. The bacterial cultures were transferred to new 5 ml tubes, centrifuged for 5 min at 8,000 rpm at room temperature, and the supernatant was discarded. The pellet was dissolved in 250 µl of P1 buffer at 4 °C. Then, 250 µl of P2 lysis buffer was added and gently mixed by inverting the tube, followed by a 4-minute incubation in the P2 buffer. After incubation, 350 µl N3 neutralisation buffer was added and gently remixed, followed by centrifugation at 13,000 rpm for 10 min at room temperature. The resulting supernatant was transferred to a QIAprep spin column, centrifuged at 10,000 rpm for 30 seconds, and the filtrate was discarded. 500 µl of PB binding buffer was added to the column and centrifuged at 10,000 rpm for 30 seconds. The column was then washed with 750 µl PE wash buffer and centrifuged at 10,000 rpm for 30 seconds. The residual PE buffer was removed by centrifuging the column at 10,000 rpm for 1 minute. Finally, the column was transferred to a new 1.5 ml tube, 50 µl of EB elution buffer was added, incubated for 1 minute at room temperature, and then centrifuged at 10,000 rpm for 1 minute. The

plasmids were sequenced using primers M13F and M13R by Sanger sequencing (Macrogen). Sequence alignment was performed using the Clustal Omega 1.2.2 algorithm in Geneious Prime software (v2021.01.1, Biomatters Ltd.).

3.5. Reagent setup.

The RNA extraction buffer I:

2% cetyltrimethylammonium bromide (CTAB)

2% polyvinylpolypyrrolidone (PVPP)

100 mM (hydroxymethyl)aminomethane [Tris–HCl (pH 8.0)]

25 mM ethylenediaminetetra acetic acid [EDTA (pH 8.0)]

2 M sodium chloride [NaCl].

Beta-mercaptoethanol was added just before use at a final concentration of 2%

The RNA extraction buffer II (prepared immediately before use):

Phenol saturated with Tris buffer to a pH of 6.7 ± 0.2

Sodium dodecyl sulfate [SDS; 0.1% (w/v)]

Sodium acetate [NaOAc; 0.32 M (w/v)]

EDTA (0.01 M final concentration, pH 8.0)

Enzymatic mixture for root treatment

6% pectinase (Sigma-Aldrich, St. Louis, MO, USA) 0.6 ml

0.5% Onozuka R-10 cellulase (Serva, Heidelberg, Germany) 0.05 g

0.5% w/v cellulase (Sigma-Aldrich) 0.05 g

Ampicillin (100 mg/ml)

100 mg of ampicillin

dH_2O - up to 1 ml

Sterilised through a 0.45 μm filter

CTAB buffer

2% hexadecyltrimethylammonium bromide (CTAB)

20 mM EDTA

100 mM Tris-HCl, pH 8

1.4 M NaCl

LB Agar medium with ampicillin, X-Gal and IPTG

8.75 g of LB Agar

dH_2O to 250 ml

Sterilised in an autoclave. After sterilisation, ampicillin (100 mg/ml) was added to the cooled medium at a ratio of 1 µl of antibiotic per 1 ml of LB medium.

LB Broth medium with ampicillin

5 g of LB Broth

dH_2O to 250 ml

Sterilised in an autoclave. After sterilisation, ampicillin (100 mg/ml) was added to the cooled medium at a ratio of 1 µl of antibiotic per 1 ml of LB medium. 30 ml of the medium was poured into each dish and left to solidify. Approximately an hour before introducing the bacteria, 40 µl of 2% X-Gal (Sigma-Aldrich) and 7 µl of 20% IPTG (Sigma-Aldrich) were added to the solid medium. The mixtures were cautiously spread over the medium using a sterile spreader, and the dishes were then placed in an incubator at 37 °C for 30 min.

RNase (10mg/ml)

10 mg RNase A

1 ml of a solution of 10 mM Tris-HCl + 15 mM NaCl

The RNase solution was stored in 15 µl aliquots at -20 °C. For the FISH reaction, 2× SSC buffer was diluted 1:99 (1485 µl of 2× SSC buffer was added).

1% formaldehyde in 1× PBS

6 ml formaldehyde (37%)

20 ml 10× PBS, pH 7.0

174 ml of dH_2O

10× PBS, pH 7.0

Solution (A): 0.1 M Na_2HPO_4 + 1.4 M NaCl

Solution (B): 0.1 M NaH_2PO_4 + 1.4 M NaCl

Solution A was supplemented with solution B until pH 7.0 was reached and sterilised in an autoclave.

20× SSC, pH 7.0

175.3 g 3 M NaCl

88.3g 0.3 M sodium citrate $C_6H_5Na_3O_7$×2H2O

DH_2O was added to the volume of 1 litre, and pH was adjusted with 1N HCl and sterilised in an autoclave.

4. RESULTS

4.1. The number and chromosomal localisation of 35S and 5S rDNA loci in different *B. hybridum* genotypes.

FISH was used to determine the number and chromosomal distribution of the 35S and 5S rDNA loci in 50 *B. hybridum* genotypes. The results are shown in Figures 5-24.

In the case of all studied genotypes (except for genotypes 7.27.1, 8.5.4, and ABR123, in which only the number of 5S rDNA was assessed based on FISH on interphase nuclei, and genotypes 13.19.2, 19.16.5, and ABR138 in the case of which the FISH with 5S rDNA as a probe was not performed), four FISH signals corresponding to 5S rDNA were observed: (i) two, proximally located ones on the chromosomal pair inherited from *B. distachyon*; and (ii) two signals located on the chromosomal pair originated from *B. stacei* in subterminal part of their short arms (Figures 5-14 and 16-22).

In the case of 35S rDNA loci, in 49 out of the 50 *B. hybridum* genotypes analysed, four hybridisation signals corresponding to the 25S rDNA were found (Figures 5-22): (i) two, terminally located ones on the chromosomal pair inherited from *B. distachyon*; and (ii) two, proximally located ones on the chromosomal pair inherited from *B. stacei* (Figures 5-13B, C and 16-22).

However, differences in FISH signal intensity corresponding to the 25S rDNA probe were observed between the D- and S-subgenome 35S rDNA loci. In general, the 25S rDNA FISH signals on the chromosomes from the S-subgenome were significantly smaller than on the D-subgenome ones. Based on the intensity of the FISH signals corresponding to 25S rDNA, the studied genotypes were classified into four groups (Table 7):

(i) Group 1 – contains the majority of investigated genotypes (30 out of 50) and is characterised by D-subgenome chromosomes having moderately stronger 25S rDNA hybridisation signals than *B. stacei*-like ones (Figures 5-15);

(ii) Group 2 – encompasses 12 out of 50 *B. hybridum* genotypes, in which the 25S rDNA FISH signals in the *B. stacei*-inherited chromosome pair are significantly smaller than in the Group 1 genotypes (Figures 16-19);

(iii) Group 3 – consists of *B. hybridum* genotypes (7 out of 50) showing very intense 25S rDNA hybridisation signals on S-subgenome chromosomes (Figures 20-22);

(iv) Group 4 – contains one *B. hybridum* genotype, in which only one chromosome pair belonging to the D-subgenome bears 35S rDNA loci. The FISH signals corresponding to 25S rDNA are also characterised by the substantial rDNA knobs at the chromosome termini in this genotype (Figure 23, A1-A4).

Table 7. Classification of *B. hybridum* genotypes.

Genotype	Number of 35S rDNA loci	Number of 5S rDNA loci	Group
1.12.1	4	4	1
1.24.1	4	4	2
2.2.2	4	4	1
2.6.1	4	4	1
3.4.2	4	4	3
3.16.1	4	4	2
5.6.5	4	4	1
5.8.3	4	4	1
6.5.1	4	4	2
7.27.1	4	4	1
8.5.4	4	4	1
8.8.2	4	4	1
9.1.3	4	4	3
9.7.6	4	4	2
10.11.2	4	4	3
10.19.5	4	4	2
11.24.1	4	4	2
12.5.3	4	4	1
12.23.2	2	4	4
13.3.5	4	4	1
13.19.2	4	n/d	1
14.2.2	4	4	1
15.3.1	4	4	2

16.2.5	4	4	2
18.5.2	4	4	1
18.6.1	4	4	1
19.16.5	4	n/d	1
21.7.2	4	4	2
21.11.1	4	4	2
24.1	4	4	1
24.3	4	4	1
26.12	4	4	1
26.24	4	4	1
28.28	4	4	1
28.29	4	4	2
29.3	4	4	2
29.5	4	4	1
ABR 103	4	4	1
ABR 118	4	4	3
ABR 121	4	4	3
ABR 123	4	4	1
ABR 124	4	4	1
ABR 127	4	4	1
ABR 129	4	4	1
ABR 130	4	4	3
ABR 132	4	4	3
ABR 134	4	4	1
ABR 135	4	4	1
ABR 136	4	4	1
ABR 138	4	n/d	1

*n/d – not determined

Figure 5

Figure 5

FISH with 25S rDNA and 5S rDNA probes on the mitotic metaphase chromosomes of *B. hybridum* genotypes 1.12.1, 2.2.2 and 4.5.2.

A1-A4	genotype 1.12.1
B1–B4	genotype 2.2.2
C1–C4	genotype 4.5.2

A1, B1, C1	Mitotic metaphase chromosomes (blue fluorescence, DAPI)
A2, B2, C2	FISH signals corresponding to the 25S rDNA probe (red fluorescence, TAMRA)
A3, B3, C3	FISH signals corresponding to the 5S rDNA probe (green fluorescence, FITC)

A4	Superimposed channels A1 - A3
B4	Superimposed channels B1 - B3
C4	Superimposed channels C1 - C3

Bd', Bd'' – *B. distachyon*-inherited chromosomes that bear 35S rDNA loci.
Bs', Bs'' – *B. stacei*-inherited chromosomes that bear 35S rDNA loci.

Scale bars: 5 µm

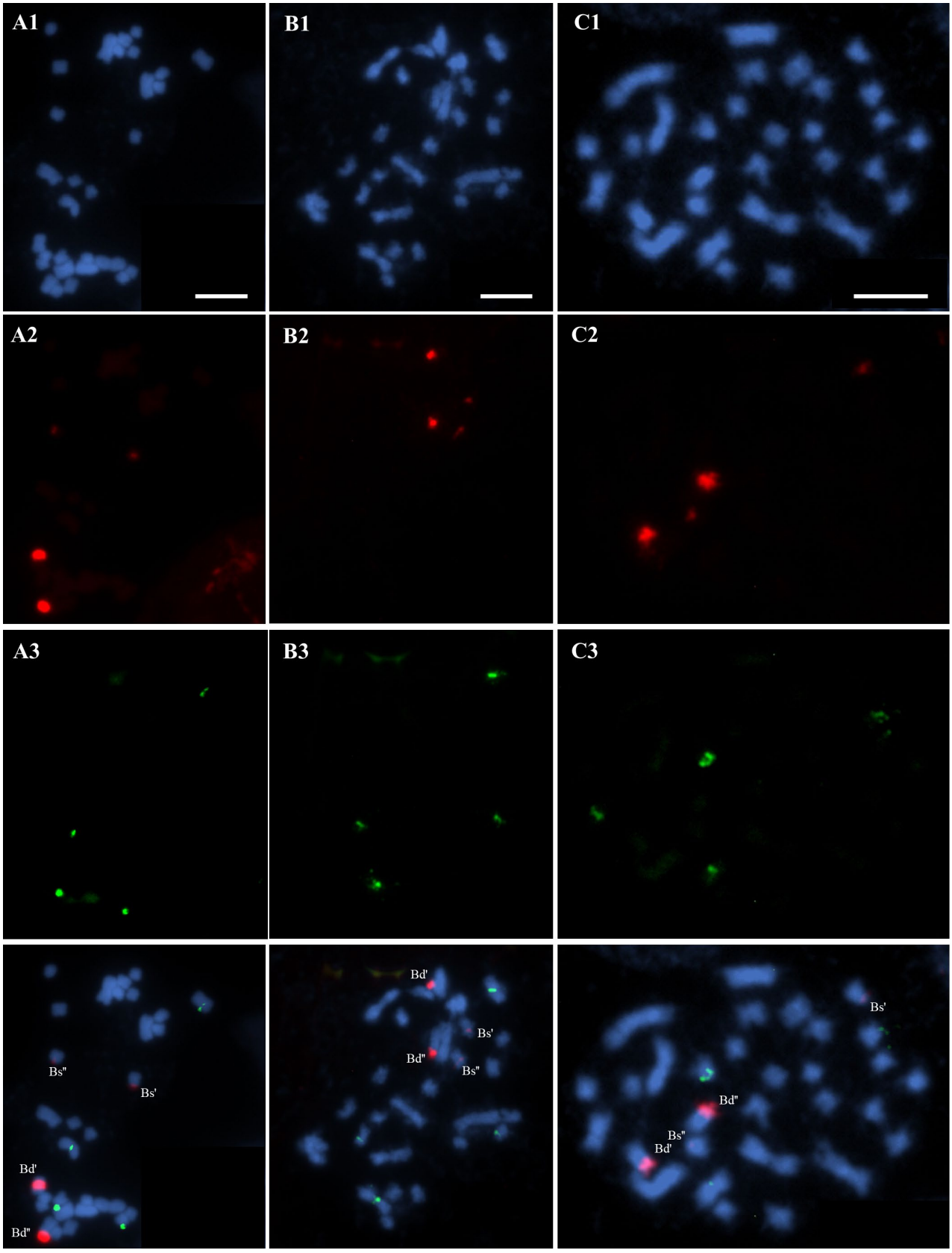
A1
B1
C1
A2
B2
C2
A3
B3
C3
Bs"
Bs'
Bd'
Bd"
Bd'
Bs'
Bd"
Bs"
Bs'
Bd"
Bs"
Bd'

Figure 6

Figure 6

FISH with 25S rDNA and 5S rDNA probes on the mitotic metaphase chromosomes of *B. hybridum* genotypes 5.6.5, 5.8.3 and 8.8.2.

A1-A4	genotype 5.6.5
B1–B4	genotype 5.8.3
C1–C4	genotype 8.8.2

A1, B1, C1	Mitotic metaphase chromosomes (blue fluorescence, DAPI)
A2, B2, C2	FISH signals corresponding to the 25S rDNA probe (red fluorescence, TAMRA)
A3, B3, C3	FISH signals corresponding to the 5S rDNA probe (green fluorescence, FITC)

A4	Superimposed channels A1 - A3
B4	Superimposed channels B1 - B3
C4	Superimposed channels C1 - C3

Bd', Bd'' – *B. distachyon*-inherited chromosomes that bear 35S rDNA loci.
Bs', Bs'' – *B. stacei*-inherited chromosomes that bear 35S rDNA loci.

Scale bars: 5 µm

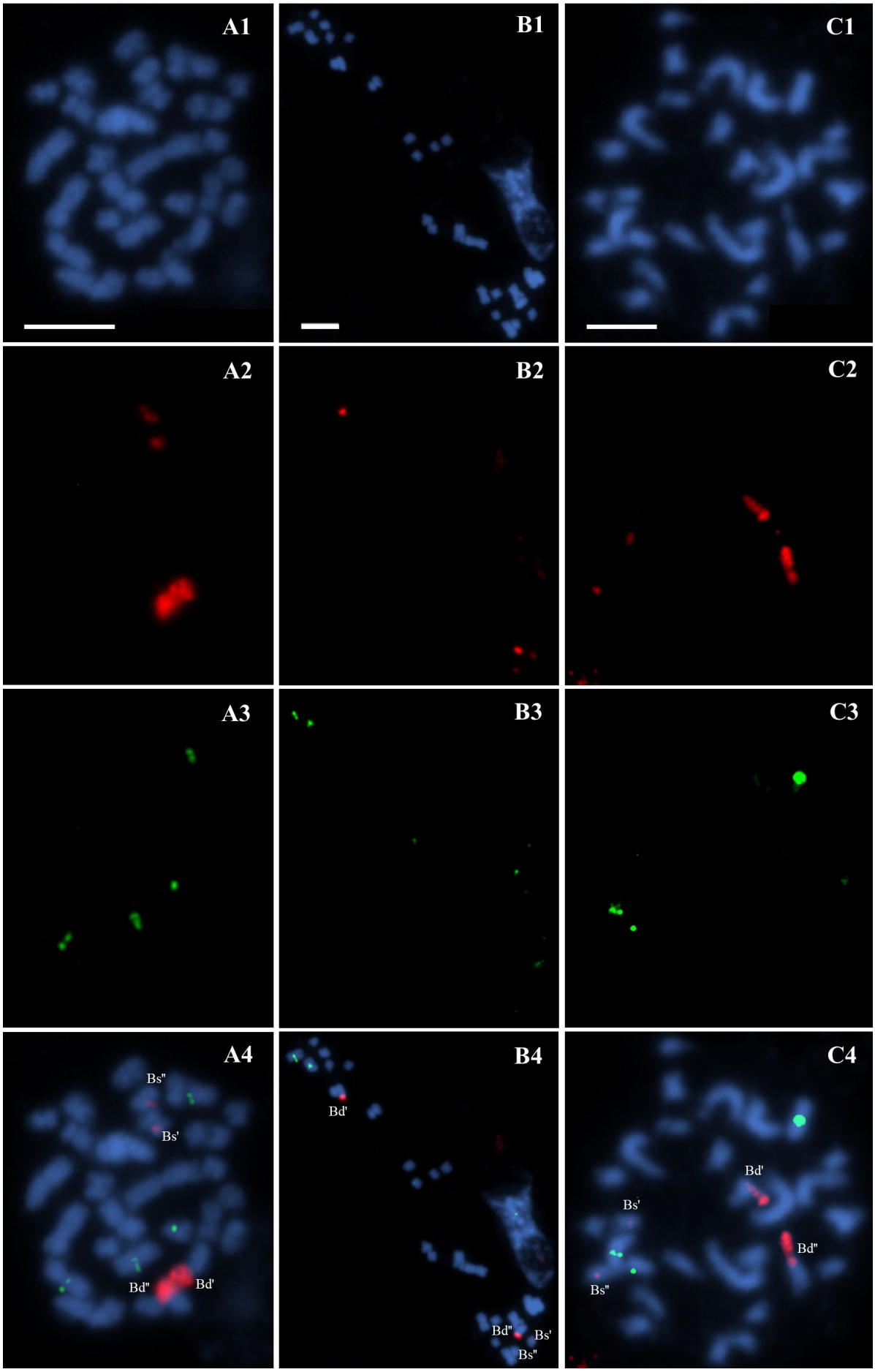

Figure 7

Figure 7

FISH with 25S rDNA and 5S rDNA probes on the mitotic metaphase chromosomes of *B. hybridum* genotypes 12.5.3, 13.3.5 and 14.2.2.

A1-A4	genotype 12.5.3
B1–B4	genotype 13.3.5
C1–C4	genotype 14.2.2

A1, B1, C1	Mitotic metaphase chromosomes (blue fluorescence, DAPI)
A2, B2, C2	FISH signals corresponding to the 25S rDNA probe (red fluorescence, TAMRA)
A3, B3, C3	FISH signals corresponding to the 5S rDNA probe (green fluorescence, FITC)

A4	Superimposed channels A1 - A3
B4	Superimposed channels B1 - B3
C4	Superimposed channels C1 - C3

Bd', Bd'' – *B. distachyon*-inherited chromosomes that bear 35S rDNA loci.

Bs', Bs'' – *B. stacei*-inherited chromosomes that bear 35S rDNA loci.

Scale bars: 5 µm

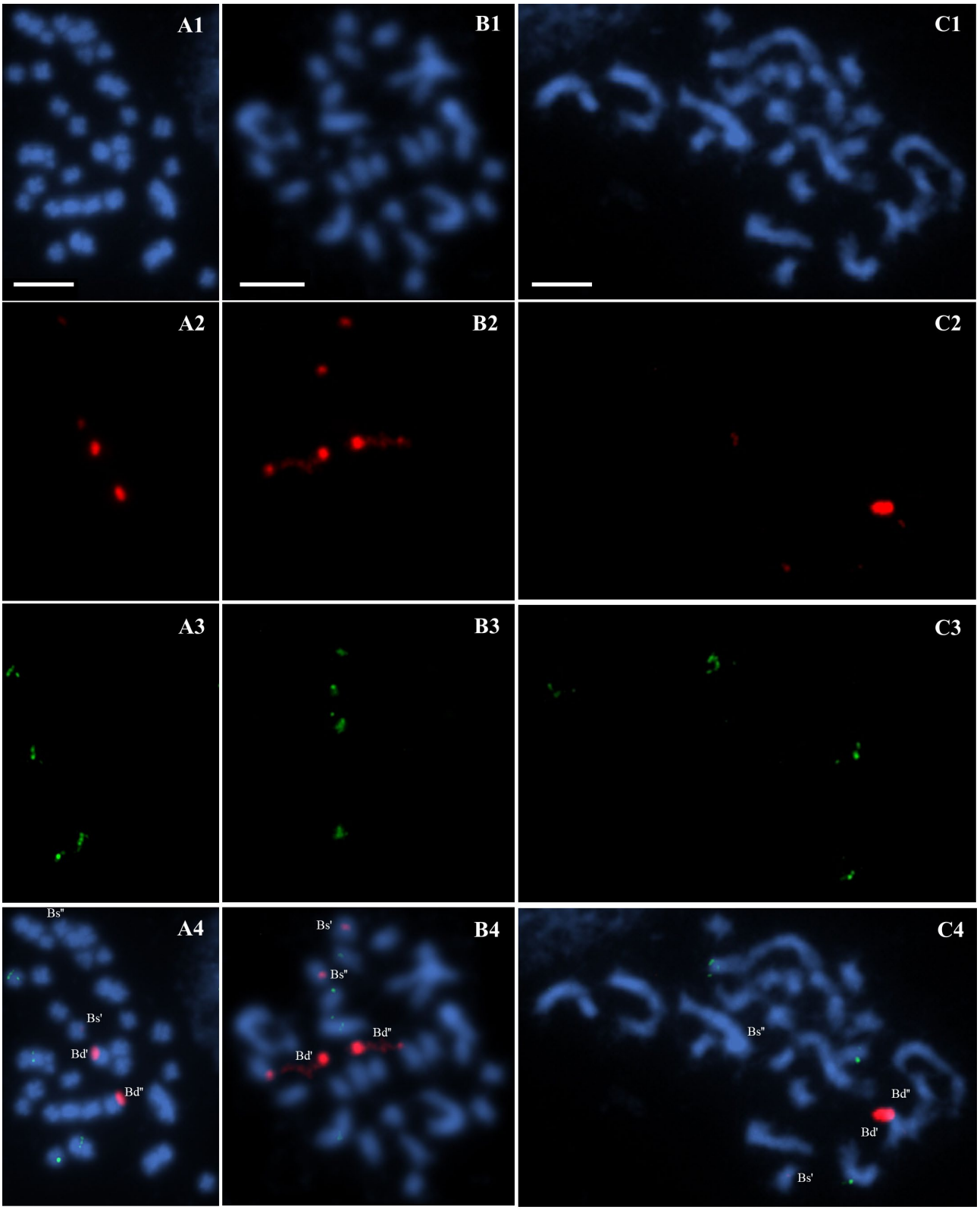
A1
B1
C1
A2
B2
C2
A3
B3
C3
A4
Bs"
Bs'
Bd'
Bd"
B4
Bs'
Bs"
Bd"
Bd'
C4
Bs"
Bd"
Bd'
Bs'

Figure 8

Figure 8

FISH with 25S rDNA and 5S rDNA probes on the mitotic metaphase chromosomes of *B. hybridum* genotypes 18.5.2 and 18.6.1.

A1-A4	genotype 18.5.2
B1–B4	genotype 18.6.1

A1, B1	Mitotic metaphase chromosomes (blue fluorescence, DAPI)
A2, B2	FISH signals corresponding to the 25S rDNA probe (red fluorescence, TAMRA)
A3, B3	FISH signals corresponding to the 5S rDNA probe (green fluorescence, FITC)
A4	Superimposed channels A1 - A3
B4	Superimposed channels B1 - B3

Bd', Bd'' – *B. distachyon*-inherited chromosomes that bear 35S rDNA loci.

Bs', Bs'' – *B. stacei*-inherited chromosomes that bear 35S rDNA loci.

Scale bars: 5 µm

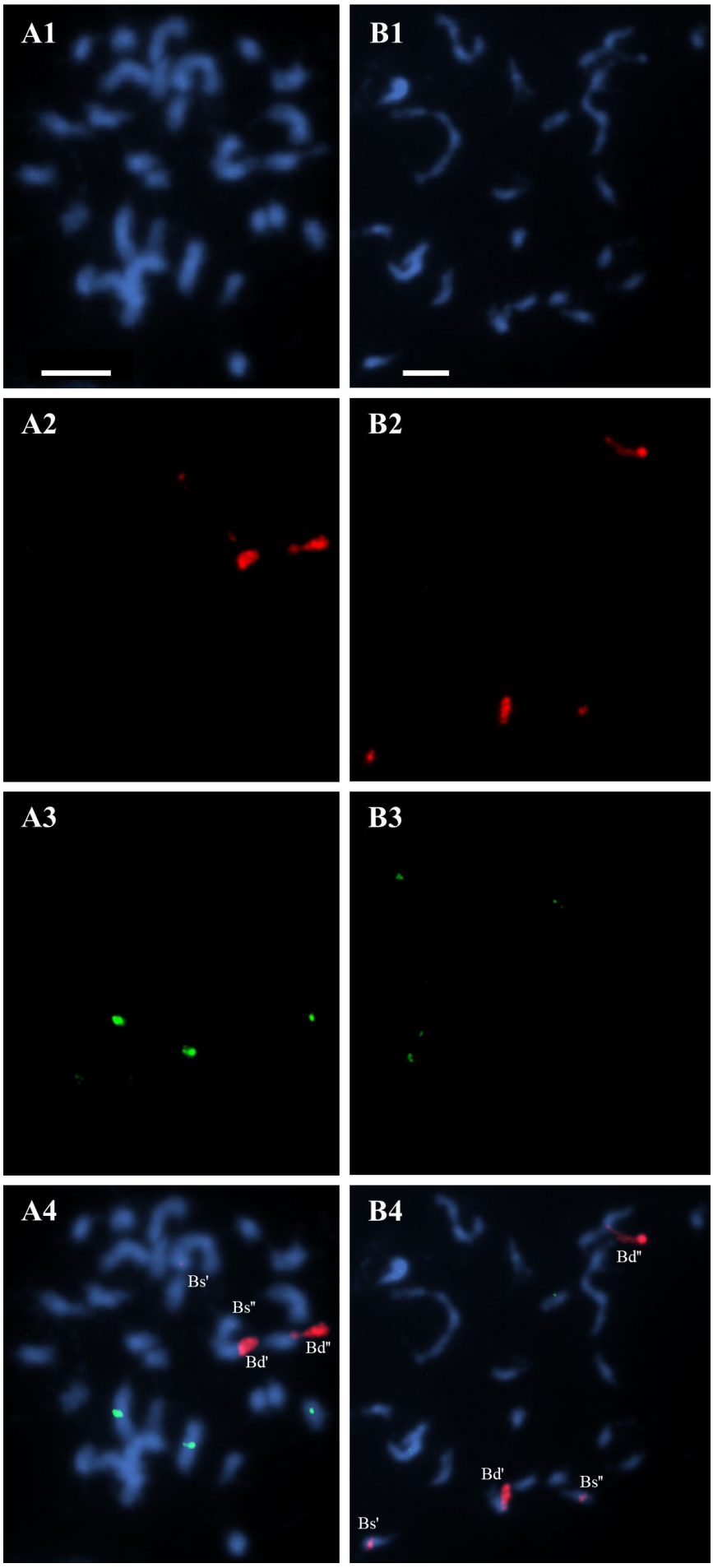

Figure 9

Figure 9

FISH with 25S rDNA and 5S rDNA probes on the mitotic metaphase chromosomes of *B. hybridum* genotypes 24.1, 24.3 and 26.24.

A1-A4	genotype 24.1
B1–B4	genotype 24.3
C1–C4	genotype 26.24

A1, B1, C1	Mitotic metaphase chromosomes (blue fluorescence, DAPI)
A2, B2, C2	FISH signals corresponding to the 25S rDNA probe (red fluorescence, TAMRA)
A3, B3, C3	FISH signals corresponding to the 5S rDNA probe (green fluorescence, FITC)

A4	Superimposed channels A1 - A3
B4	Superimposed channels B1 - B3
C4	Superimposed channels C1 - C3

Bd', Bd'' – *B. distachyon*-inherited chromosomes that bear 35S rDNA loci.

Bs', Bs'' – *B. stacei*-inherited chromosomes that bear 35S rDNA loci.

Scale bars: 5 µm

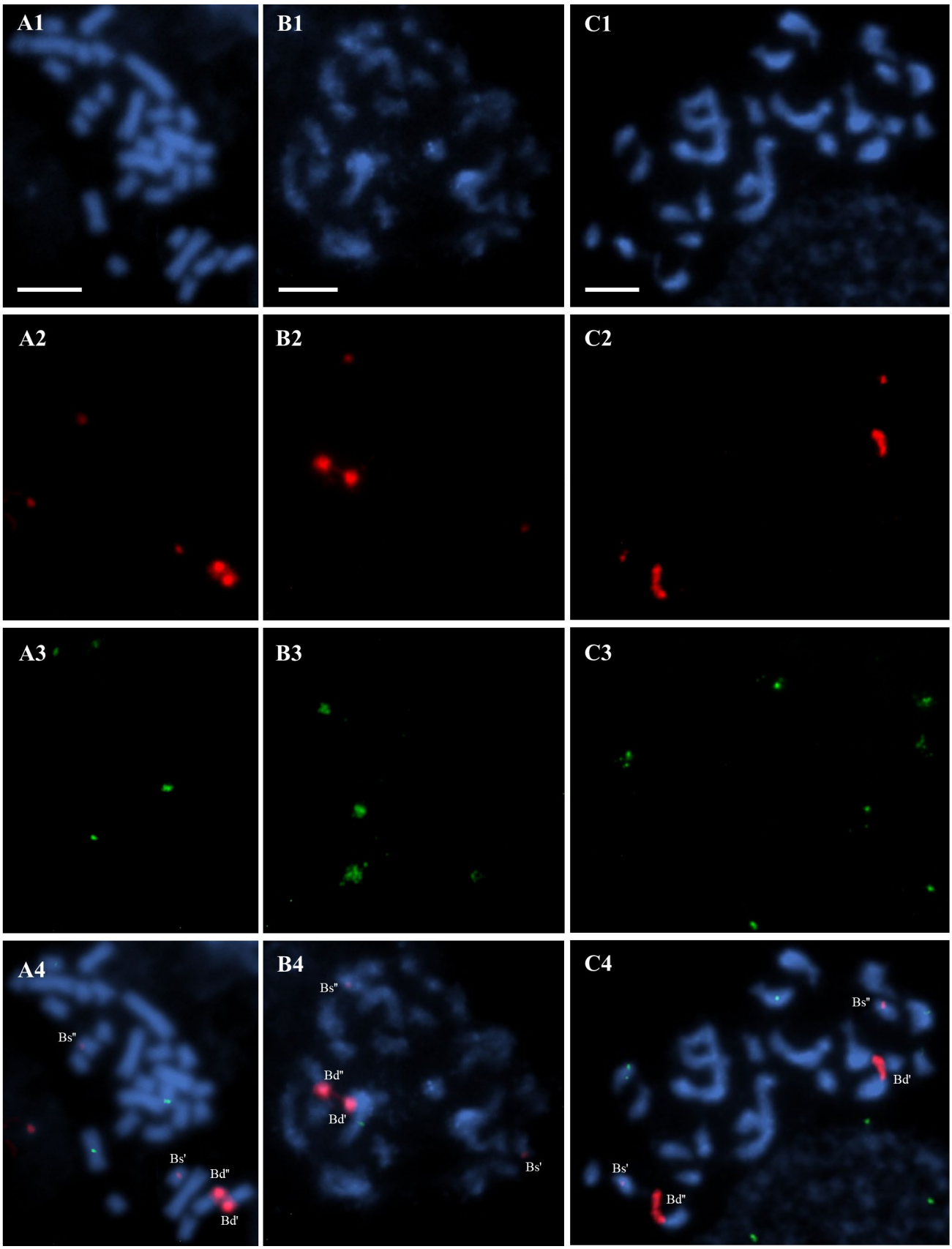

Figure 10

Figure 10

FISH with 25S rDNA and 5S rDNA probes on the mitotic metaphase chromosomes of *B. hybridum* genotypes 26.12, 28.28 and 29.5.

A1-A4	genotype 26.12
B1–B4	genotype 28.28
C1–C4	genotype 29.5

A1, B1, C1	Mitotic metaphase chromosomes (blue fluorescence, DAPI)
A2, B2, C2	FISH signals corresponding to the 25S rDNA probe (red fluorescence, TAMRA)
A3, B3, C3	FISH signals corresponding to the 5S rDNA probe (green fluorescence, FITC)

A4	Superimposed channels A1 - A3
B4	Superimposed channels B1 - B3
C4	Superimposed channels C1 - C3

Bd', Bd'' – *B. distachyon*-inherited chromosomes that bear 35S rDNA loci.

Bs', Bs'' – *B. stacei*-inherited chromosomes that bear 35S rDNA loci.

Red dashed line – distended secondary constrictions in the chromosomes from the D-subgenome.

Scale bars: 5 μm

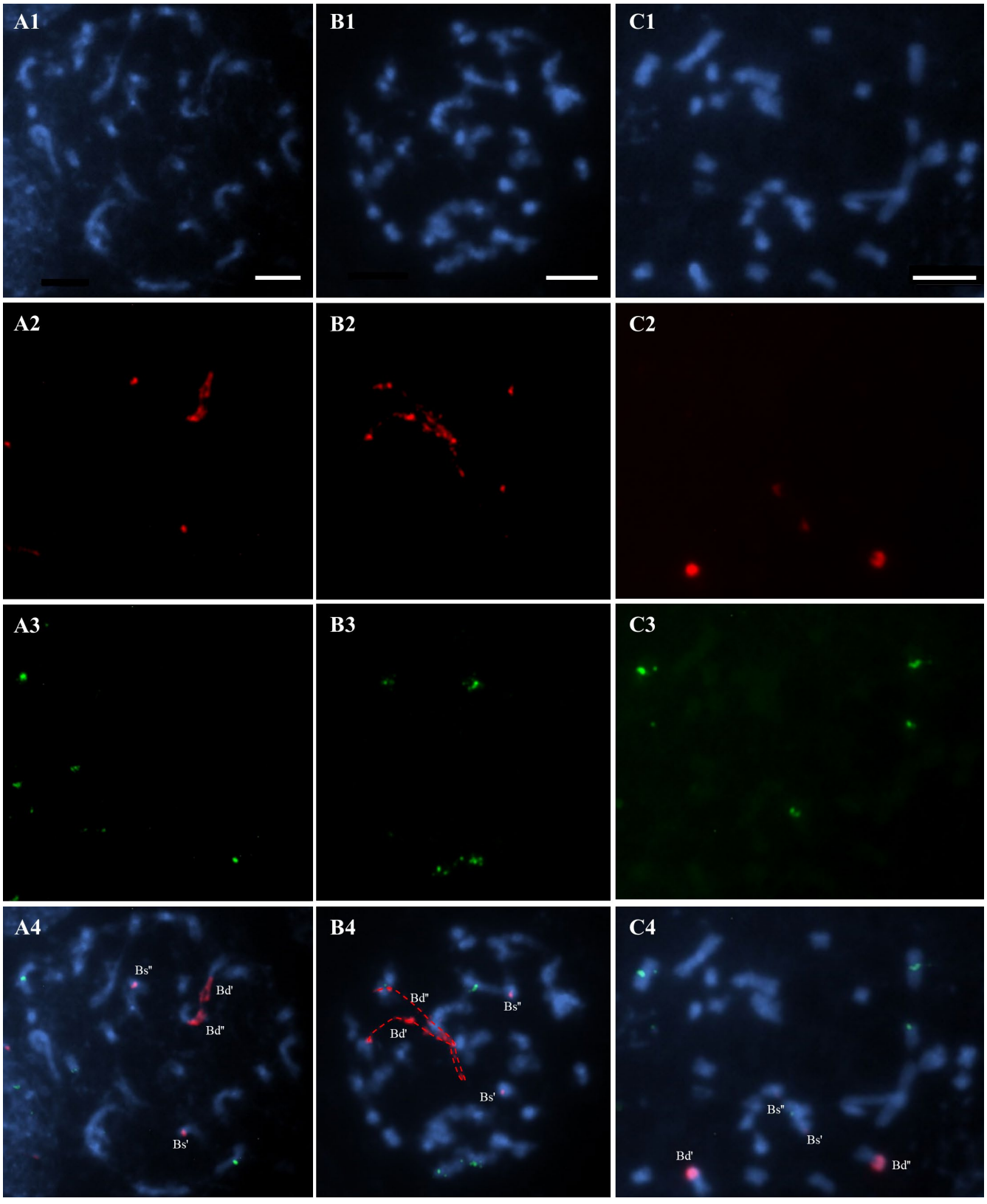

Figure 11

Figure 11

FISH with 25S rDNA and 5S rDNA probes on the mitotic metaphase chromosomes of *B. hybridum* genotypes ABR103, ABR124 and ABR129.

A1-A4	genotype ABR103
B1–B4	genotype ABR124
C1–C4	genotype ABR129
A1, B1, C1	Mitotic metaphase chromosomes (blue fluorescence, DAPI)
A2, B2, C2	FISH signals corresponding to the 25S rDNA probe (red fluorescence, TAMRA)
A3, B3, C3	FISH signals corresponding to the 5S rDNA probe (green fluorescence, FITC)
A4	Superimposed channels A1 - A3
B4	Superimposed channels B1 - B3
C4	Superimposed channels C1 - C3

Bd', Bd'' – *B. distachyon*-inherited chromosomes that bear 35S rDNA loci.

Bs', Bs'' – *B. stacei*-inherited chromosomes that bear 35S rDNA loci.

Scale bars: 5 µm

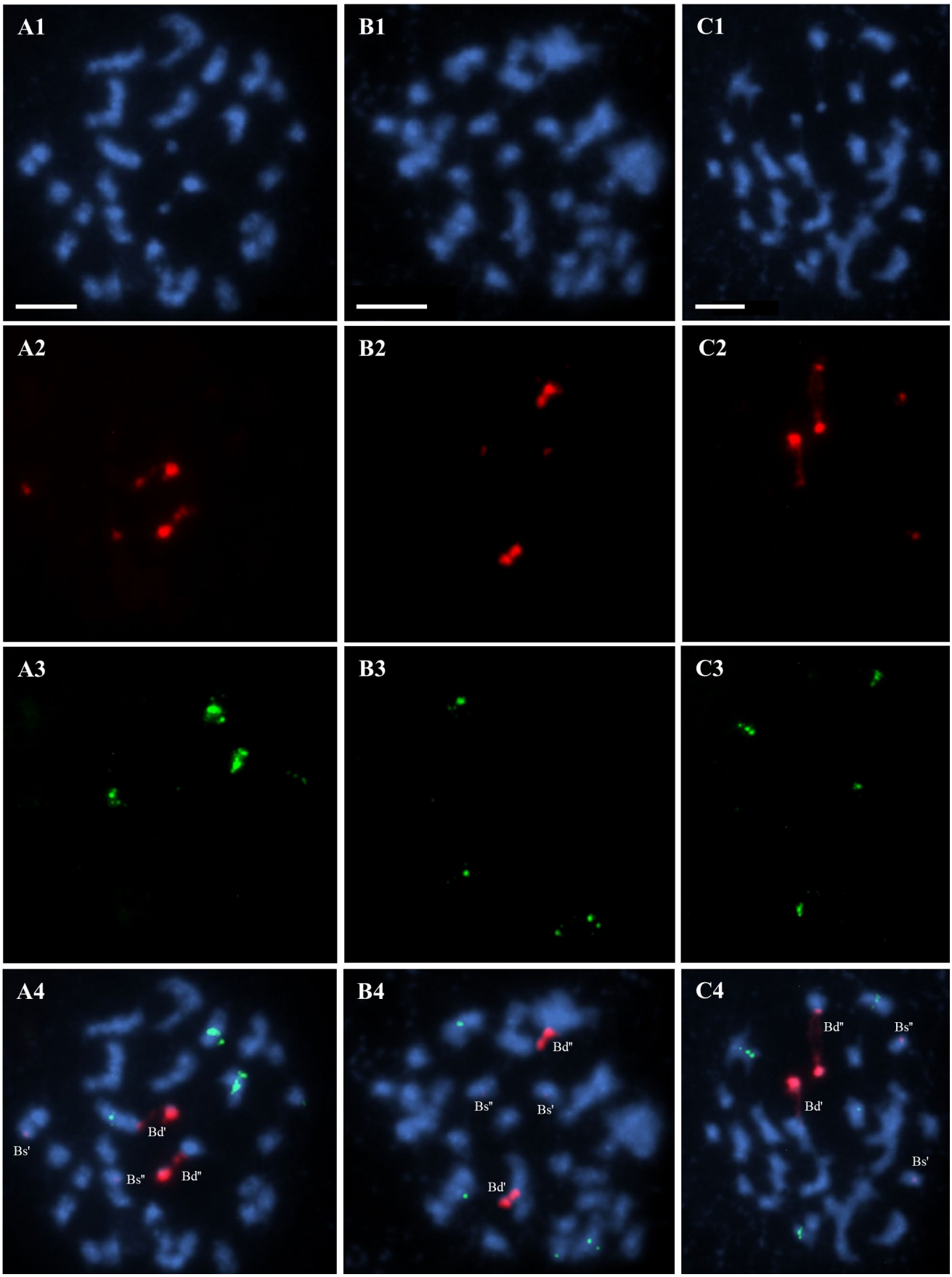

Figure 12

Figure 12

FISH with 25S rDNA and 5S rDNA as probes on the mitotic metaphase chromosomes of *B. hybridum* genotypes ABR134, ABR135 and ABR136.

A1-A4	genotype ABR134
B1–B4	genotype ABR135
C1–C4	genotype ABR136

A1, B1, C1	Mitotic metaphase chromosomes (blue fluorescence, DAPI)
A2, B2, C2	FISH signals corresponding to the 25S rDNA probe (red fluorescence, TAMRA)
A3, B3, C3	FISH signals corresponding to the 5S rDNA probe (green fluorescence, FITC)

A4	Superimposed channels A1 - A3
B4	Superimposed channels B1 - B3
C4	Superimposed channels C1 - C3

Bd', Bd'' – *B. distachyon*-inherited chromosomes that bear 35S rDNA loci.
Bs', Bs'' – *B. stacei*-inherited chromosomes that bear 35S rDNA loci.

Scale bars: 5 µm

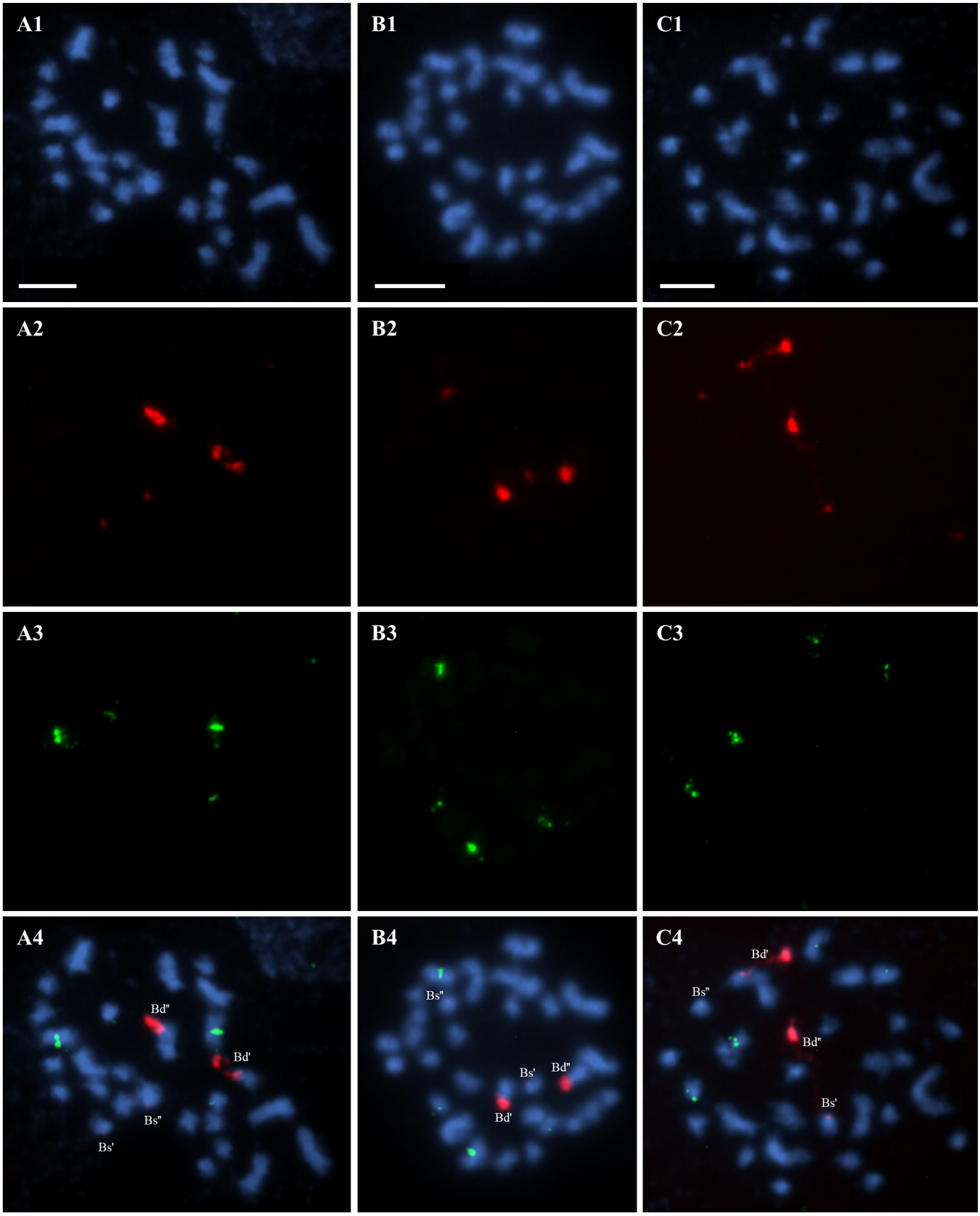

Figure 13

Figure 13

FISH with 25S rDNA and 5S rDNA probes on the mitotic metaphase chromosomes of *B. hybridum* genotypes 2.6.1, ABR138 and ABR127.

A1-A3	genotype 2.6.1
B1–B4	genotype ABR138
C1–C4	genotype ABR127
A1, B1, C1	Mitotic metaphase chromosomes (blue fluorescence, DAPI)
A2, B2, C2	FISH signals corresponding to the 25S rDNA probe (red fluorescence, TAMRA)
B3, C3	FISH signals corresponding to the 5S rDNA probe (green fluorescence, FITC)
A3	Superimposed channels A1 - A2
B4	Superimposed channels B1 - B3
C4	Superimposed channels C1 - C3

Bd', Bd'' – *B. distachyon*-inherited chromosomes that bear 35S rDNA loci.

Bs', Bs'' – *B. stacei*-inherited chromosomes that bear 35S rDNA loci.

Scale bars: 5 µm

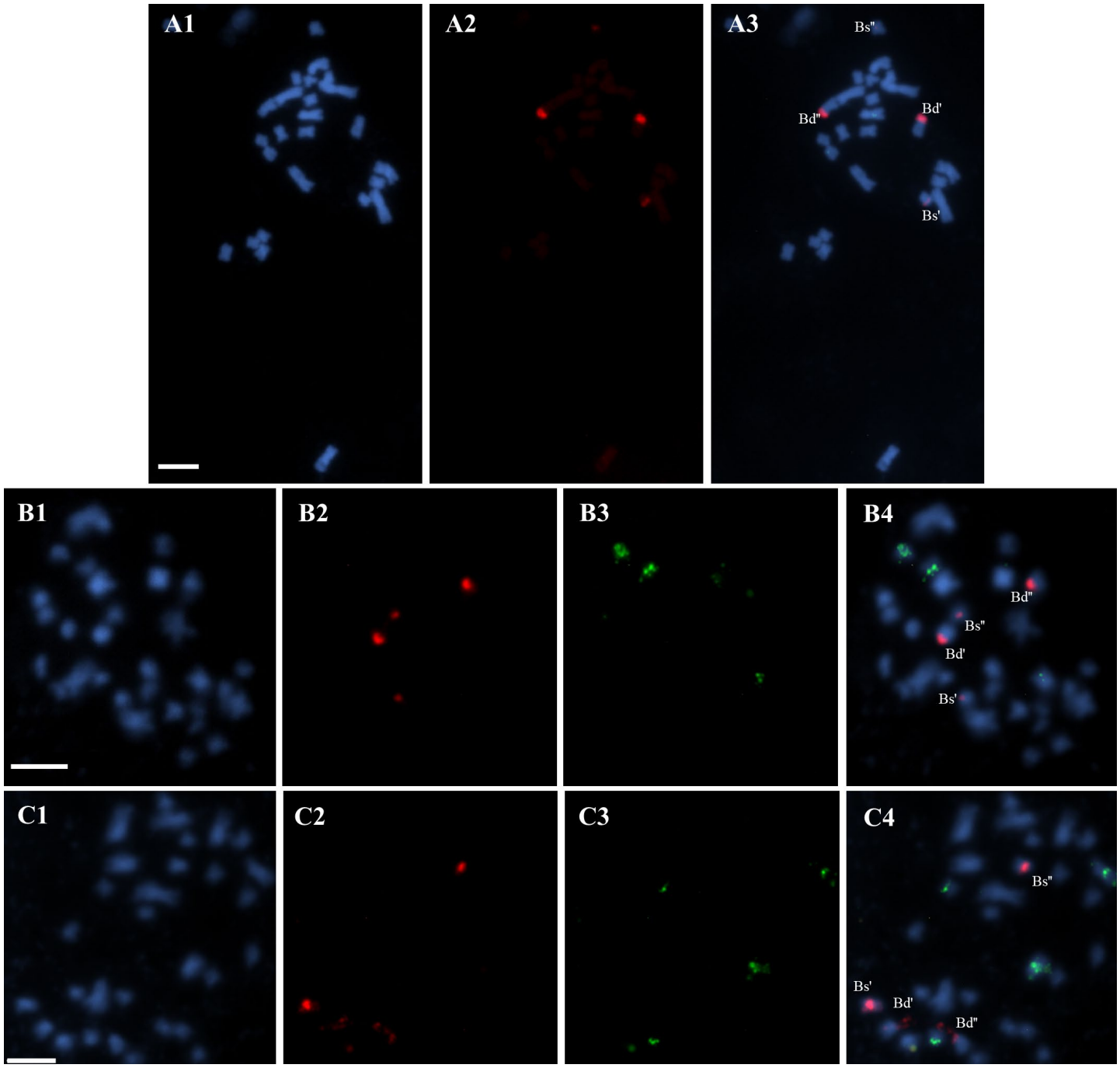
A1
A2
A3
Bs"
Bd"
Bd'
Bs'
B1
B2
B3
B4
Bd"
Bs"
Bd'
Bs'
C1
C2
C3
C4
Bs"
Bs'
Bd'
Bd"

Figure 14

Figure 14

FISH with 25S rDNA and 5S rDNA as probes on the interphase nuclei of *B. hybridum* genotypes 7.27.1, 8.5.4 and ABR123.

A1-A4	genotype 7.27.1
B1–B4	genotype 8.5.4
C1–C4	genotype ABR123
A1, B1, C1	Interphase nuclei (blue fluorescence, DAPI)
A2, B2, C2	FISH signals corresponding to the 25S rDNA probe (red fluorescence, TAMRA)
A3, B3, C3	FISH signals corresponding to the 5S rDNA probe (green fluorescence, FITC)
A4	Superimposed channels A1 - A3
B4	Superimposed channels B1 - B3
C4	Superimposed channels C1 - C3

Bd', Bd'' – the signal presumably originating from D-subgenome 35S rDNA loci.
Bs', Bs'' – the signal presumably originating from S-subgenome 35S rDNA loci.

Scale bars: 5 µm

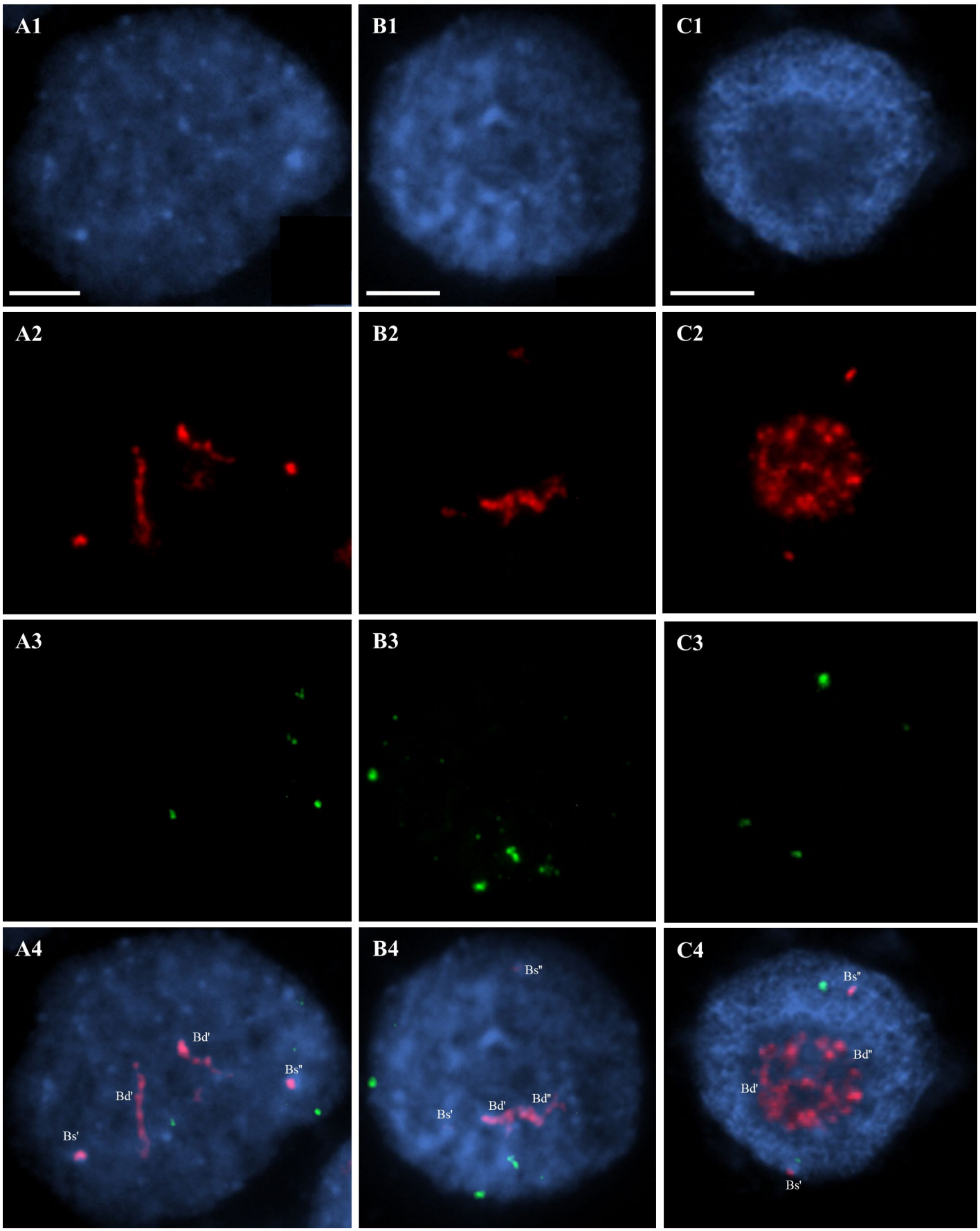
A1
B1
C1
A2
B2
C2
A3
B3
C3
A4
Bd'
Bs"
Bd'
Bs'
B4
Bs"
Bs'
Bd'
Bd"
C4
Bs"
Bd"
Bd'
Bs'

Figure 15

Figure 15

FISH with 25S rDNA probe on the mitotic metaphase chromosomes of *B. hybridum* genotypes 13.19.2 and 19.16.5.

A1-A3	genotype 13.19.2
B1-B3	genotype 19.16.5
A1, B1	Mitotic metaphase chromosomes (blue fluorescence, DAPI)
A2, B2	FISH signals corresponding to the 25S rDNA probe (red fluorescence, TAMRA)
A3	Superimposed channels A1 – A2
B3	Superimposed channels B1 – B2

Bd', Bd" – *B. distachyon*-inherited chromosomes that bear 35S rDNA loci.
Bs', Bs" – *B. stacei*-inherited chromosomes that bear 35S rDNA loci.

Scale bars: 5 μm

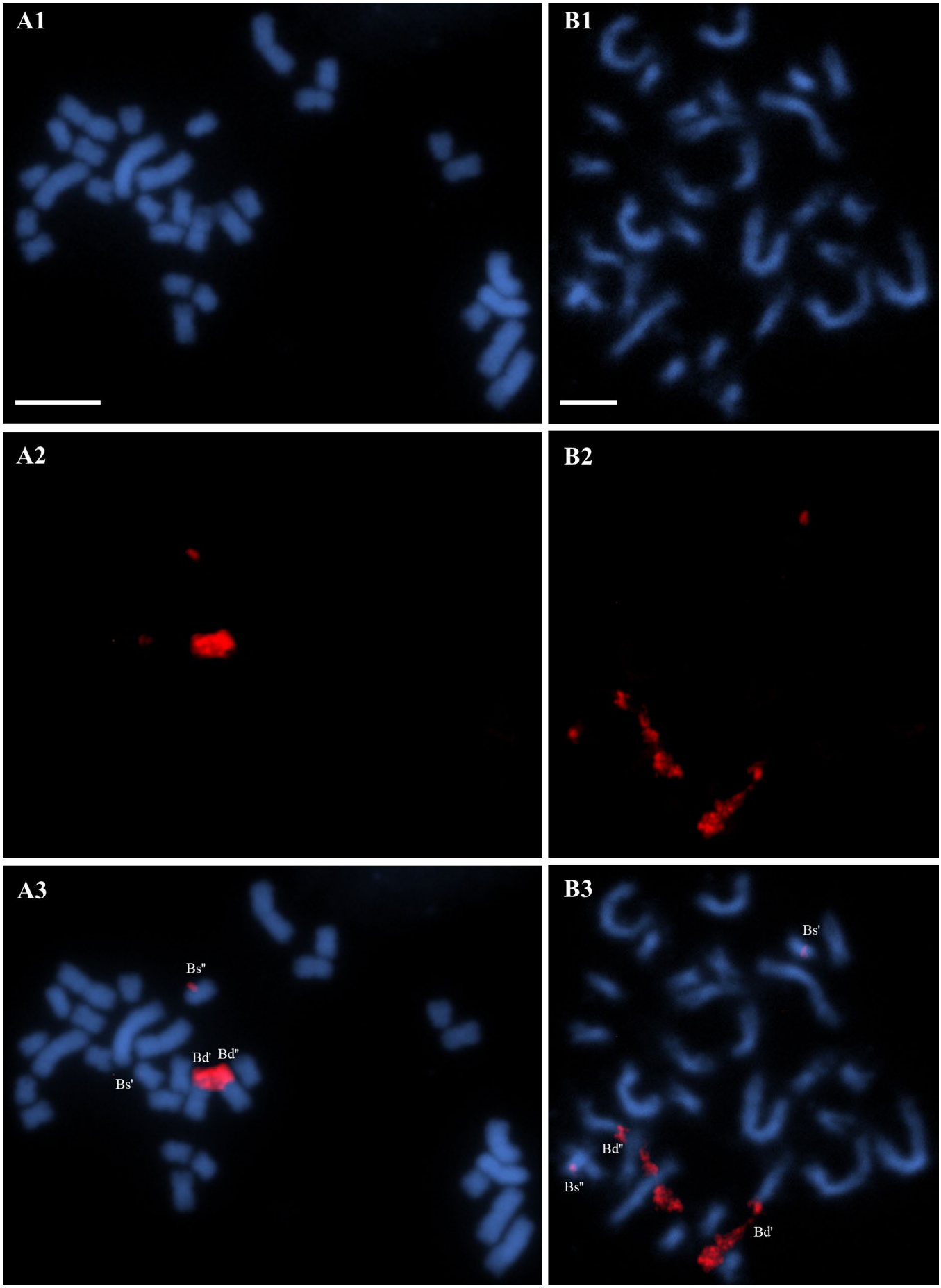
A1
B1
A2
B2
A3
Bs"
Bd'
Bd"
Bs'
B3
Bs'
Bd"
Bs"
Bd'

Figure 16

Figure 16

FISH with 25S rDNA and 5S rDNA probes on the mitotic metaphase chromosomes of *B. hybridum* genotypes 1.24.1, 6.5.1 and 10.19.5.

A1-A4	genotype 1.24.1
B1–B4	genotype 6.5.1
C1–C4	genotype 10.19.5

A1, B1, C1	Mitotic metaphase chromosomes (blue fluorescence, DAPI)
A2, B2, C2	FISH signals corresponding to the 25S rDNA probe (red fluorescence, TAMRA)
A3, B3, C3	FISH signals corresponding to the 5S rDNA probe (green fluorescence, FITC)

A4	Superimposed channels A1 - A3
B4	Superimposed channels B1 - B3
C4	Superimposed channels C1 - C3

Bd', Bd'' – *B. distachyon*-inherited chromosomes that bear 35S rDNA loci.
Bs', Bs'' – *B. stacei*-inherited chromosomes that bear 35S rDNA loci.

Scale bars: 5 µm

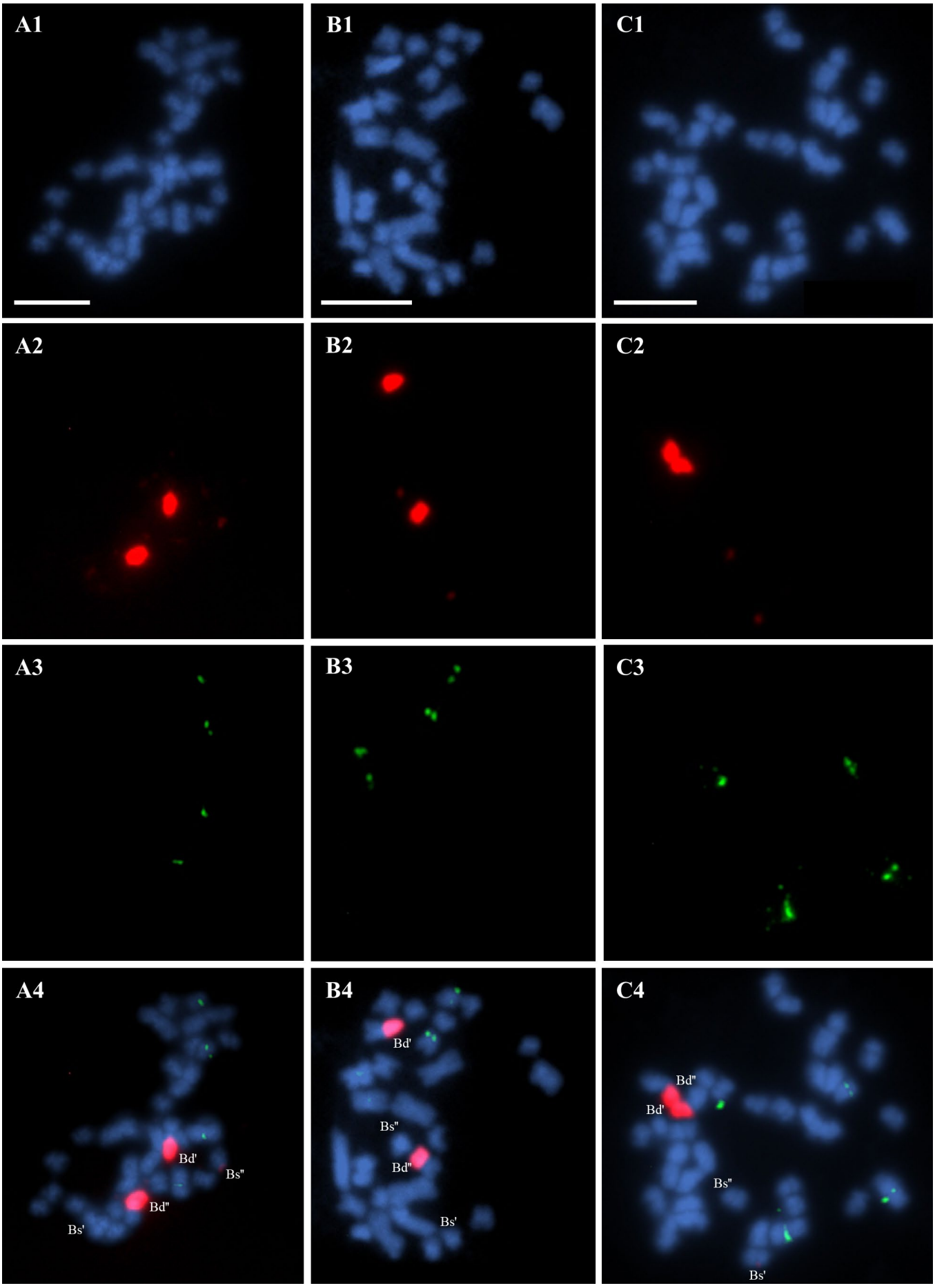
A1
B1
C1
A2
B2
C2
A3
B3
C3
A4
Bd'
Bs"
Bd"
Bs'
B4
Bd'
Bs"
Bd"
Bs'
C4
Bd"
Bd'
Bs"
Bs'

Figure 17

Figure 17

FISH with 25S rDNA and 5S rDNA probes on the mitotic metaphase chromosomes of *B. hybridum* genotypes 9.7.6, 3.16.1 and 21.11.1.

A1-A4	genotype 9.7.6
B1–B4	genotype 3.16.1
C1–C4	genotype 21.11.1

A1, B1, C1	Mitotic metaphase chromosomes (blue fluorescence, DAPI)
A2, B2, C2	FISH signals corresponding to the 25S rDNA probe (red fluorescence, TAMRA)
A3, B3, C3	FISH signals corresponding to the 5S rDNA probe (green fluorescence, FITC)

A4	Superimposed channels A1 - A3
B4	Superimposed channels B1 - B3
C4	Superimposed channels C1 - C3

Bd', Bd'' – *B. distachyon*-inherited chromosomes that bear 35S rDNA loci.
Bs', Bs'' – *B. stacei*-inherited chromosomes that bear 35S rDNA loci.

Scale bars: 5 µm

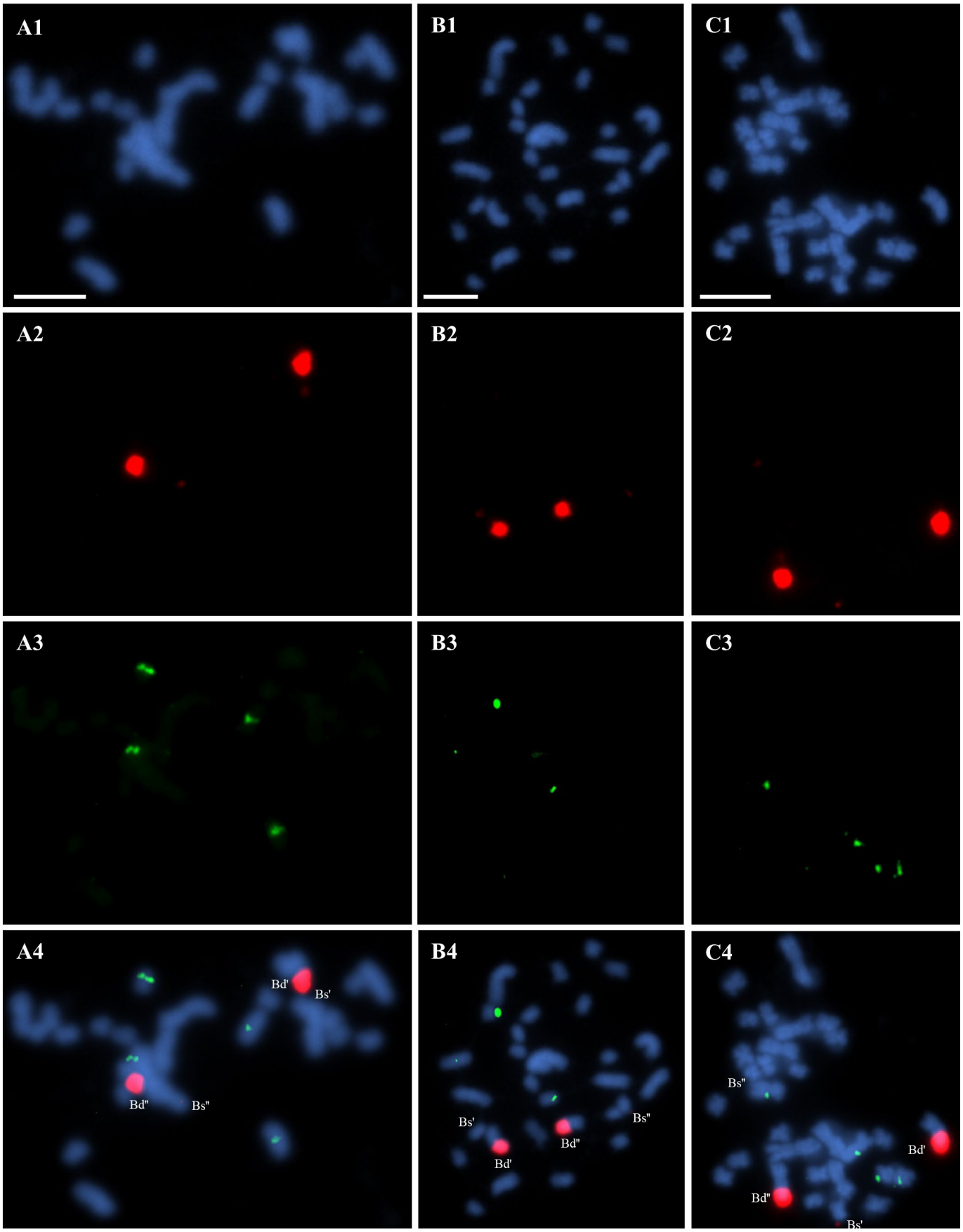

Figure 18

Figure 18

FISH with 25S rDNA and 5S rDNA probes on the mitotic metaphase chromosomes of *B. hybridum* genotypes 16.2.5, 28.29 and 29.3.

A1-A4	genotype 16.2.5
B1–B4	genotype 28.29
C1–C4	genotype 29.3
A1, B1, C1	Mitotic metaphase chromosomes (blue fluorescence, DAPI)
A2, B2, C2	FISH signals corresponding to the 25S rDNA probe (red fluorescence, TAMRA)
A3, B3, C3	FISH signals corresponding to the 5S rDNA probe (green fluorescence, FITC)
A4	Superimposed channels A1 - A3
B4	Superimposed channels B1 - B3
C4	Superimposed channels C1 - C3

Bd', Bd'' – *B. distachyon*-inherited chromosomes that bear 35S rDNA loci.

Bs', Bs'' – *B. stacei*-inherited chromosomes that bear 35S rDNA loci.

Scale bars: 5 µm

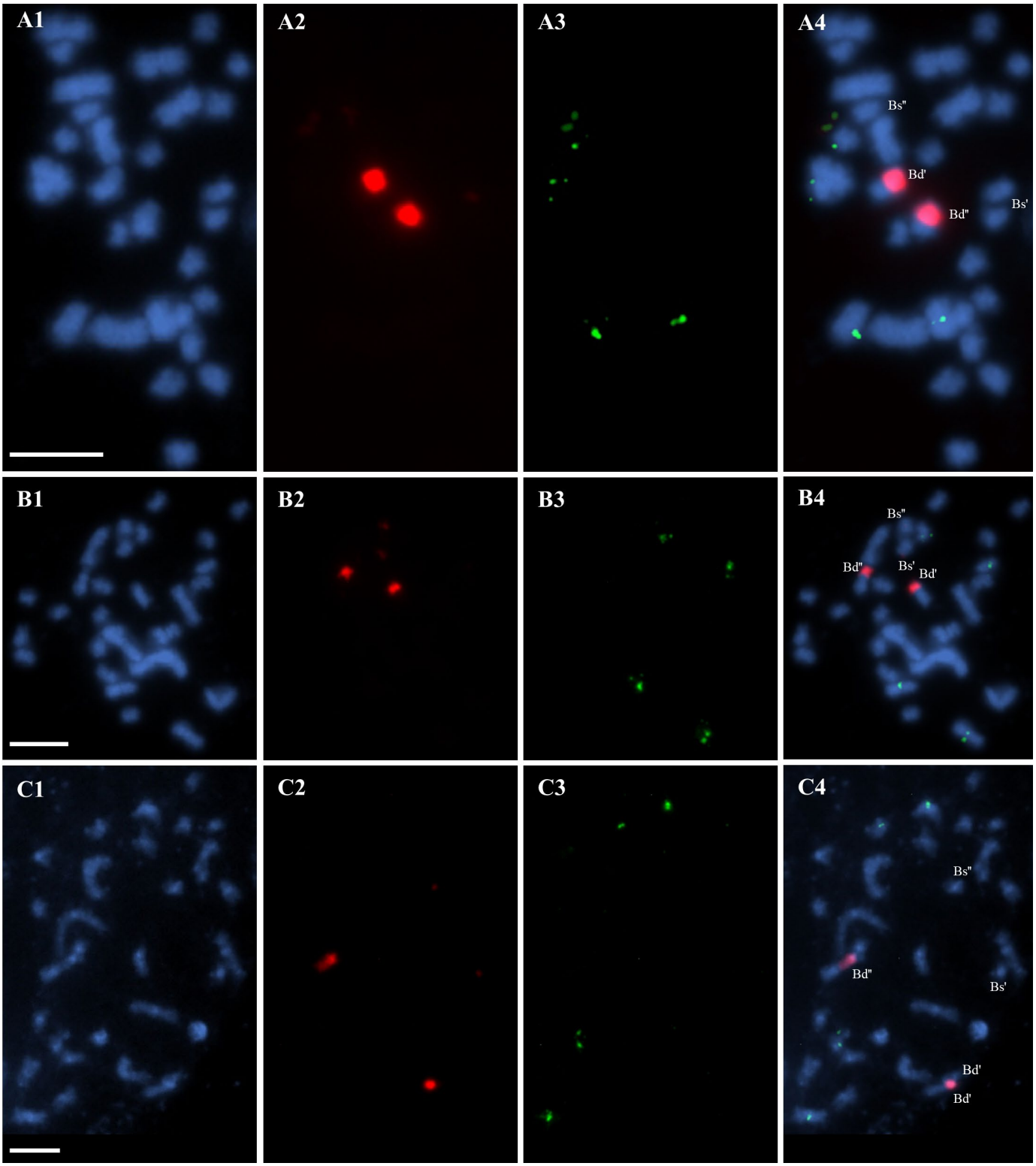

Figure 19

Figure 19

FISH with 25S rDNA and 5S rDNA probes on the mitotic metaphase chromosomes of *B. hybridum* genotypes 21.7.2, 15.3.1 and 11.24.1.

A1-A4	genotype 21.7.2
B1-B4	genotype 15.3.1
C1-C4	genotype 11.24.1

A1, B1, C1	Mitotic metaphase chromosomes (blue fluorescence, DAPI)
A2, B2, C2	FISH signals corresponding to the 25S rDNA probe (red fluorescence, TAMRA)
A3, B3, C3	FISH signals corresponding to the 5S rDNA probe (green fluorescence, FITC)

A4	Superimposed channels A1 - A3
B4	Superimposed channels B1 - B3
C4	Superimposed channels C1 - C3

Bd', Bd'' – *B. distachyon*-inherited chromosomes that bear 35S rDNA loci.

Bs', Bs'' – *B. stacei*-inherited chromosomes that bear 35S rDNA loci.

Scale bars: 5 µm

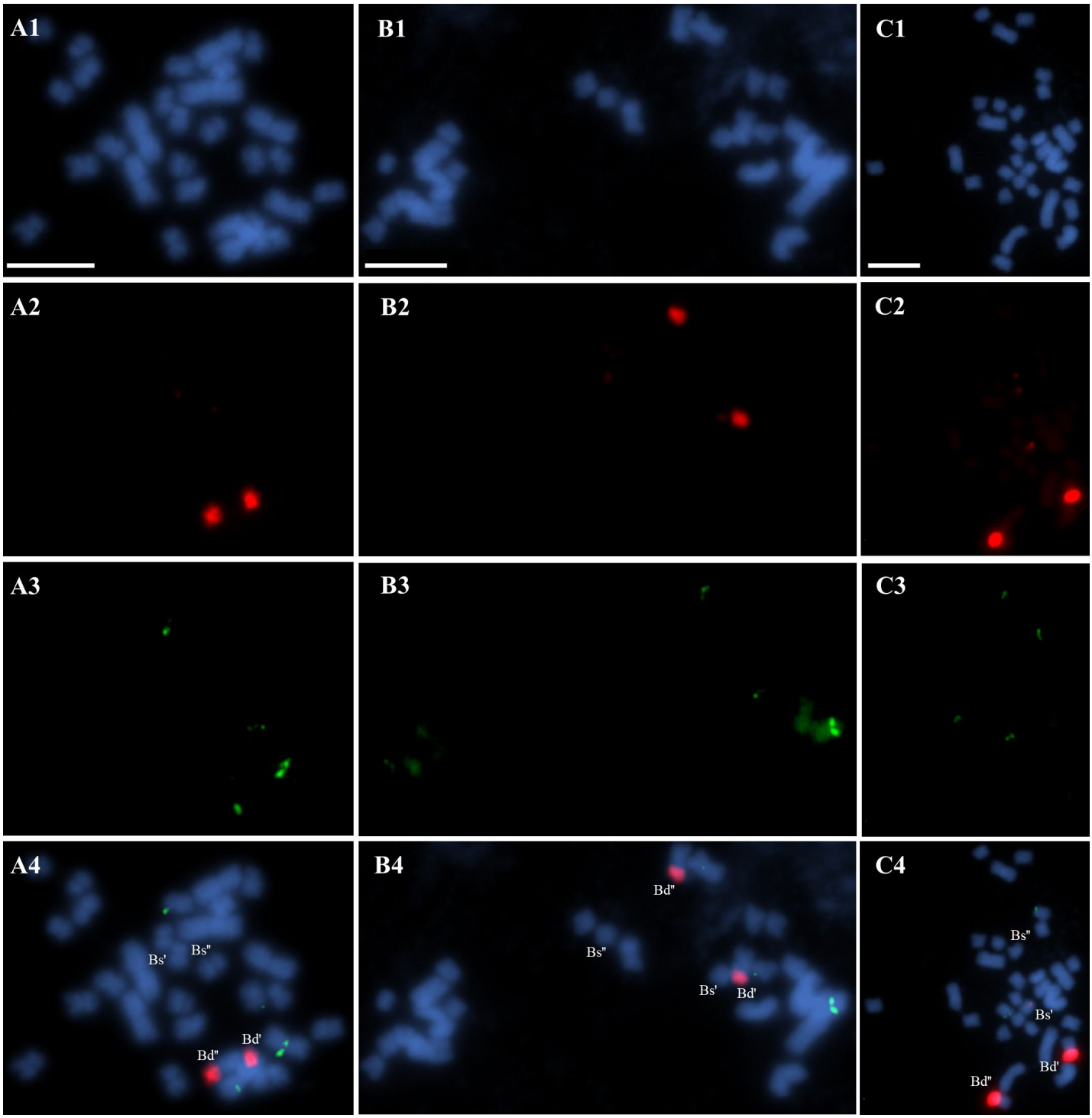

Figure 20

Figure 20

FISH with 25S rDNA and 5S rDNA probes on the mitotic metaphase chromosomes of *B. hybridum* genotypes 3.4.2, 9.1.3 and 10.11.2.

A1-A4	genotype 3.4.2
B1–B4	genotype 9.1.3
C1–C4	genotype 10.11.2

A1, B1, C1	Mitotic metaphase chromosomes (blue fluorescence, DAPI)
A2, B2, C2	FISH signals corresponding to the 25S rDNA probe (red fluorescence, TAMRA)
A3, B3, C3	FISH signals corresponding to the 5S rDNA probe (green fluorescence, FITC)

A4	Superimposed channels A1 - A3
B4	Superimposed channels B1 - B3
C4	Superimposed channels C1 - C3

Bd', Bd'' – *B. distachyon*-inherited chromosomes that bear 35S rDNA loci.
Bs', Bs'' – *B. stacei*-inherited chromosomes that bear 35S rDNA loci.

Scale bars: 5 µm

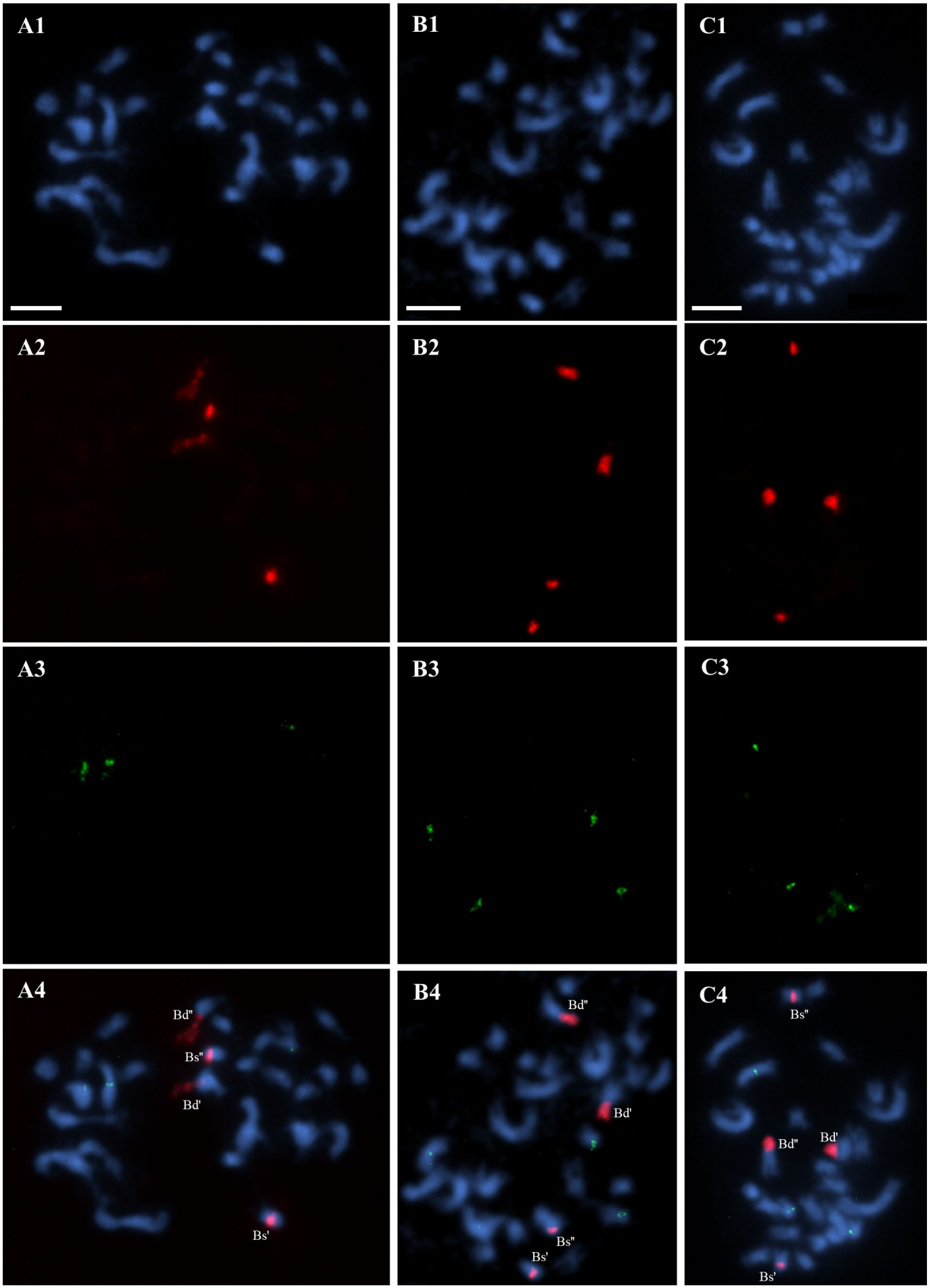

Figure 21

Figure 21

FISH with 25S rDNA and 5S rDNA probes on the mitotic metaphase chromosomes of *B. hybridum* genotypes ABR118, ABR121 and ABR130.

A1-A4	genotype ABR118
B1–B4	genotype ABR121
C1–C4	genotype ABR130
A1, B1, C1	Mitotic metaphase chromosomes (blue fluorescence, DAPI)
A2, B2, C2	FISH signals corresponding to the 25S rDNA probe (red fluorescence, TAMRA)
A3, B3, C3	FISH signals corresponding to the 5S rDNA probe (green fluorescence, FITC)
A4	Superimposed channels A1 - A3
B4	Superimposed channels B1 - B3
C4	Superimposed channels C1 - C3

Bd', Bd'' – *B. distachyon*-inherited chromosomes that bear 35S rDNA loci.

Bs', Bs'' – *B. stacei*-inherited chromosomes that bear 35S rDNA loci.

Scale bars: 5 µm

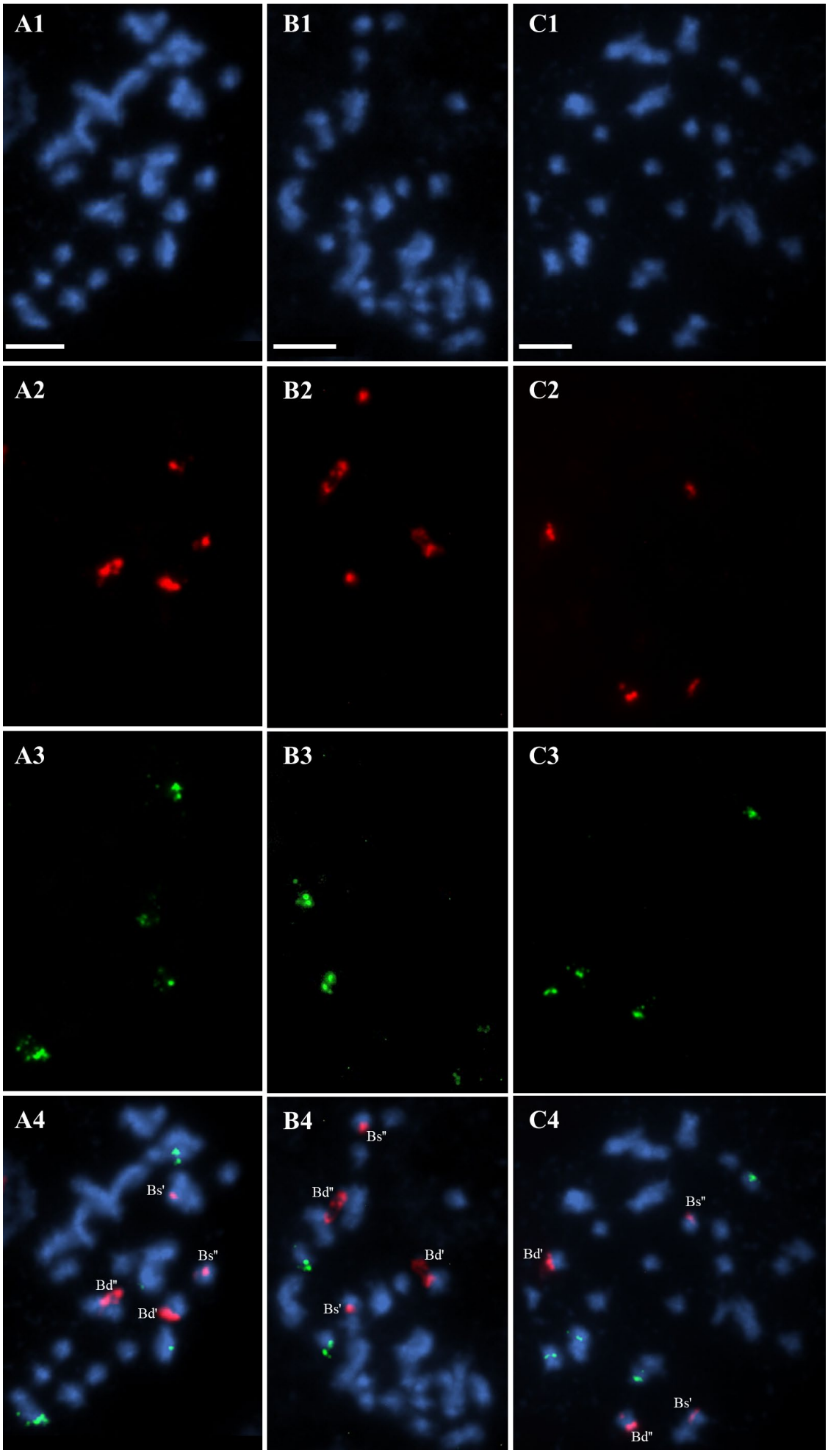

Figure 22

Figure 22

FISH with 25S rDNA and 5S rDNA probes on the mitotic metaphase chromosomes of *B. hybridum* genotype ABR132.

A1-A4	genotype ABR132
A1	Mitotic metaphase chromosomes (blue fluorescence, DAPI)
A2	FISH signals corresponding to the 25S rDNA probe (red fluorescence, TAMRA)
A3	FISH signals corresponding to the 5S rDNA probe (green fluorescence, FITC)
A4	Superimposed channels A1 - A3

Bd', Bd" – *B. distachyon*-inherited chromosomes that bear 35S rDNA loci.
Bs', Bs" – *B. stacei*-inherited chromosomes that bear 35S rDNA loci.

Scale bars: 5 μm

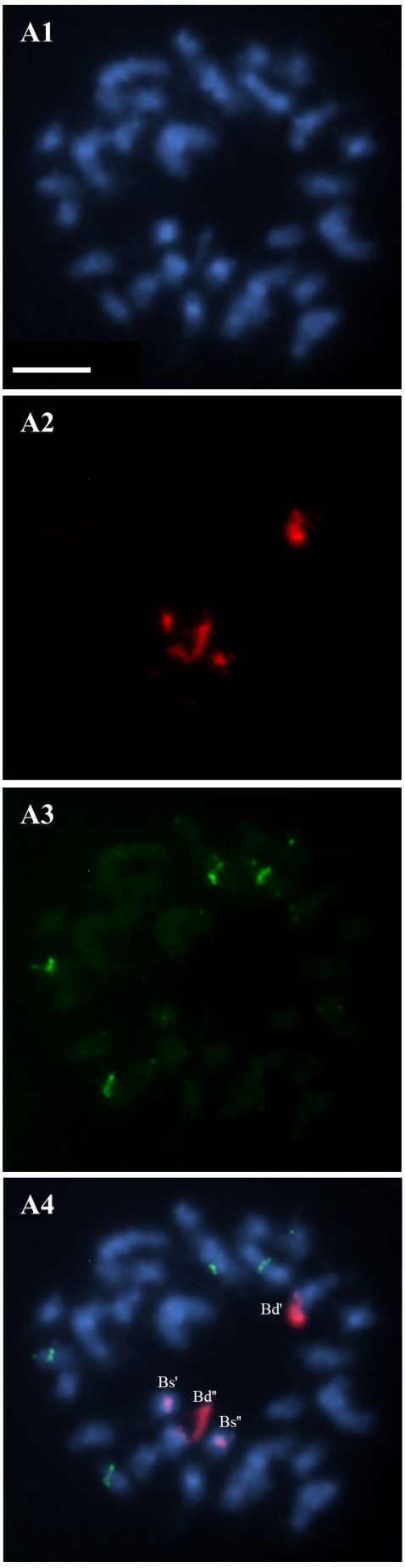

Figure 23

Figure 23

FISH with 25S rDNA and 5S rDNA probes on the mitotic metaphase chromosomes of *B. hybridum* genotype 12.23.2.

A1-A4	genotype 12.23.2
A1	Mitotic metaphase chromosomes (blue fluorescence, DAPI)
A2	FISH signals corresponding to the 25S rDNA probe (red fluorescence, TAMRA)
A3	FISH signals corresponding to the 5S rDNA probe (green fluorescence, FITC)
A4	Superimposed channels A1 - A3

Bd', Bd" – *B. distachyon*-inherited chromosomes that bear 35S rDNA loci.
Bs', Bs" – *B. stacei*-inherited chromosomes that bear 35S rDNA loci.

Scale bars: 5 μm

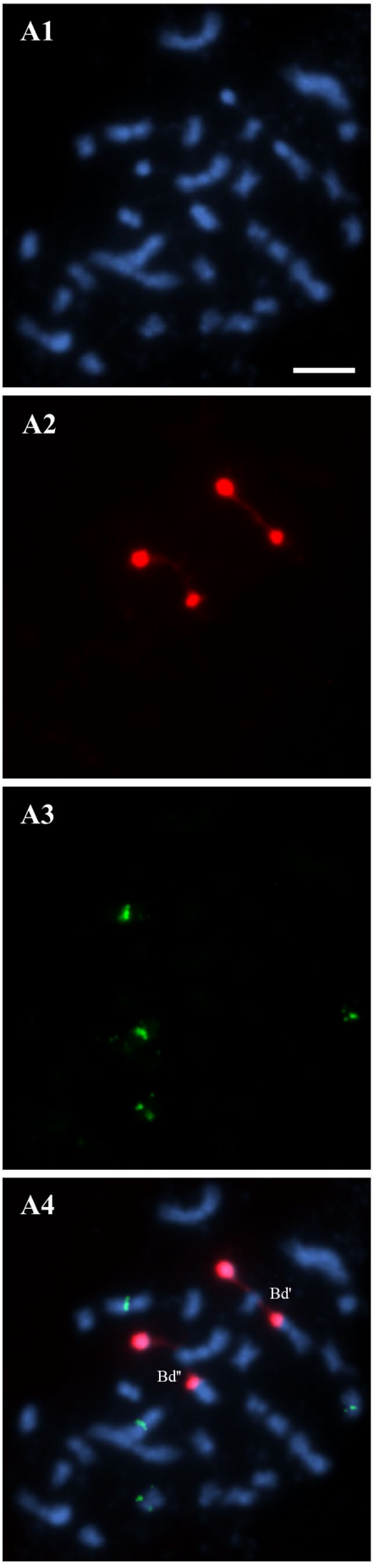
A1
A2
A3
A4
Bd'
Bd"

Figure 24

Figure 24

FISH with 25S rDNA and 5S rDNA probes on the mitotic metaphase chromosomes of *B. hybridum* genotype 2.2.2.

A1-A4	genotype 2.2.2
A1	Mitotic metaphase chromosomes (blue fluorescence, DAPI)
A2	FISH signals corresponding to the 25S rDNA probe (red fluorescence, TAMRA)
A3	FISH signals corresponding to the 5S rDNA probe (green fluorescence, FITC)
A4	Superimposed channels A1 - A3

Bd', Bd" – *B. distachyon*-inherited chromosomes that bear 35S rDNA loci.
Bs', Bs" – *B. stacei*-inherited chromosomes that bear 35S rDNA loci.

Scale bars: 5 μm

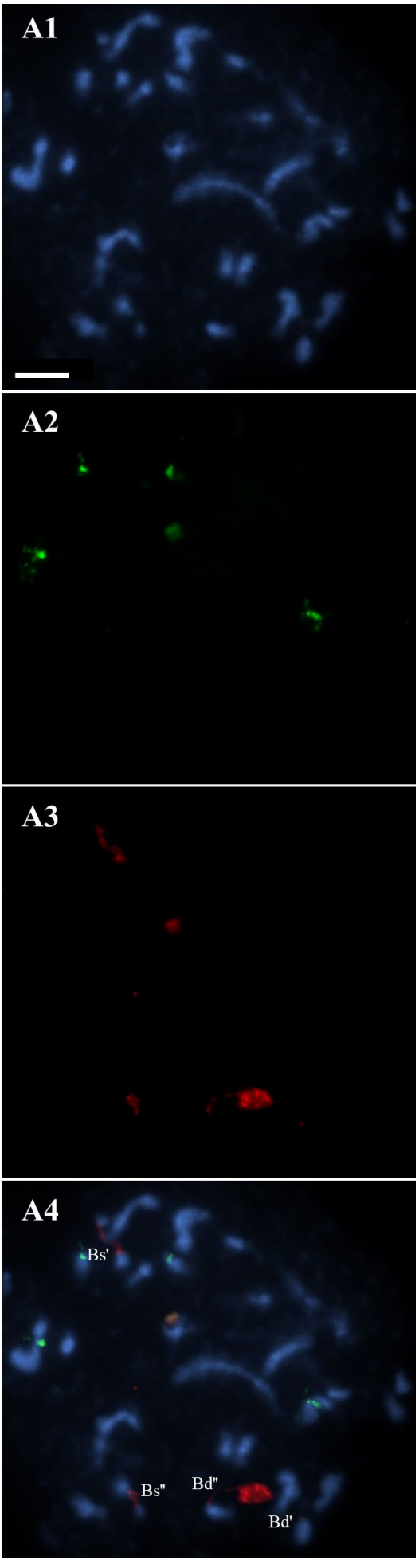
A1
A2
A3
A4
Bs'
Bs"
Bd"
Bd'

4.2. Determination of the 35S rDNA homoeologue ratios among the *B. hybridum* genotypes.

The gCAPS method was employed to verify the presence of both ancestral 35S rDNA homoeologues in 58 *B. hybridum* genotypes (Figure 25). Due to the divergence in the ITS1 region between the D- and S-subgenome homoeologues, only the D-subgenome PCR product was cut by *Mlu*I, giving two bands on the agarose gel. In contrast, the *B. stacei*-like PCR product remained uncut due to a lack of the *Mlu*I recognition site (see Figure 2). The intensity of the uncut, S-subgenome band differed between the studied *B. hybridum* genotypes. For example, genotypes 3.4.2 and 10.11.2, characterised by strong bands corresponding to S-subgenome fragments (Figure 25), also demonstrated strong S-subgenome hybridisation signals after FISH (Figure 20, A1-A4 and C1-C4). In contrast, genotypes 1.24.1 and 21.11.1 were characterised by the presence of S-subgenome 25S rDNA FISH signals of very low intensity (Figure 16, A1-A4 and Figure 17, C1-C4, respectively) after gCAPS showed weak bands corresponding to S-subgenome PCR products (Figure 25). Genotype 12.23.2 showed an almost undetectable *B. stacei*-like band after gCAPS (Figure 25) and no 25S rDNA FISH signal on S-subgenome chromosomes (Figure 23, A1-A4).

Figure 25

Figure 25

The *Mlu*I gel restriction profiles of the '18S rDNA fragment-ITS1' PCR products obtained from the leaf gDNA from 58 *B. hybridum* genotypes.

Bs – the uncut S-subgenome PCR product with a molecular mass of 678 base pairs.
Bd – D-subgenome bands with a molecular mass of 370 and 308 base pairs.

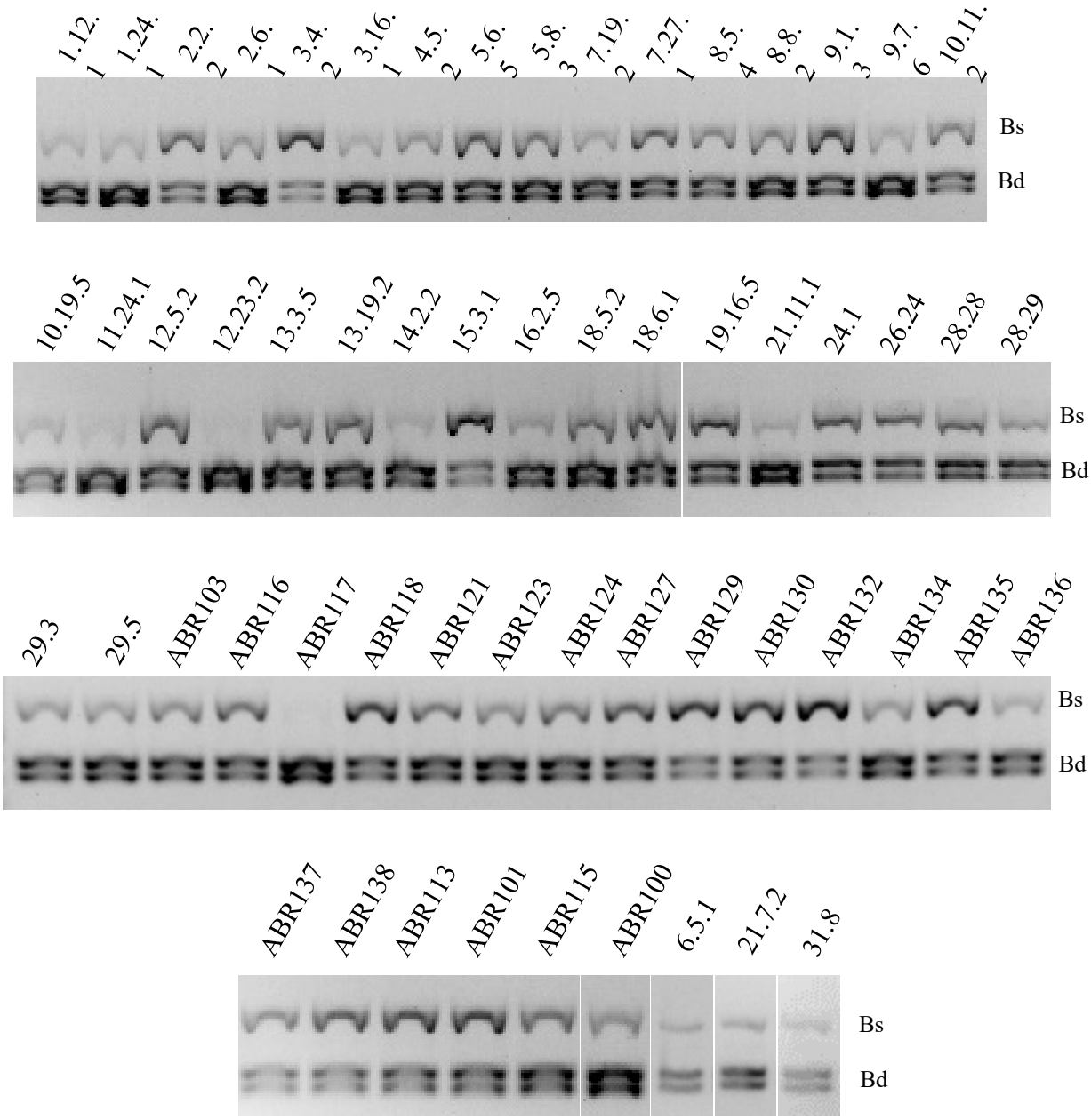
1.12.1
1.24.1
2.2.2
2.6.1
3.4.2
3.16.1
4.5.2
5.6.5
5.8.3
7.19.2
7.27.1
8.5.4
8.8.2
9.1.3
9.7.6
10.11.2
Bs
Bd
10.19.5
11.24.1
12.5.2
12.23.2
13.3.5
13.19.2
14.2.2
15.3.1
16.2.5
18.5.2
18.6.1
19.16.5
21.11.1
24.1
26.24
28.28
28.29
Bs
Bd
29.3
29.5
ABR103
ABR116
ABR117
ABR118
ABR121
ABR123
ABR124
ABR127
ABR129
ABR130
ABR132
ABR134
ABR135
ABR136
Bs
Bd
ABR137
ABR138
ABR113
ABR101
ABR115
ABR100
6.5.1
21.7.2
31.8
Bs
Bd

4.2.1. 35S rDNA homoeologue ratios among the *B. hybridum* genotypes determined by Southern blot.

Southern blot hybridisation with a fragment of 25S rDNA as a probe was performed on gDNAs from nine *B. hybridum* genotypes to determine the ancestral 35S rDNA ratios (Figure 26). Two *B. stacei* genotypes (ABR114 and Bsta5) and one *B. distachyon* genotype (Bd21) were analysed as references. To determine the contribution of the *B. distachyon*- and *B. stacei*-inherited rDNA loci, the radioactivity of the bands was quantified using a phosphorimager. It was shown that the D-subgenome 35S rDNA units were more abundant than the S-subgenome units for all but one (genotype 3.4.2) of the studied genotypes (Table 8, Figure 26B). *B. hybridum* genotype 12.23.2 has rDNA homeologs from the D-subgenome, but an additional rDNA family with a molecular weight similar (but not the same) to the rDNA from the S-subgenome was identified on the membrane (Figure 26A, Table 8). Interestingly, in *B. stacei* genotype Bsta5, the presence of two 35S rDNA families was found – the units of one 35S rDNA family cleaved twice by the *Bgl*II enzyme; however, the units from the other 35S rDNA family were cleaved only once, which is most likely due to mutations in one of the restriction sites. In *B. stacei* genotype ABR114, only one 35S rDNA family is present.

Table 8. The D- and S-subgenome rDNA content of selected *B. hybridum* genotypes quantified based on Southern blot results. The homoeologue gene number is denoted as a proportion of the Bd-like 35S rDNA or Bs-like 35S rDNA to the total rDNA and shown as percentages.

Genotype	Bd-like 35S rDNA (%)	Bs-like 35S rDNA (%)
ABR113	71.2	28.8
3-7-2	61.7	38.3
2.2.2	72.7	27.3
12.23.2	78.0	22.0
3.4.2	46.7	53.3
10.11.2	68.8	31.2
10.19.5	73.5	26.5
24.1	64.8	35.2
ABR132	68.0	32.0

Figure 26

Figure 26

The structure of the 35S rDNA loci in nine genotypes of *B. hybridum*.

A. Southern blot hybridisation of the gDNA from *B. distachyon, B. stacei* and nine *B. hybridum* genotypes subjected to *Bgl*II restriction. The blot was hybridised with the 25S rDNA probe.

B. The quantification of D- and S-subgenome 35S rDNA homoeologous ratio.

S – S-subgenome 35SrDNA after *Bgl*II treatment.
D – D-subgenome 35S rDNA after *Bgl*II treatment.

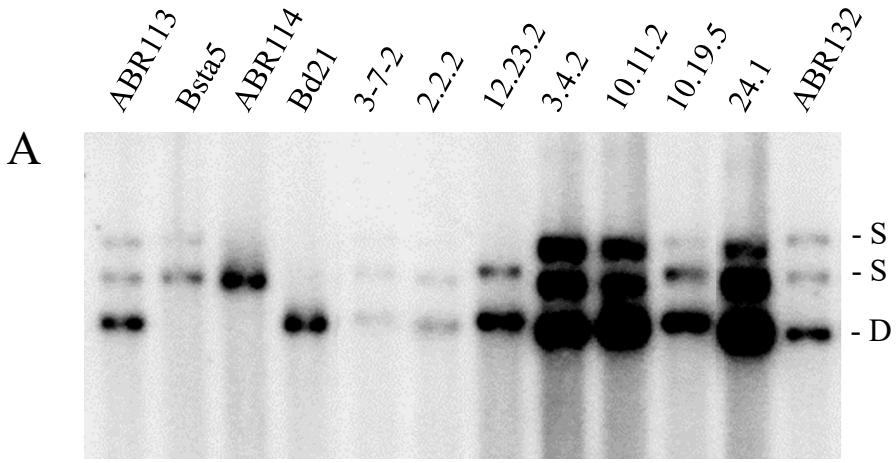

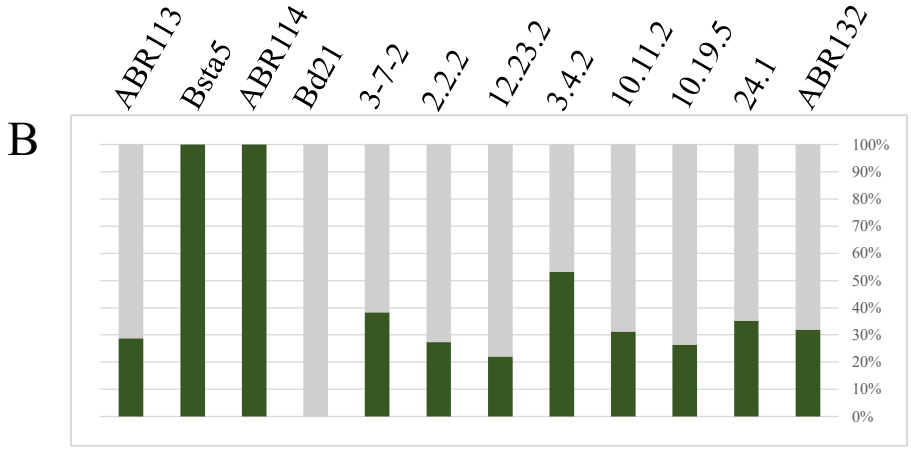

– S-subgenome 35S rDNA content.

– D-subgenome 35S rDNA content.

4.2.2. The D- and S-subgenome 35S rDNA ancestral contributions in selected *B. hybridum* genotypes based on bioinformatic analysis.

As the Material and Methods section outlined, the bioinformatic analysis was conducted to estimate the approximate D- and S-subgenome 35S rDNA ratio in selected *B. hybridum* genotypes. Raw reads from *B. hybridum* genotypes 3-7-2, 2.2.2, 12.23.2, 3.4.2, 10.11.2, 10.19.5, 24.1, and ABR132 were used to determine D- and S-subgenome rDNA contributions. A 50-bp sequence, originating from the ITS1 that shows approximately 10% divergence between the D- and S-subgenome rDNA consensus sequences, was chosen. The ITS1 fragment from the S-subgenome was subjected to BLAST analysis against the *B. hybridum* raw Illumina reads local libraries of each genotype. The identified sequences were extracted, trimmed, sampled, and aligned, following the procedures outlined in the Material and Methods. Subsequently, an alignment comprising 500 reads was used to construct a neighbour-joining phylogenetic tree (Figure 27).

In genotype ABR113, the ancestral 35S rDNA ratio was presented in Borowska-Zuchowska et al. (2020) and showed that the D-genome-like rDNA constitutes 74% of the total 35S rDNA, while the S-genome one accounted for 26%. The ancestral 35S rDNA contributions of the rest of the genotypes are shown in Table 9. *B. hybridum* genotypes 12.23.2 and 10.19.5 demonstrate the low amount of Bs-like 35S rDNA according to the Illumina reads count, which is congruent with data from FISH and Southern blot techniques.

The bioinformatic analysis was conducted to determine 35S rDNA read coverage in selected *B. hybridum* genotypes. The 35S rDNA consensus sequences of different *B. hybridum* genotypes, including 3-7-2, 2.2.2, 12.23.2, 3.4.2, 10.11.2, 10.19.5, 24.1 and ABR132, were extracted as outlined in the Material and Methods section. Genotypes 12.23.2 and 10.19.5 showed low reads coverage (Figure 28) to S-subgenome S2 consensus, which, in congruence with FISH and Southern blot data, can also serve as indirect proof of low copy number S-subgenome 35S rDNA units in these genotypes.

Table 9. The D- and S-subgenome rDNA contributions of selected *B. hybridum* genotypes quantified by raw Illumina reads.

Genotype	D-subgenome 35S rDNA (%)	S-subgenome 35S rDNA (%)
ABR113	74	26
3-7-2	57.5	42.5
2.2.2	62.4	37.6
12.23.2	98.4	1.6
3.4.2	47	53
10.11.2	66.2	33.8
10.19.5	91.6	8.4
24.1	83	17
ABR132	53	47

Figure 27

Figure 27

Circular phylogenetic trees of selected *B. hybridum* genotypes for ratio estimation of 35S rDNA homoeologues content.

Blue colour – S-subgenome clade
Red colour – D-subgenome clade
Scale – tree scale
Numbers – bootstrap values

* 500 reads were used for each tree

3-7-2*

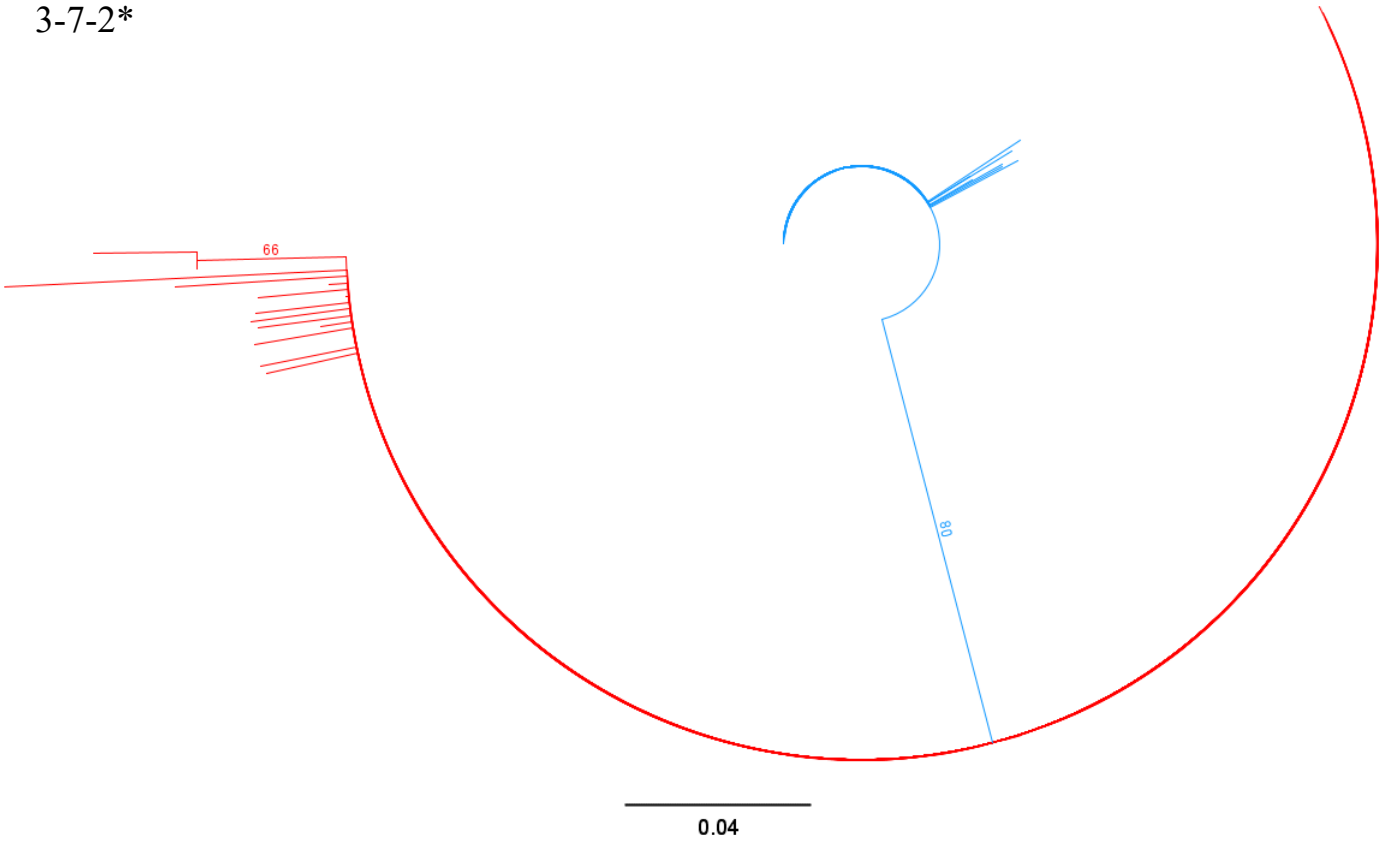

2.2.2

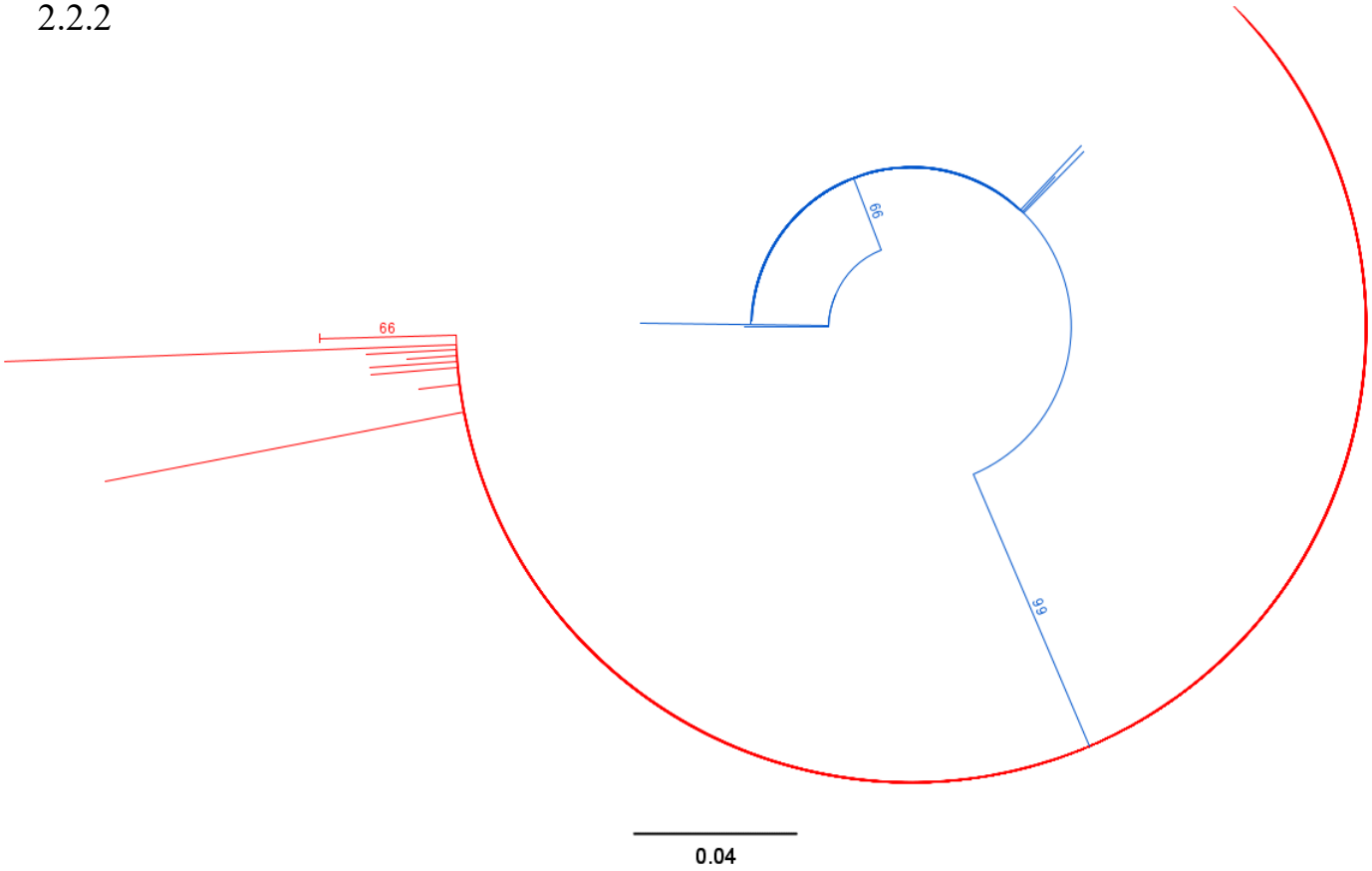

3.4.2

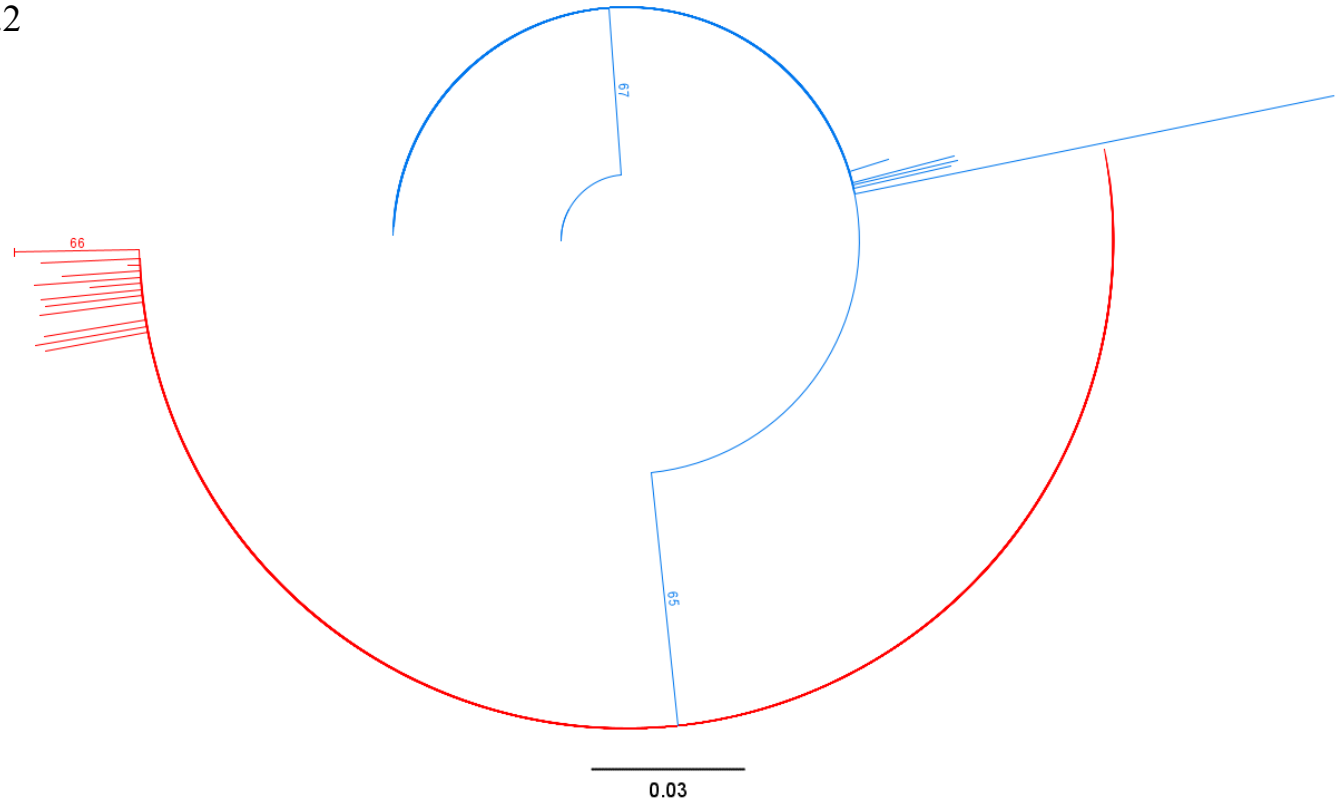

10.11.2

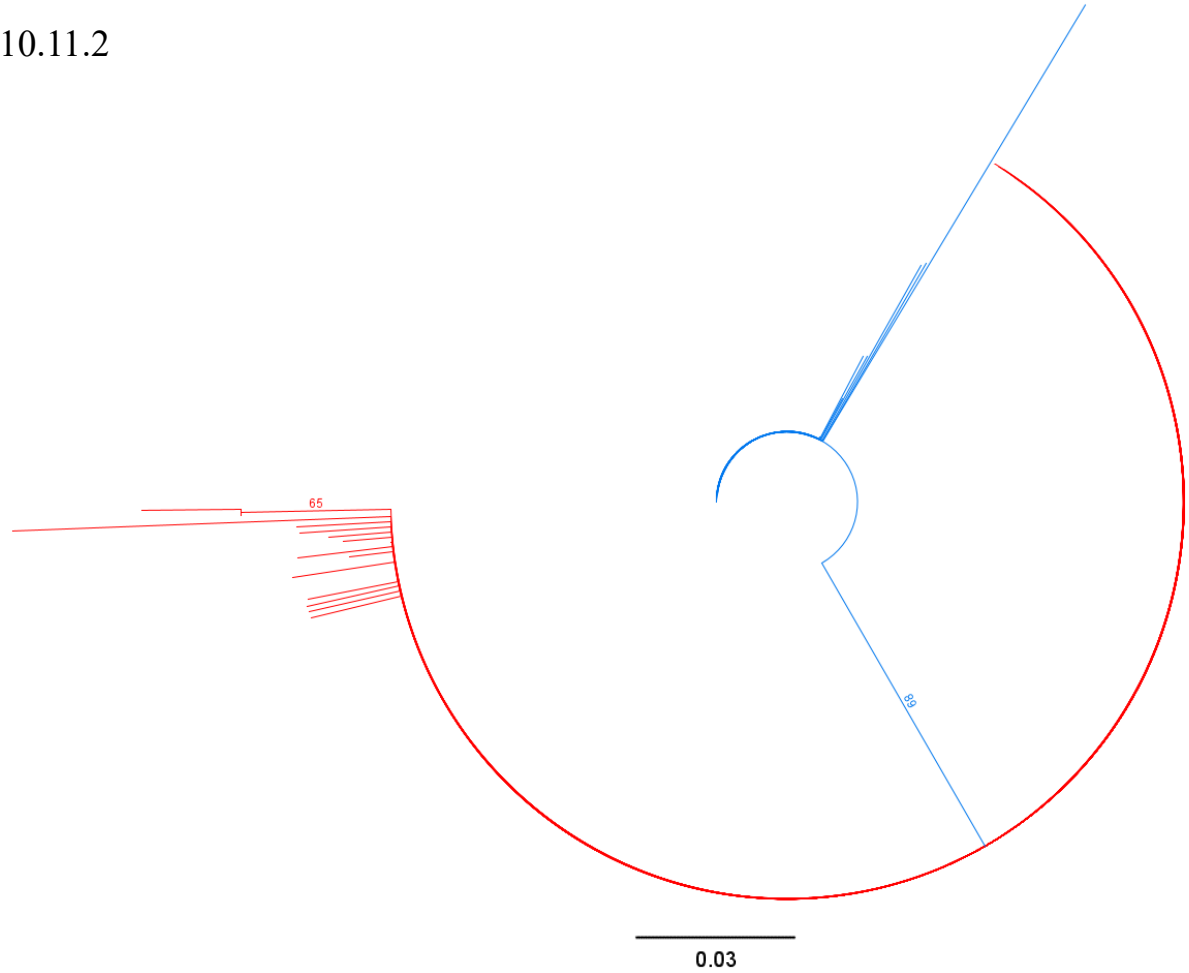

10.19.5

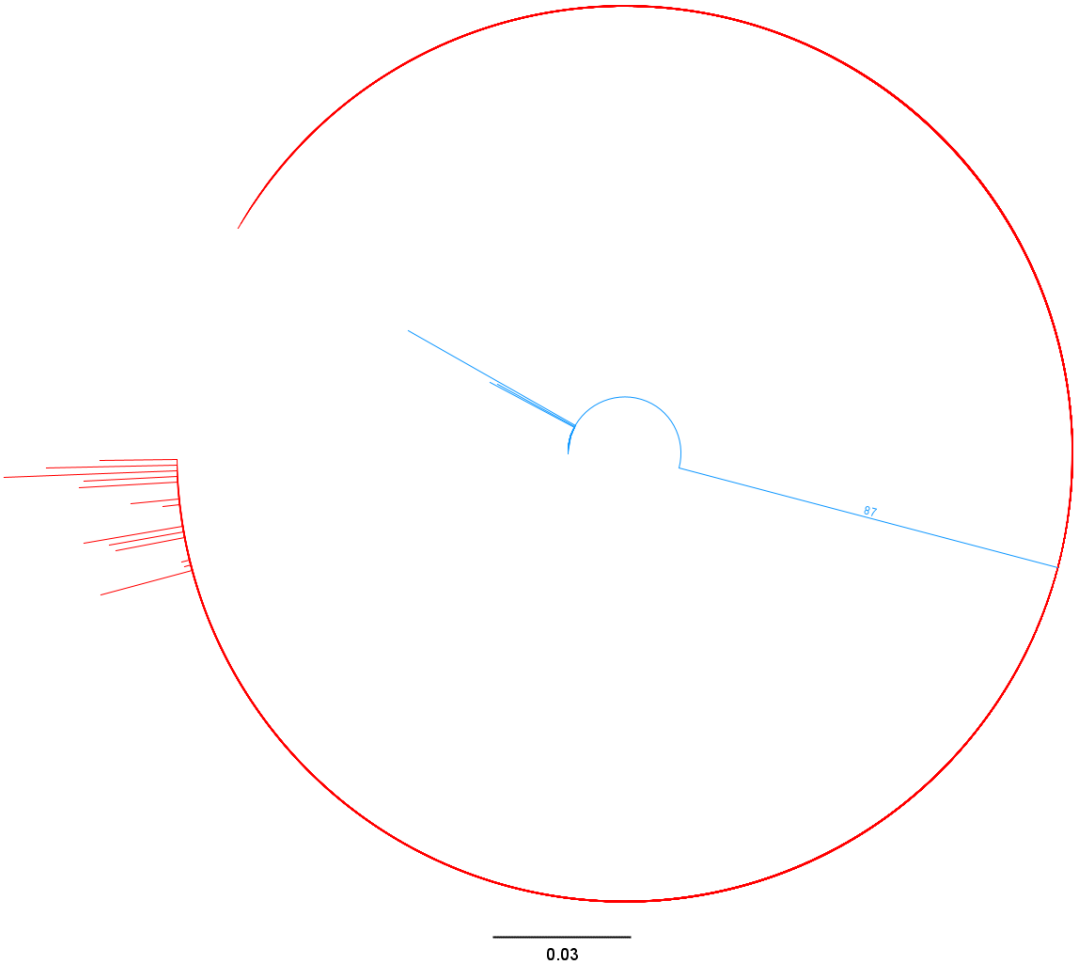

12.23.2

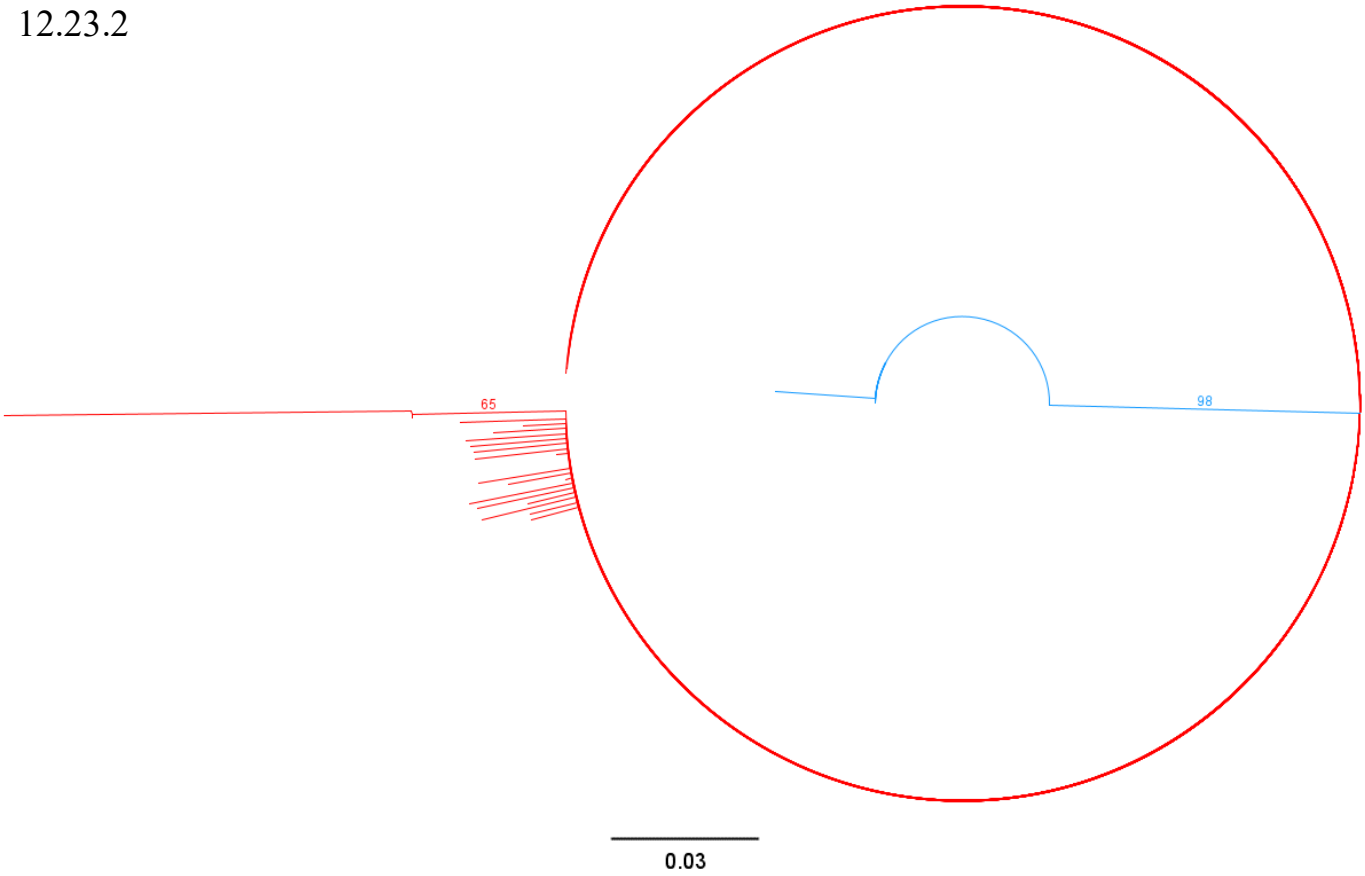

24.1

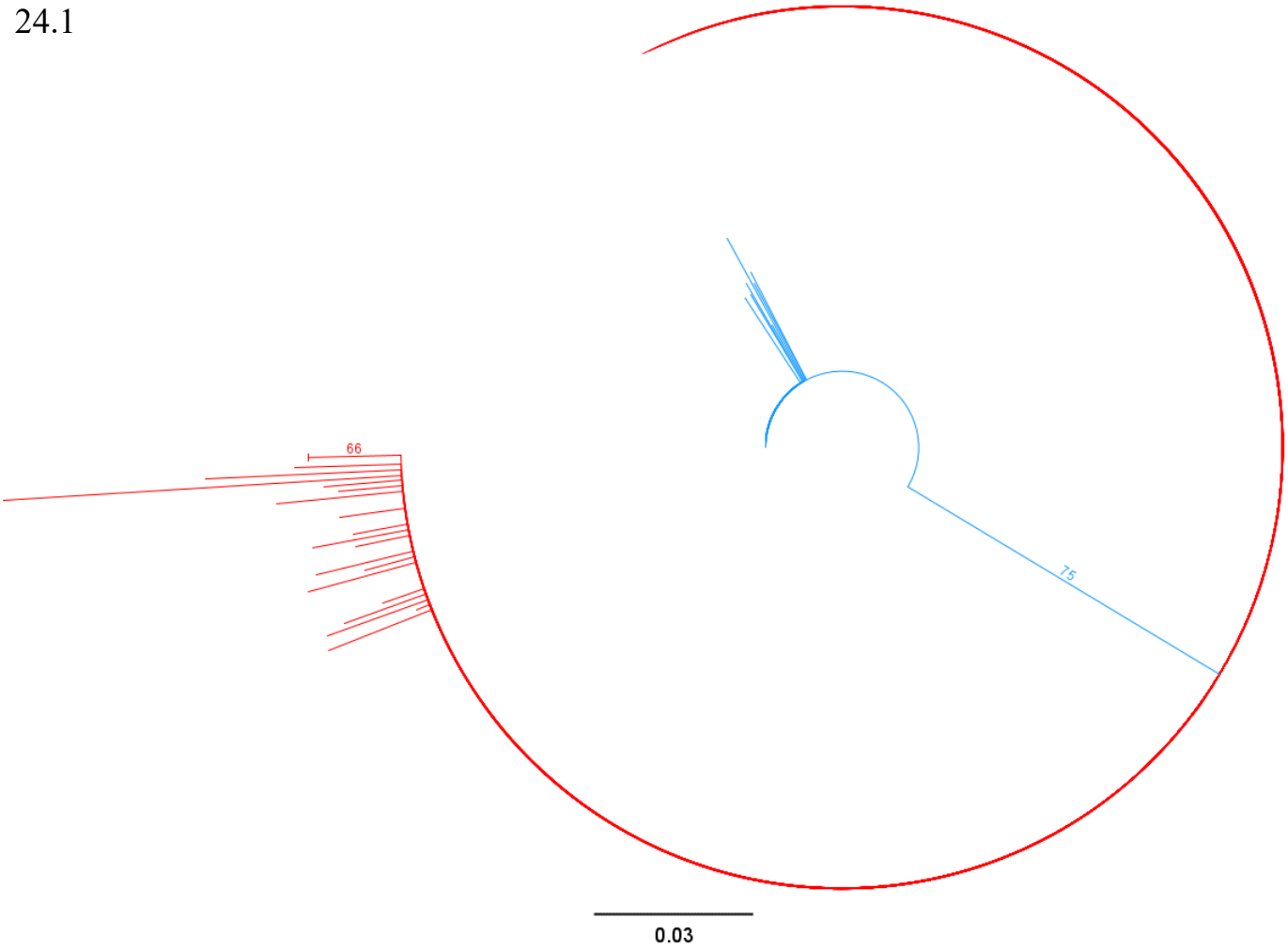

ABR132

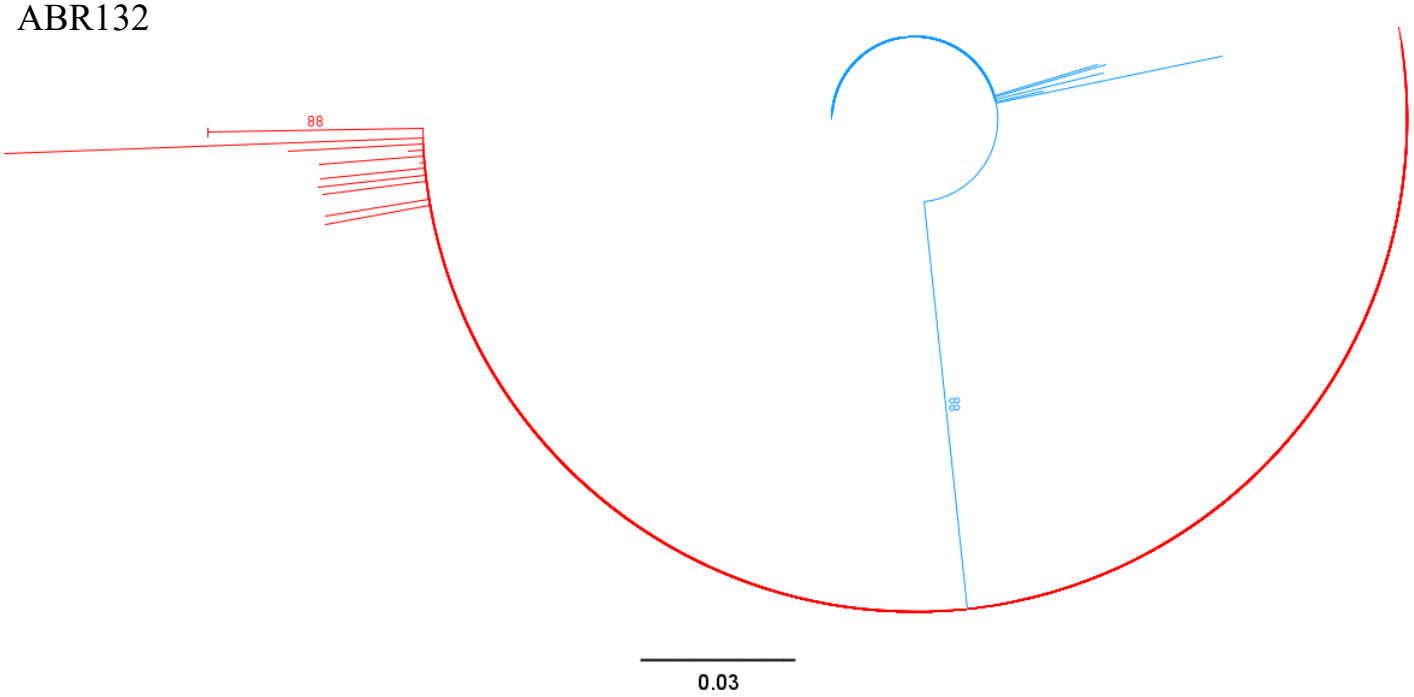

Figure 28

Figure 28

Read coverage of 35S rDNA unit in selected *B. hybridum* genotypes.

Raw Illumina reads mapped to Bd- and Bs-specific 35S rDNA consensus sequences of *B. hybridum* (Consensus D2 and S2).

Red triangles indicate IGS regions of D-subgenome (~2.3 kb) and S-subgenome (~3.5 kb) 35S rDNA.

* – number of reads

2.2.2

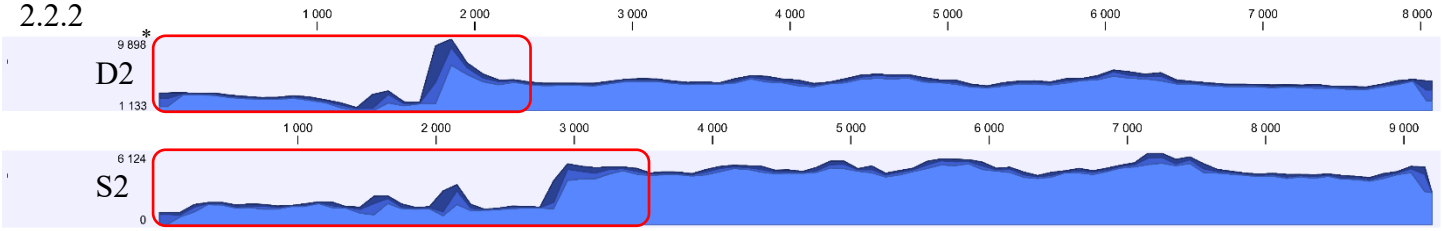

3.4.2

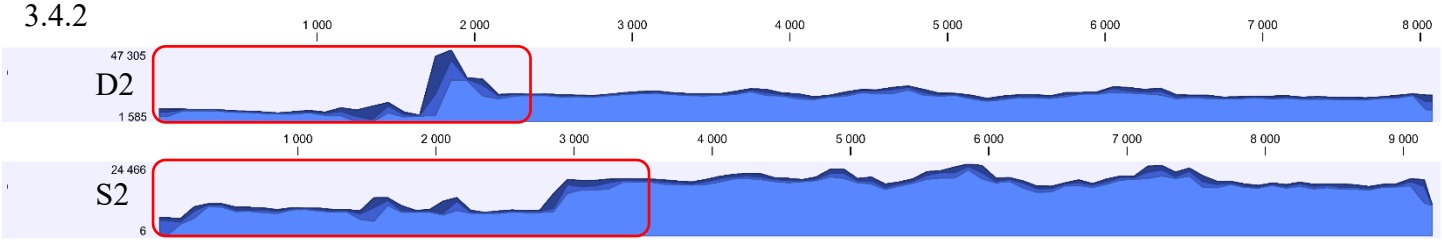

3-7-2

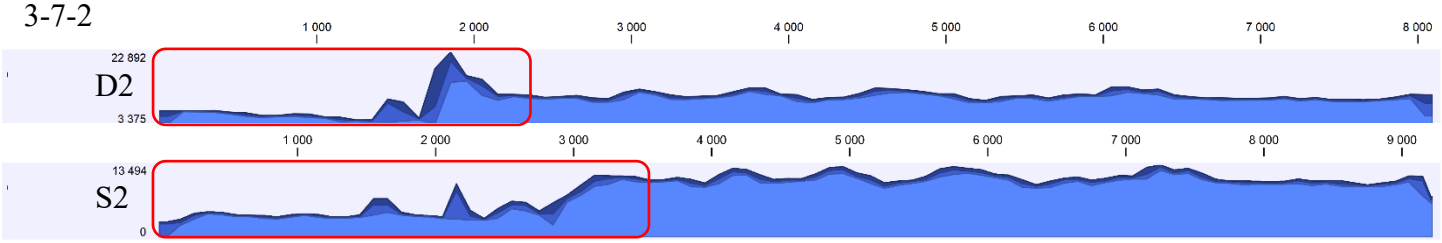

10.11.2

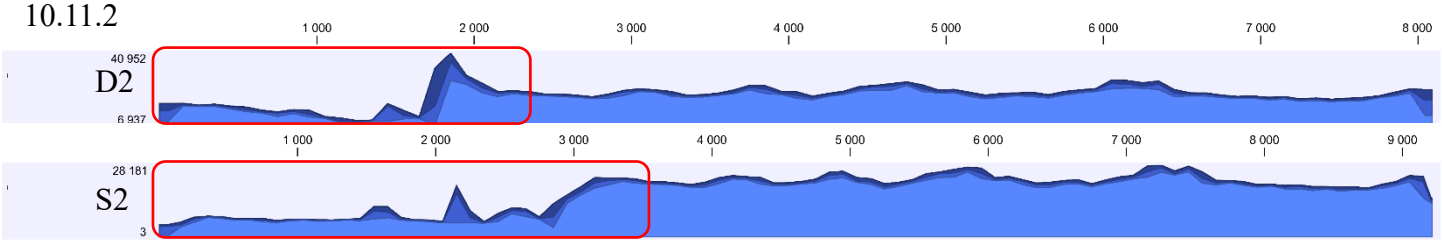

10.19.5

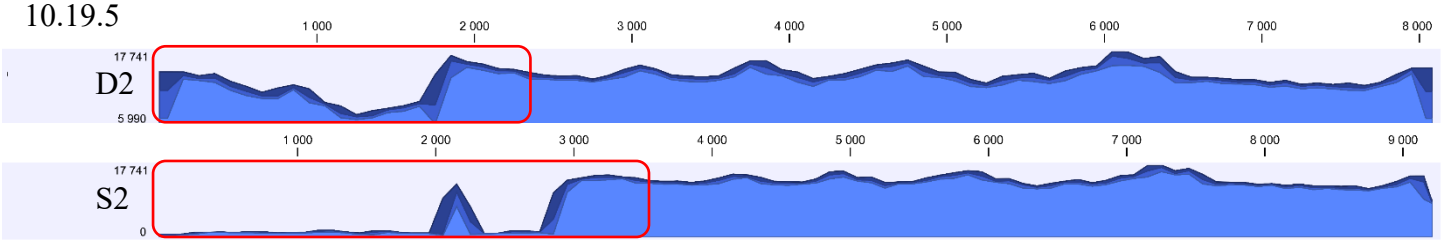

12.23.2

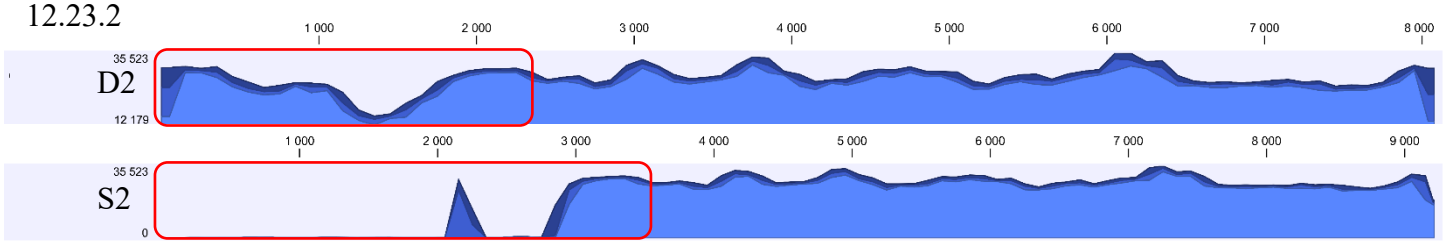

24.1

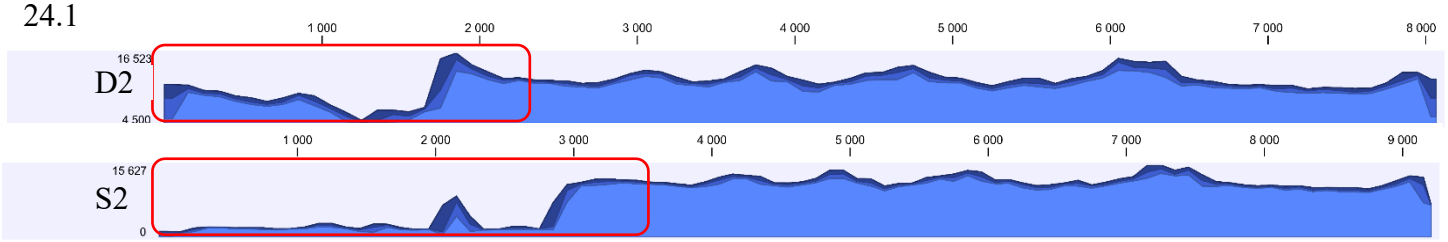

ABR132

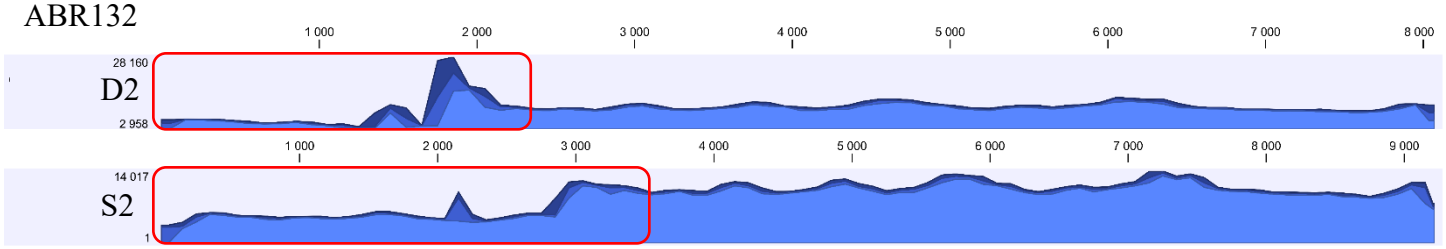

4.3. 18S rDNA and ITS1 homogeneity in selected *B. hybridum* genotypes.

In order to investigate the homogeneity of the whole ITS1 region and a part of the 18S rDNA, the cloned 18S rDNA-ITS1 sequences of *B. stacei* genotype ABR114 (15 clones), *B. hybridum* genotype ABR113 (30 clones) and *B. hybridum* genotypes ABR101 and 2.2.2 (15 clones) were analysed. *B. stacei* genotype ABR114 showed a high level of homogeneity in both 18S rDNA and ITS1 (Figure 29). In the case of *B. hybridum* genotype 2.2.2, four clones belonging to the D-subgenome demonstrated a high level of homogeneity, while, among S-clade clones, one (indicated in red in Figure 29) was probably a pseudogene having 11 SNPs in the coding region. Genotype ABR113 demonstrated high homogeneity among all clones analysed except one clone from the S-subgenome having 10 SNPs in the ITS1 region. Genotype ABR101 had only two clones from the D-subgenome, and both clones showed a low number of SNPs.

Overall, the ITS1 sequence was more homogeneous in *B. stacei* than *B. stacei*-derived ITS1 in *B. hybridum.* 18S rDNA sequence is more homogeneous than the ITS1 sequence in both studied species.

Figure 29

Figure 29

***B. hybridum* and *B. stacei* 18S rDNA and ITS1 sequences aligned to the reference D- and S-subgenome 18S rDNA and ITS1 sequences for homogeneity level assessment.**

Red rectangle – possible pseudogene sequence.

ABR114

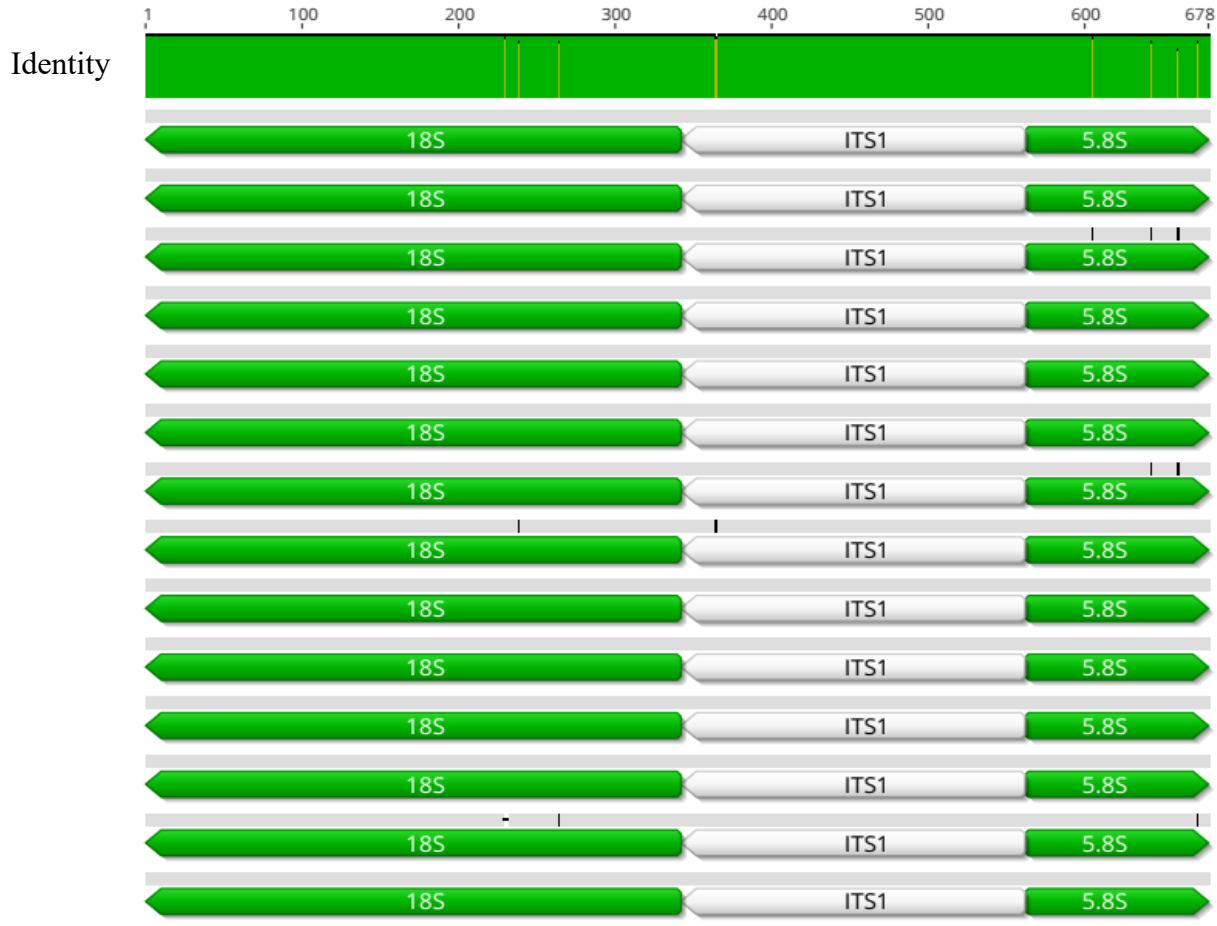

2.2.2

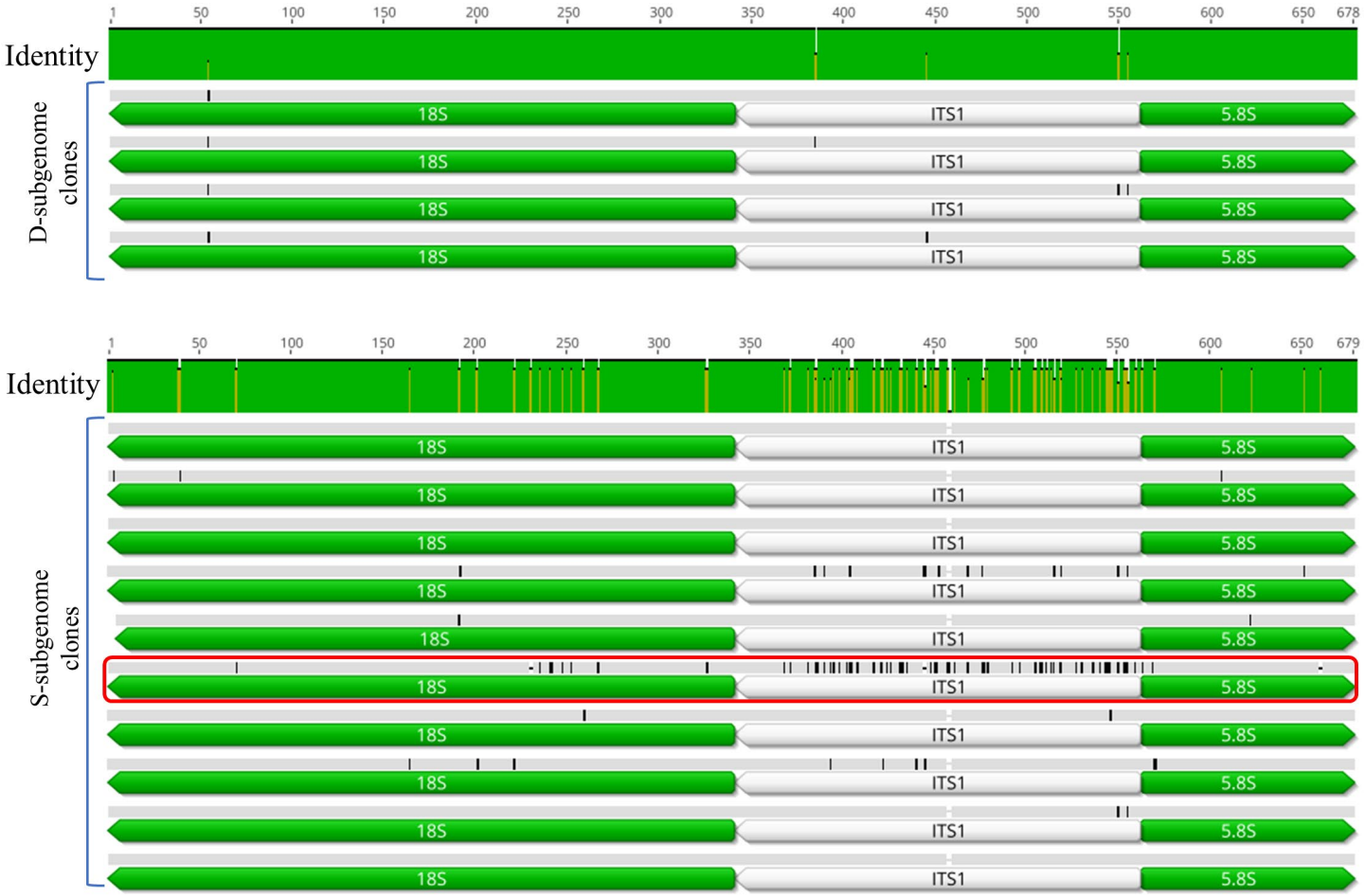
Identity
1
50
100
150
200
250
300
350
400
450
500
550
600
650
678
D-subgenome clones
18S
ITS1
5.8S
Identity
1
50
100
150
200
250
300
350
400
450
500
550
600
650
679
S-subgenome clones
18S
ITS1
5.8S

ABR113

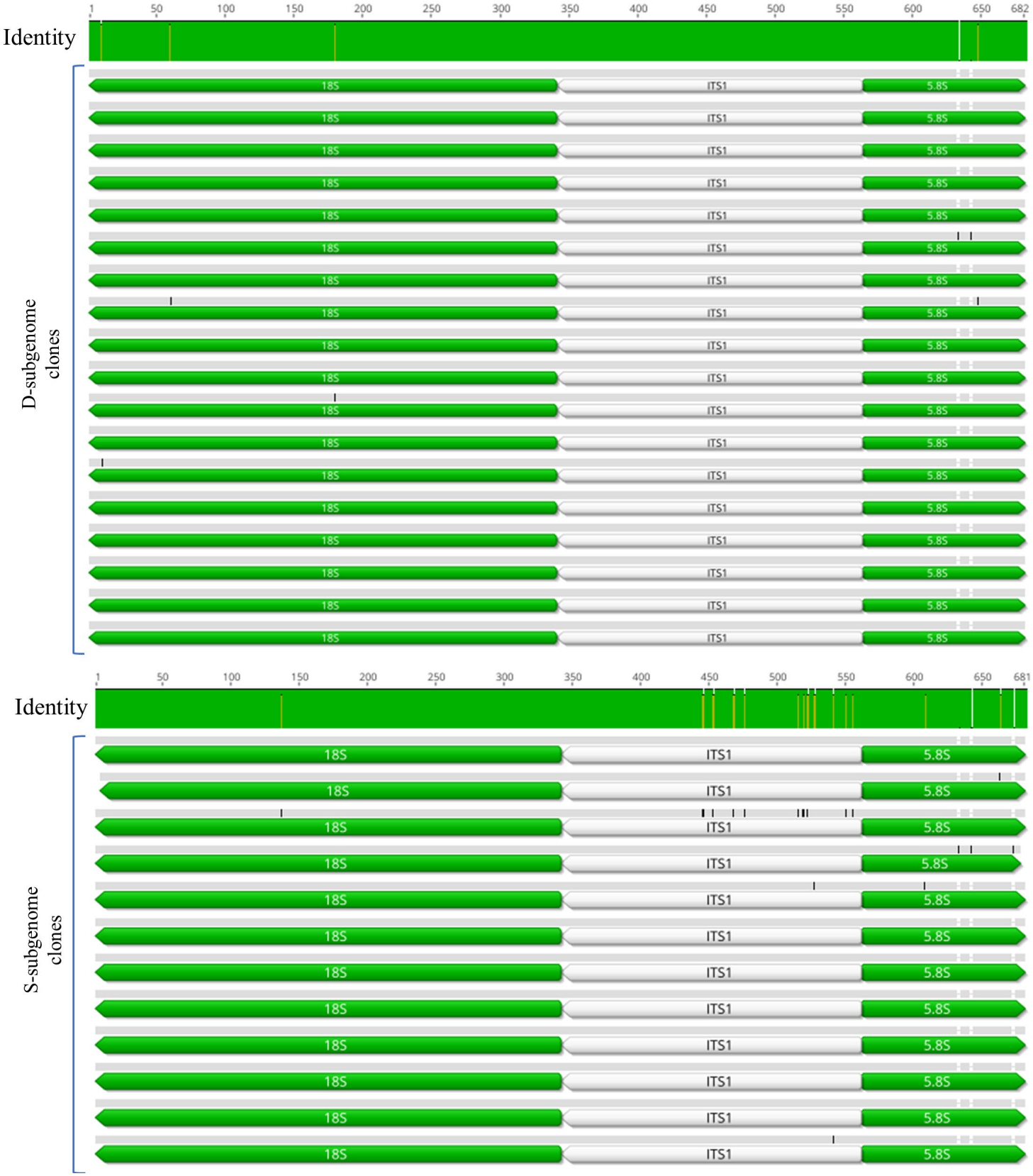
Identity
1
50
100
150
200
250
300
350
400
450
500
550
600
650
682
D-subgenome clones
18S
ITS1
5.8S
Identity
1
50
100
150
200
250
300
350
400
450
500
550
600
650
681
S-subgenome clones
18S
ITS1
5.8S

ABR101

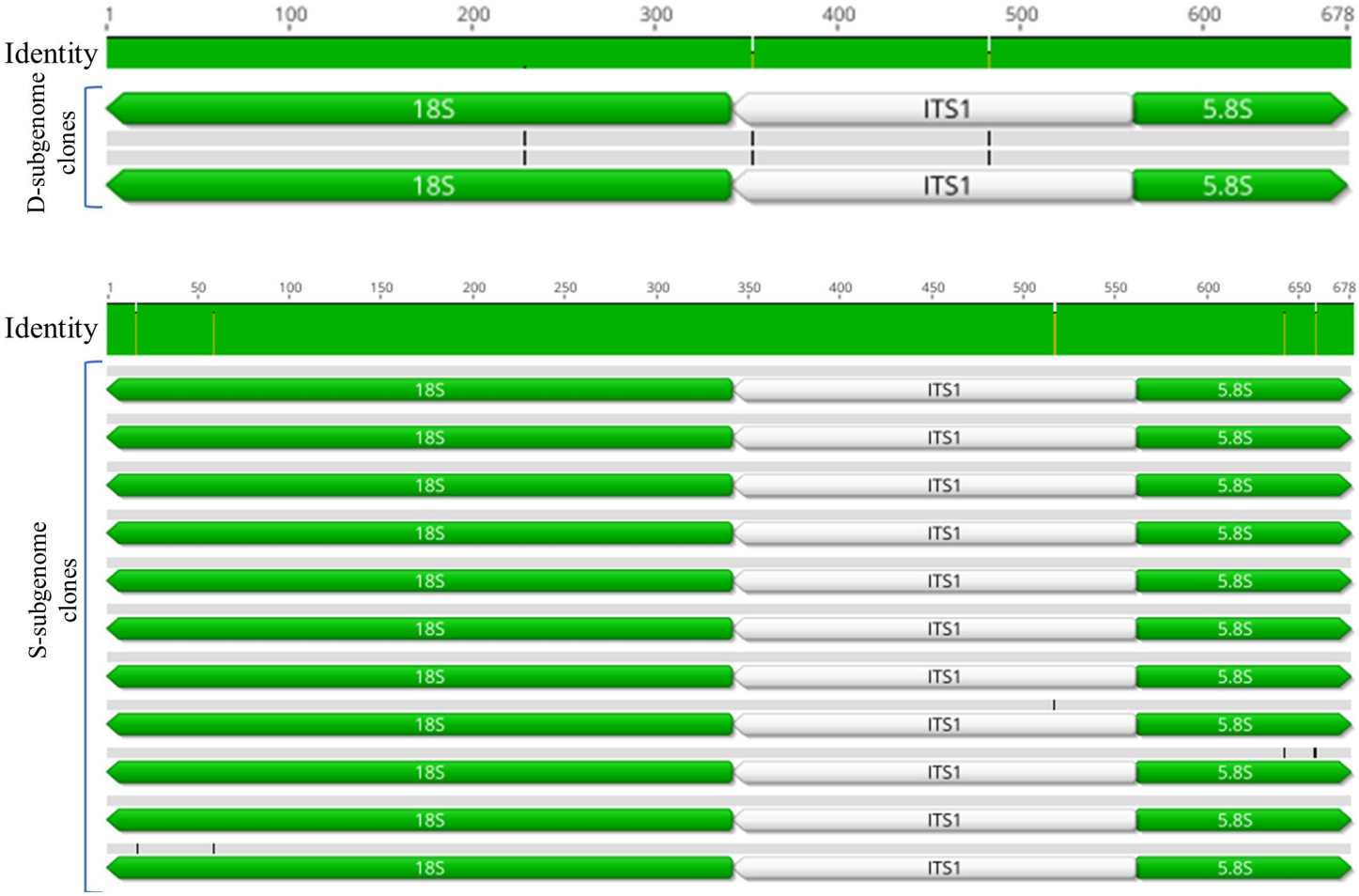
1
100
200
300
400
500
600
678
Identity
D-subgenome clones
18S
ITS1
5.8S
18S
ITS1
5.8S

1
50
100
150
200
250
300
350
400
450
500
550
600
650
678
Identity
S-subgenome clones
18S
ITS1
5.8S

4.4. Chloroplast haplotype analysis of selected *B. hybridum* genotypes.

In order to determine the maternal lineage of the chloroplast DNA (cpDNA) among the studied *B. hybridum* genotypes, a fragment of the chloroplast *trn*LF gene was amplified, sequenced and aligned. The linkage between chloroplast origin and the presence of the S-subgenome rRNA gene expression can provide evidence for the impact of the maternal effect on ND. The 1.12.1, 1.24.1, 2.2.2, 2.6.1, 3.4.2, 3.16.1, 4.5.2, 5.6.5, 5.8.3, 6.5.1, 7.19.2, 7.27.1, 8.5.4, 8.8.2, 9.1.3, 9.7.6, 10.11.2, 10.19.5, 11.24.1, 12.5.3, 12.23.2, 13.3.5, 13.19.2, 14.2.2, 15.3.1, 16.2.5, 18.5.2, 18.6.1, 19.16.5, 21.7.2, 21.11.1, 23.101, 24.1, 26.12, 26.24, 28.28, 28.29, 29.3, 29.5, 31.8, ABR103, ABR113, ABR116, ABR118, ABR119, ABR121, ABR123, ABR124, ABR127, ABR129, ABR130, ABR132, ABR134, ABR135, ABR136, ABR137, ABR138 and 3-7-2 *B. hybridum* genotypes were used for haplotype analysis. The S-subgenome cpDNA origin was found in all 58 *B. hybridum* genotypes with a confidence level of 90 through sequencing, alignment, and phylogenetic analyses (Figure 30). Interestingly, the genotypes that exhibited strong S-subgenome 35S rRNA gene activation in their adventitious roots and leaves were found to possess cpDNA inherited from *B. stacei*, implying the lack of correlation between the maternal origin and ND.

Figure 30

Figure 30

A phylogenetic tree based on the *trn*LF chloroplast gene fragment in 58 *B. hybridum* genotypes.

The bootstrap value is highlighted in a red circle.

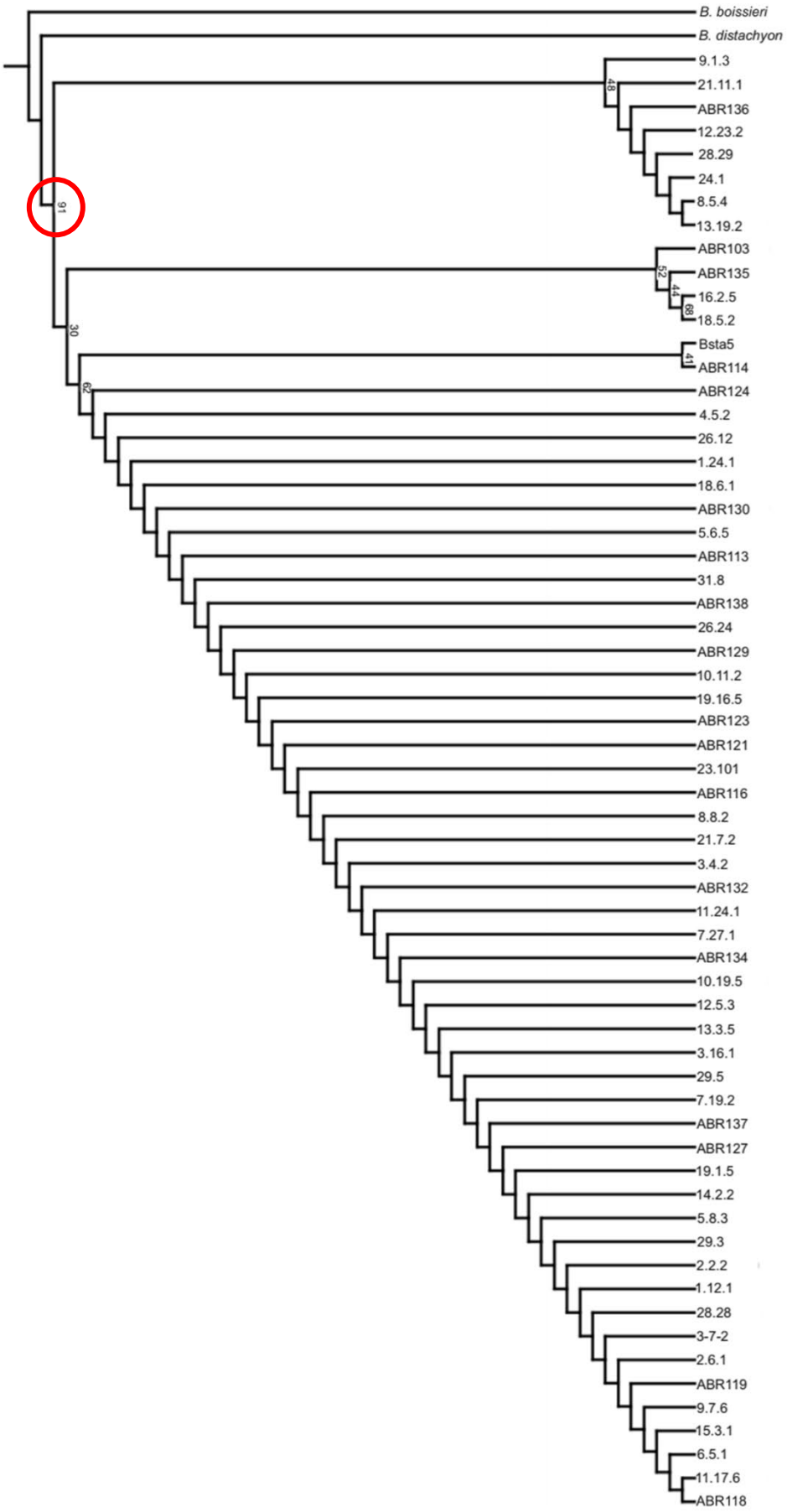
B. boissieri
B. distachyon
9.1.3
21.11.1
ABR136
12.23.2
28.29
24.1
8.5.4
13.19.2
ABR103
ABR135
16.2.5
18.5.2
Bsta5
ABR114
ABR124
4.5.2
26.12
1.24.1
18.6.1
ABR130
5.6.5
ABR113
31.8
ABR138
26.24
ABR129
10.11.2
19.16.5
ABR123
ABR121
23.101
ABR116
8.8.2
21.7.2
3.4.2
ABR132
11.24.1
7.27.1
ABR134
10.19.5
12.5.3
13.3.5
3.16.1
29.5
7.19.2
ABR137
ABR127
19.1.5
14.2.2
5.8.3
29.3
2.2.2
1.12.1
28.28
3-7-2
2.6.1
ABR119
9.7.6
15.3.1
6.5.1
11.17.6
ABR118
48
91
52
44
98
30
41
62

4.5. The expression patterns of *B. hybridum* 35S rDNA homoeologues.

4.5.1. Ancestral 35S rDNA expression status in *B. hybridum* using RT-CAPS technique.

In order to assess the ancestral 35S rDNA expression patterns in *B. hybridum,* the RT-CAPS approach (Sochorova et al., 2017) was performed taking advantage of the ITS1 sequence polymorphism. As shown in Figure 2, the upper band represents the uncut *B. stacei* ITS1 region, and the lower bands represent the cut D-subgenome ITS1 region. Total RNA from the leaf tissue of 61 *B. hybridum* genotypes was isolated and converted to cDNA with the subsequent RT-CAPS analysis. The results of the RT-CAPS approach are presented in Figure 31A. The D-subgenome ITS1 bands were present in all analysed tissues if all genotypes, showing their presence in 35S pre-rRNA transcripts. Interestingly, none of the genotypes showed the presence of a *B. stacei*-originated ITS1, indicating a strong ND in the leaves of the studied genotypes. The next generation of plants was analysed using the same approach, and two genotypes (2.2.2 and 3.4.2) showed the presence of the S-subgenome band, indicating the ND abolishment (Figure 31B).

The 35S rRNA gene expression patterns were also analysed in adventitious roots of 60 *B. hybridum* genotypes. As in the case of leaves, the D-subgenome 35S rRNA genes were transcribed in all analysed genotypes (Figure 32). Interestingly, almost half of the studied genotypes showed the presence of the S-subgenome band, indicating the expression of the S-subgenome 35S rRNA genes (Figure 32). Moreover, the intensity of S-subgenome bands varied among genotypes, demonstrating differences in the expression level of 35S rRNA genes.

During the RT-CAPS experiment on adventitious roots, *B. hybridum* genotypes 13.19.2, 24.1, ABR103, ABR123, ABR129 and ABR138 showed differences in 35S rRNA gene expression between generations. To investigate the generation-specific 35S rRNA gene expression, the pre-rRNA transcripts from adventitious roots of *B. hybridum* genotypes 13.19.2, 24.1, ABR103, ABR123, ABR129 and ABR138 were analysed. All genotypes, apart from genotypes ABR138 and ABR123, were analysed in two generations of plants and genotypes 13.19.2 and ABR129 showed a difference in S-subgenome rRNA gene expression in T2 and T3 generations (see Figure 33). Interestingly, genotypes 13.19.2, ABR123, ABR129 and ABR138 showed differences in 35S rRNA homoeologues expression between individual plants belonging to the same generation.

4.5.2. Ancestral 35S rDNA units expression in *B. hybridum* using RT-qPCR.

Three *B. hybridum* genotypes (ABR113, 3-7-2 and 2.2.2) were analysed by RT-qPCR in order to shed more light on the changes in the ancestral 35S rRNA gene expression during the plant development. The genotypes used in the experiment were chosen based on their differential expression of 35S rDNA homoeologues, as shown by the RT-CAPS approach. Primers specific to either the D- or S-subgenome ITS1 were used in each reaction to assess their presence among the pre-rRNA transcripts. Total RNA was isolated from primary roots, adventitious roots, leaves from 4-, 6-, and 8-week-old plants, and spikes that contain meiocytes. The obtained cDNAs were used as templates in RT-qPCR reactions.

The D-subgenome 35S pre-rRNA transcripts were present in all analysed tissues and genotypes (Figures 31-34). The expression patterns of the S-subgenome rRNA genes were more variable. In the case of the reference genotype ABR113, a strong ND towards the D-subgenome 35S rDNA was observed. No S-subgenome PCR products were detected in all but one studied tissue (Figure 34A). The adventitious roots were the only tissue where S-subgenome pre-rRNA transcripts were found. However, the expression level of the S-subgenome 35S rRNA genes was 60-140 times lower than the D-subgenome ones, reaching only up to 1.5% of total pre-rRNA transcripts that were detected (Figure 34A). It should be noted that the RT-qPCR cycle threshold was detected at the 24th cycle, indicating the first discovery of expression of *B. stacei*-specific rRNA genes in the ABR113 genotype of *B. hybridum*.

In genotype 3-7-2, the S-subgenome 35S rRNA genes were expressed in the leaves from the 6-week-old plants, adventitious roots and primary roots (Figure 34A). Primary roots showed expression of S-subgenome rRNA genes in the range of 17-20% of total pre-rRNA gene transcripts; at the same time, adventitious roots demonstrated this expression at 50-65%. Surprisingly, among all the leaf tissues analysed, only leaves from 6-week-old plants showed some traces of S-subgenome 35S pre-rRNA transcripts, amounting to 1-2% of total pre-rRNA.

Interestingly, genotype 2.2.2 demonstrated the prevailing expression of S-subgenome rRNA genes in primary and adventitious roots, amounting to 81% and 93% of total pre-rRNA transcripts, respectively. The expression of the S-subgenome rRNA genes in the leaves of 4-, 6-, and 8-week-old plants showed a variation, with a general trend of decreasing the expression level as the plants aged (see Figure 34A). To shed more

light on the variability in S-subgenome rRNA gene expression in leaf tissue, the leaves from 6-week-old plants of 10 individuals were studied by RT-qPCR and RT-CAPS techniques. The ancestral pre-rRNA ratio, in this case, was dependent on the specific plant and not on the genotype itself. Spike tissue demonstrated slight S-subgenome rRNA gene expression in the range of 1-3% of the total 35S pre-rRNA transcripts. The standard deviation calculation based on three biological replicates is presented in Figure 34B.

Figure 31

Figure 31

Expression analysis of the 35S rRNA genes in the leaf tissue of 61 *B. hybridum* genotypes using the RT-CAPS method.

A. The gel restriction profiles of the ITS1 PCR products were obtained from the leaf cDNA of 61 *B. hybridum* genotypes.

B. The gel restriction profiles of the ITS1 PCR products were obtained from the leaf cDNA of the first and the second generation of *B. hybridum* genotypes 2.2.2 and 3.4.2.

S – S-subgenome RT-CAPS fragment after *Mlu*I treatment.
D – D-subgenome RT-CAPS fragment after *Mlu*I treatment.

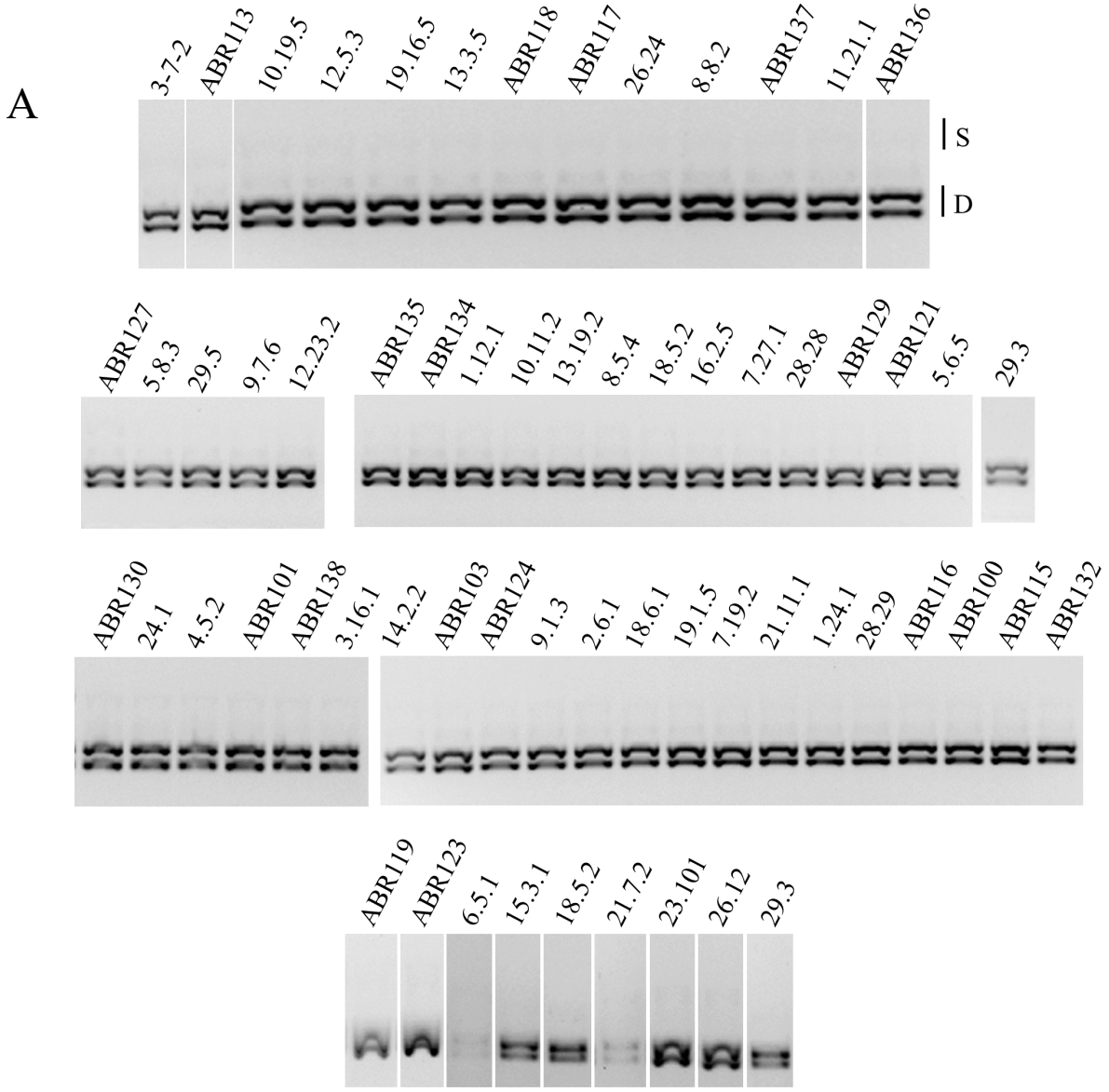
A
3-7-2
ABR113
10.19.5
12.5.3
19.16.5
13.3.5
ABR118
ABR117
26.24
8.8.2
ABR137
11.21.1
ABR136
S
D
ABR127
5.8.3
29.5
9.7.6
12.23.2
ABR135
ABR134
1.12.1
10.11.2
13.19.2
8.5.4
18.5.2
16.2.5
7.27.1
28.28
ABR129
ABR121
5.6.5
29.3
ABR130
24.1
4.5.2
ABR101
ABR138
3.16.1
14.2.2
ABR103
ABR124
9.1.3
2.6.1
18.6.1
19.1.5
7.19.2
21.11.1
1.24.1
28.29
ABR116
ABR100
ABR115
ABR132
ABR119
ABR123
6.5.1
15.3.1
18.5.2
21.7.2
23.101
26.12
29.3

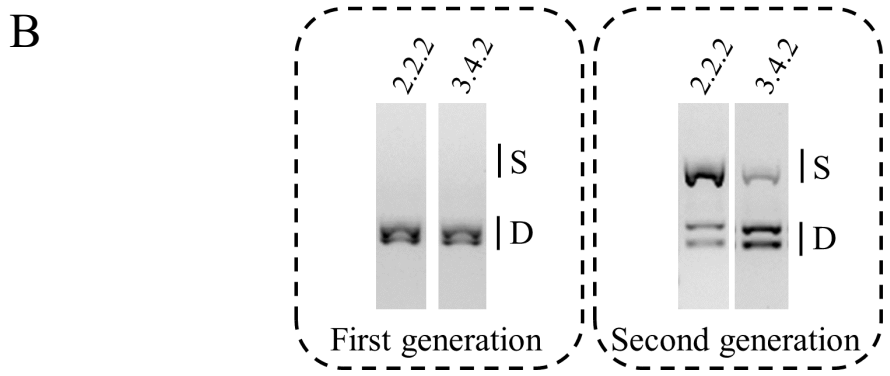
B
2.2.2
3.4.2
S
D
First generation
2.2.2
3.4.2
S
D
Second generation

Figure 32

Figure 32

Analysis of the 35S rRNA gene expression in the adventitious root tissue of 60 *B. hybridum* genotypes using the RT-CAPS method.

The gel restriction profiles of the ITS1 PCR products were obtained from the adventitious root cDNA of 60 *B. hybridum* genotypes.

S – S-subgenome RT-CAPS fragment after *Mlu*I treatment.
D – D-subgenome RT-CAPS fragment after *Mlu*I treatment.

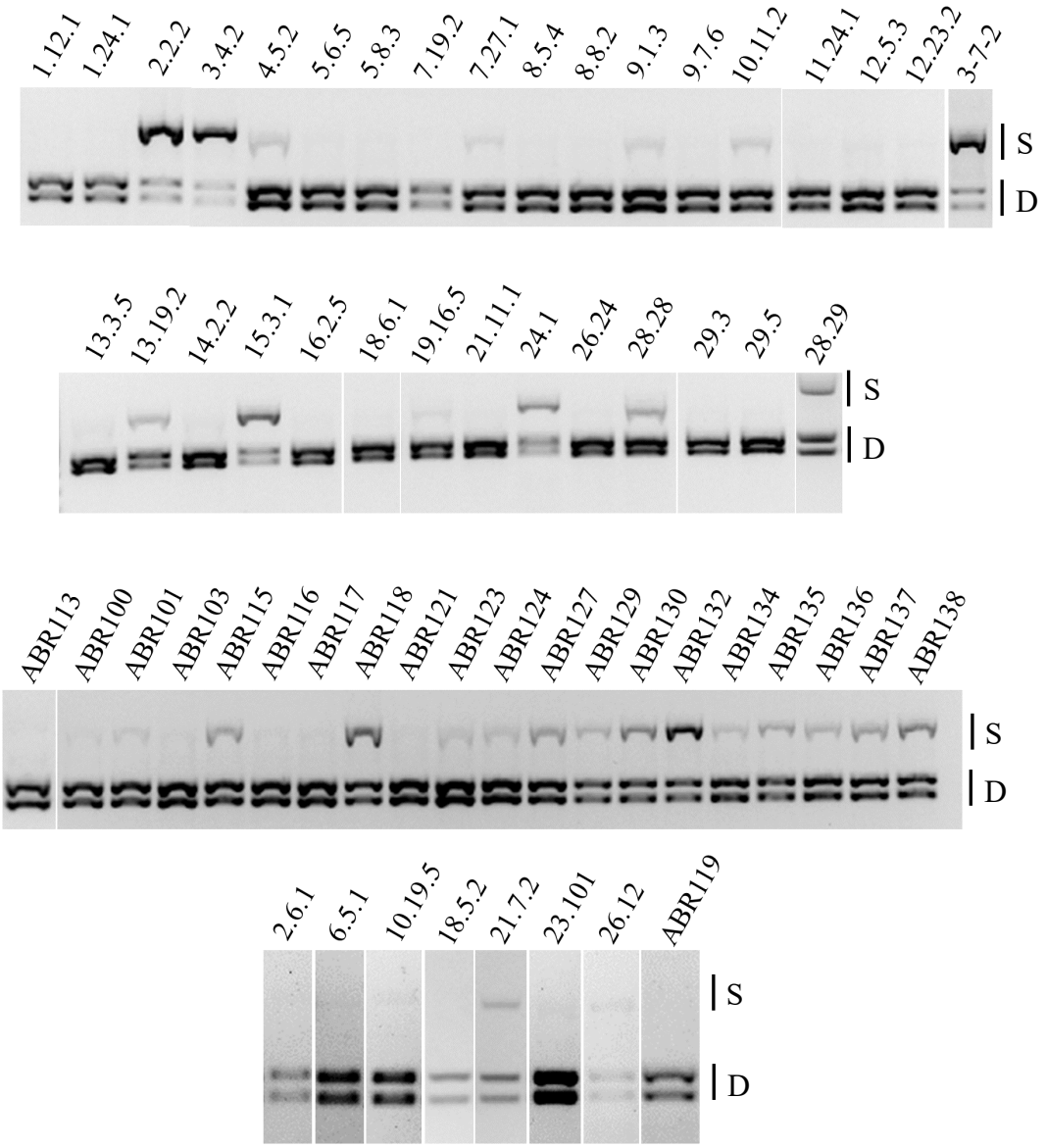
1.12.1
1.24.1
2.2.2
3.4.2
4.5.2
5.6.5
5.8.3
7.19.2
7.27.1
8.5.4
8.8.2
9.1.3
9.7.6
10.11.2
11.24.1
12.5.3
12.23.2
3-7-2
S
D
13.3.5
13.19.2
14.2.2
15.3.1
16.2.5
18.6.1
19.16.5
21.11.1
24.1
26.24
28.28
29.3
29.5
28.29
S
D
ABR113
ABR100
ABR101
ABR103
ABR115
ABR116
ABR117
ABR118
ABR121
ABR123
ABR124
ABR127
ABR129
ABR130
ABR132
ABR134
ABR135
ABR136
ABR137
ABR138
S
D
2.6.1
6.5.1
10.19.5
18.5.2
21.7.2
23.101
26.12
ABR119
S
D

Figure 33

Figure 33

Analysis of the 35S rRNA gene expression in adventitious roots of six *B. hybridum* genotypes using the RT-CAPS method.

The gel restriction profiles of the ITS1 PCR products were obtained from adventitious roots cDNA of 6 *B. hybridum* genotypes in the T2 and T3 generations.

S – S-subgenome RT-CAPS fragment after *Mlu*I treatment.
D – D-subgenome RT-CAPS fragment after *Mlu*I treatment.

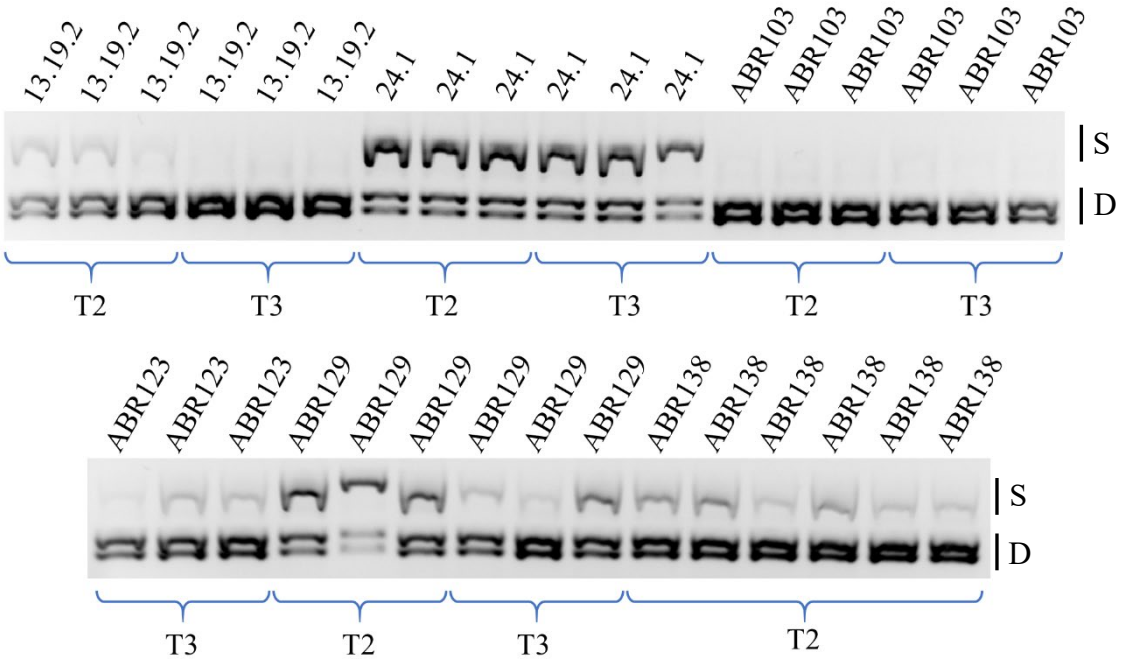
13.19.2
13.19.2
13.19.2
13.19.2
13.19.2
13.19.2
24.1
24.1
24.1
24.1
24.1
24.1
ABR103
ABR103
ABR103
ABR103
ABR103
ABR103
S
D
T2
T3
T2
T3
T2
T3
ABR123
ABR123
ABR123
ABR129
ABR129
ABR129
ABR129
ABR129
ABR129
ABR138
ABR138
ABR138
ABR138
ABR138
ABR138
S
D
T3
T2
T3
T2

Figure 34

Figure 34

S- and D-subgenome 35S rRNA gene expression ratio in *B. hybridum* genotypes ABR113, 3-7-2 and 2.2.2 at different developmental stages.

A. Quantification of D- and S-subgenome 35S pre-rRNA transcripts in different tissues of genotypes ABR113, 3-7-2, and 2.2.2 using primers specific to *B. distachyon* and *B. stacei* ITS1 region.

B. Standard deviation calculation based on three biological replicates. No significant differences were observed between the values indicated by the same letter. Due to the high standard deviation in the leaves of the 2.2.2 line (marked with *), these values were excluded from the statistical analysis.

Orange colour – Bs-like rRNA gene expression.
Grey colour – Bd-like rRNA gene expression.
d – days
w – weeks
Adv. roots – adventitious roots

A

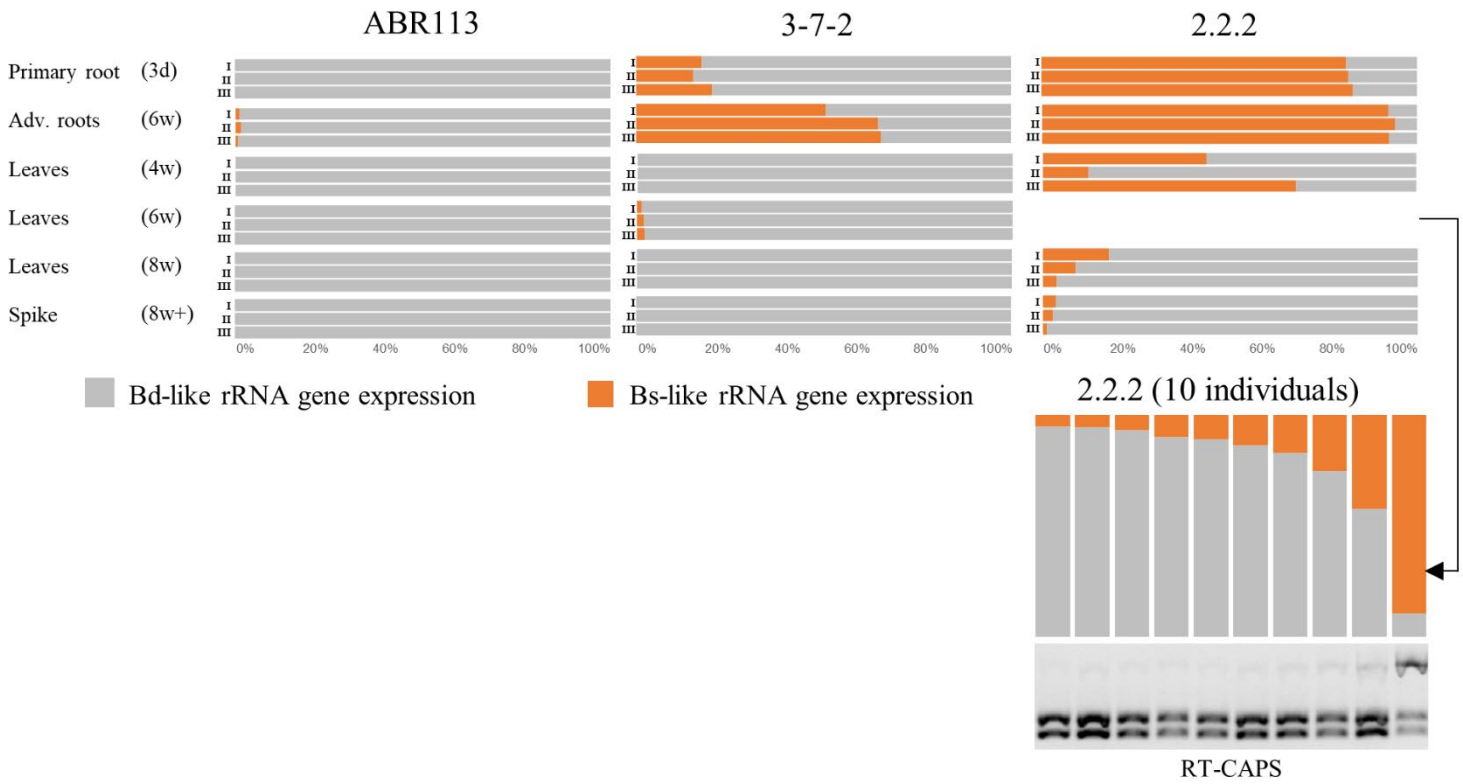

B

	ABR113	3-7-2	2.2.2
Primary root (3d)	D-genome only	1:0.21 ±0.037[a]	1:5.36 ±1.65[a]
Adv. Roots (6w)	1:0.011 ±0.003	1:1.5 ±0.47[b]	1:13.36 ±2.14[b]
Leaves (4w)	D-genome only	D-genome only	1:0.61 ±1*
Leaves (6w)	D-genome only	1:0.018 ±0.003[c]	1:0.15 ±0.38* (3 replicates) 1:0.27 ±0.39*
Leaves (8w)	D-genome only	D-genome only	1:0.93 ±0.089*
Spike (8w+)	D-genome only	D-genome only	1:0.022 ±0.013[d]

4.6. DNA methylation analysis of the 35S rDNA in selected *B. hybridum* genotypes using Southern blot hybridisation.

In order to establish the DNA methylation status of ancestral 35S rDNA units in different *B. hybridum* genotypes, the Southern blot hybridisation with 25S rDNA as a probe on the gDNAs subjected to restriction with methylation-sensitive enzyme *Pst*I was applied. Overall, one *B. distachyon* genotype Bd21, two *B. stacei* genotypes Bsta5 and ABR114 and eight *B. hybridum* genotypes: ABR113, 3-7-2, 2.2.2, 12.23.2, 3.4.2, 10.11.2, 10.19.5, 28.29, 24.1 and ABR132 were analysed. The *B. distachyon* and *B. stacei* genotypes were used as controls. *Pst*I restriction maps of the 35S rDNA units of *B. distachyon* and *B. stacei* are presented in Figure 4 in the Materials and Methods section. Only *B. hybridum* genotypes 2.2.2 and 3.4.2 showed the presence of the S-subgenome unmethylated 35S rDNA units. No S-subgenome bands corresponding to the unmethylated 35S rDNA units were observed in the other analysed genotypes (Figure 35A).

To verify whether DNA methylation affects the rRNA gene expression, total gDNA was also isolated from the plants in which the expression of 35S rRNA genes at various stages of ontogenesis was analysed (genotypes ABR113, 2.2.2, and 3-7-2) and subjected to *Pst*I digestion. As shown in Figure 35A, genotype ABR113 lacks the S-subgenome unmethylated 35S rDNA in all studied tissues, confirming that methylation of 35S rDNA units is correlated with the absence of their expression. In contrast, in the case of all studied tissues of genotype 2.2.2, the S-subgenome unmethylated rDNA units were observed. Among genotype 3-7-2 and ABR113, only gDNA isolated from adventitious roots of genotype 3-7-2 showed the presence of the S-subgenome unmethylated rDNA units (Figure 35B). In all tissues and genotypes, the presence or absence of DNA methylation correlated with the expression of 35S rRNA genes.

The analysis of methylation in the gDNA of leaves isolated from eight individuals of the *B. hybridum* genotype 2.2.2 revealed the presence of an unmethylated fragment resembling *B. stacei* in all of the individuals examined (as shown in Figure 35C).

Figure 35

Figure 35

DNA methylation analysis of the 35S rDNA homoeologues in eight *B. hybridum* genotypes.

A. Southern blot hybridisation of the gDNAs from *B. distachyon* (Bd21), *B. stacei* (Bsta5, ABR114) and the eight *B. hybridum* genotypes (ABR113, 12.23.2, 3.4.2, 10.11.2, 10.19.5, 28.29, 24.1 and ABR132) digested with *Pst*I.
B. Southern blot hybridisation of the gDNAs from *B. hybridum* genotypes ABR113, 3-7-3, 2.2.2 digested with *Pst*I. The gDNAs subjected to restriction were isolated at different stages of *B. hybridum* development: 6-week-old adventitious roots, 4-week-old leaves, 6-week-old leaves and 8-week-old leaves.
C. Southern blot hybridisation of the gDNAs from *B. hybridum* genotype 2.2.2 digested with *Pst*I. The gDNAs were isolated from eight individuals (eight biological replicates) from the greenish leaves of 6-week-old plants.

S – S-subgenome unmethylated component after *Pst*I treatment.
D – D-subgenome unmethylated component after *Pst*I treatment.
AR – adventitious root
L – leaf
w – week
I-VIII – individual plants

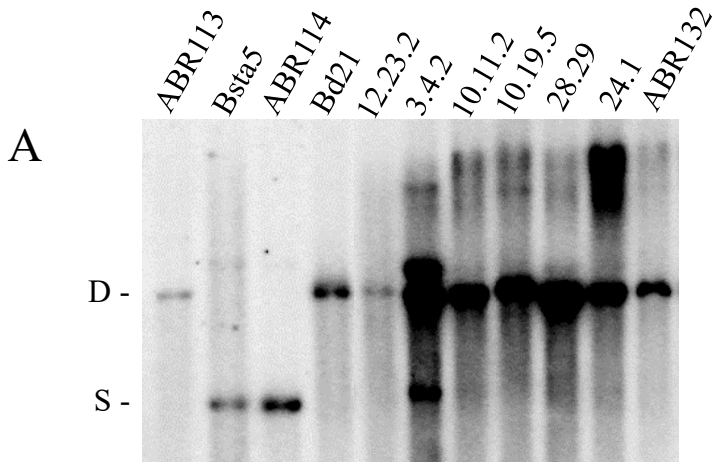

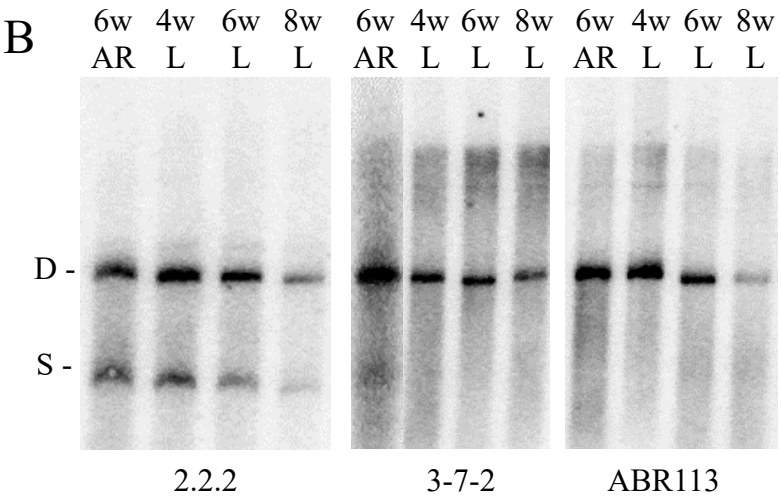

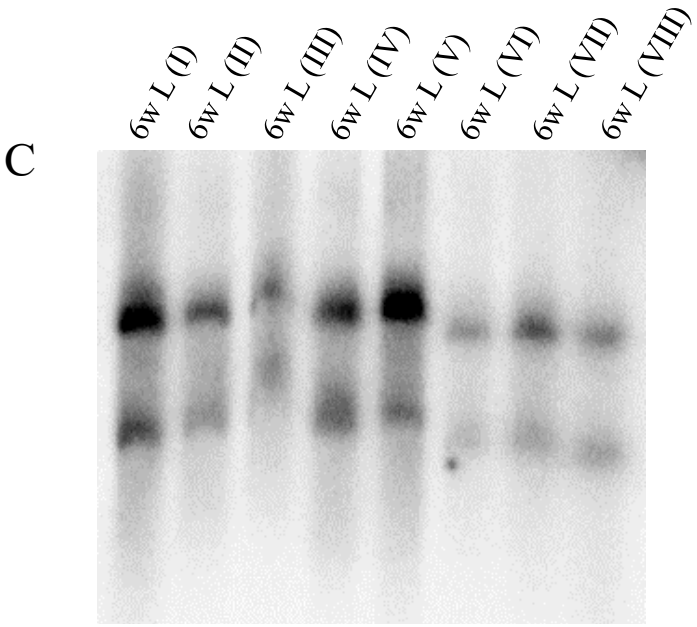

4.7. Geographical localisation of the selected *B. hybridum* genotypes across the annual average rainfall in Israel.

In order to discover a possible correlation between aridity level and S-subgenome rRNA gene expression, the GPS coordinates of selected *B. hybridum* genotype locations were set on the Israel map (see Figure 36). Overall, 41 collected *B. hybridum* genotypes were placed on the aridity map – 1.12.1, 1.24.1, 2.2.2, 2.6.1, 3.4.2, 3.16.1, 4.5.2, 5.6.5, 5.8.3, 6.5.1, 7.19.2, 7.27.1, 8.5.4, 8.8.2, 9.1.3, 9.7.6, 10.11.2, 10.19.5, 11.24.1, 12.5.3, 12.23.2, 13.3.5, 13.19.2, 14.2.2, 15.3.1, 16.2.5, 18.5.2, 18.6.1, 19.16.5, 21.7.2, 21.11.1, 23.101, 24.1, 24.3, 26.12, 26.24, 28.28, 28.29, 29.3, 29.5, 31.8. The genotypes that were analysed encompassed all of the primary aridity zones in Israel. *B. hybridum* genotypes with S-subgenome rDNA expression exceeding 10% in adventitious roots were located in different aridity zones, implying that aridity level does not seem to affect the nucleolar dominance in *B. hybridum*.

Figure 36

Figure 36

Geographical localisation of selected *B. hybridum* genotypes along aridity gradient in Israel.

Rainfall data represent mean (mm) for the 1981-2010 years.

Blue stars – *B. hybridum* genotypes with S-subgenome rDNA expression exceeding 10% in adventitious roots.

The population number on the map corresponds to the first number in the genotype name; e.g., **1** on the map of Israel corresponds to the collection site of genotypes **1**.12.1 and **1**.24.1.

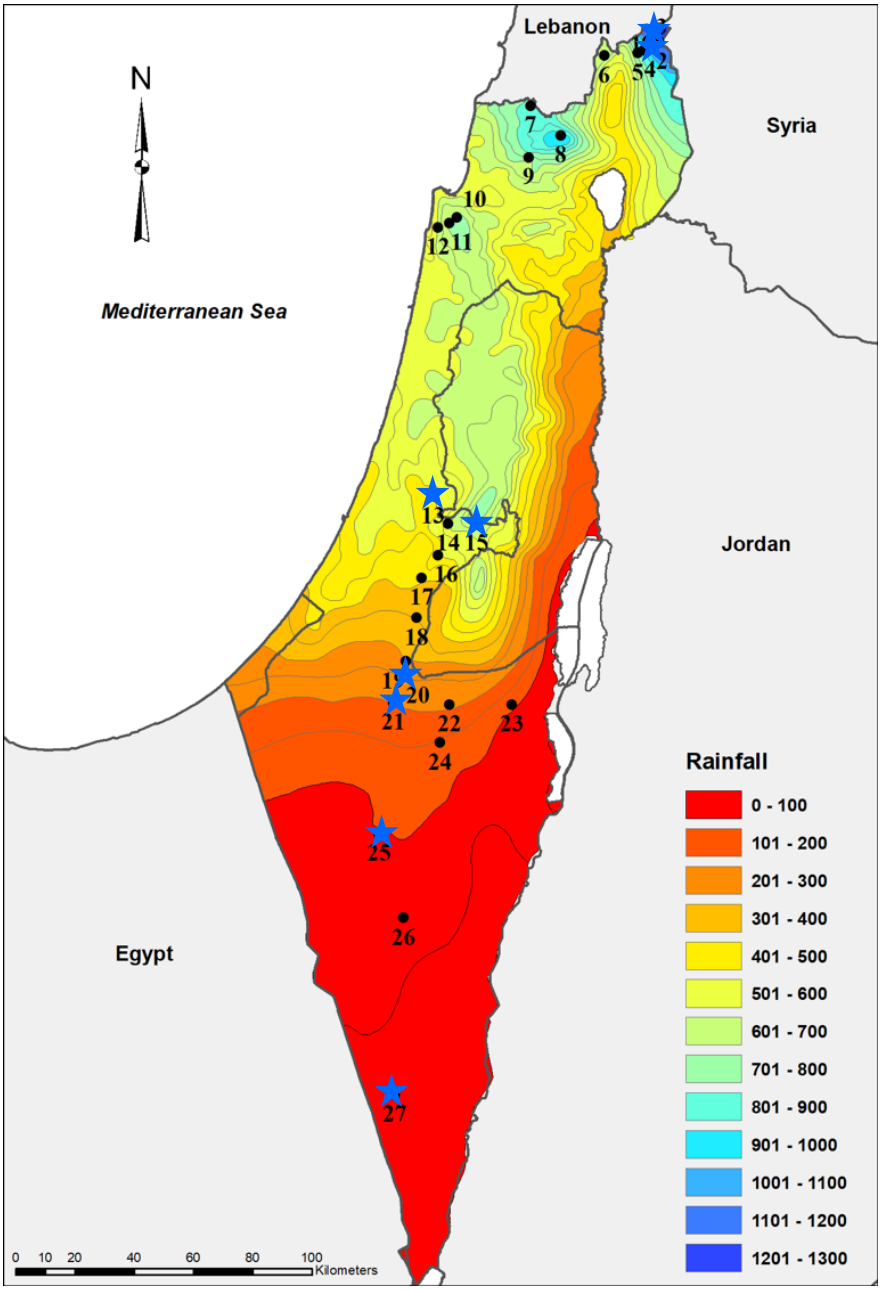
Lebanon
Syria
Jordan
Egypt
Mediterranean Sea
N
Rainfall
0 - 100
101 - 200
201 - 300
301 - 400
401 - 500
501 - 600
601 - 700
701 - 800
801 - 900
901 - 1000
1001 - 1100
1101 - 1200
1201 - 1300
0 10 20 40 60 80 100
Kilometers

5. DISCUSSION

5.1. The evolution of the ancestral 35S rDNA homoeologues in different *B. hybridum* genotypes.

The evolutionary history of the 35S rDNA homoeologues in allopolyploids can be accompanied by various scenarios (Volkov et al., 2007), including (i) the maintenance of both rDNA homoeologues without changes (Volkov et al., 2003); (ii) the elimination or conversion of the rDNA units of one ancestral species resulting in the uniparental inheritance (Wendel et al., 1995; Kotseruba et al., 2003); and (iii) the uniparental inheritance followed by structural changes that give rise to new rDNA families (Kovarik et al., 2008; Borowska-Zuchowska et al., 2020). To better understand the 35S rDNA evolutionary pathways in *B. hybridum*, the number, chromosomal localisation, and ancestral contributions of these rRNA gene loci were determined in the genotypes originating from different geographical locations, including the natural habitats in Israel.

In most analysed genotypes (49 out of 50), FISH with 25S rDNA as a probe showed the presence of two chromosomal pairs bearing the 35S rDNA loci. The diploid species that resemble the ancestors of *B. hybridum* – *B. distachyon* and *B. stacei* – possess one 35S rDNA locus and one 5S rDNA locus per genome (Hasterok et al., 2004; Lusinska et al., 2018). Thus, most of the *B. hybridum* genotypes studied in this work had the sum of the rDNA loci expected from the numbers present in the putative ancestors. These results were further supported by the Southern blot hybridisation and gCAPS screening, in which both the D- and S-subgenome 35S rDNA homoeologues were detected in all but one of the studied *B. hybridum* genotypes.

An example of the first scenario of the 35 rDNA homoeologues evolution in allopolyploids – the maintenance of both rDNA homoeologues without detectable changes – can be demonstrated by seven *B. hybridum* genotypes, which showed very intense 25S rDNA FISH signal corresponding to the *B. stacei*-like rDNA and includes two ABR genotypes and five genotypes originated from Israel. This scenario is also supported by the observation that genotypes ABR132 and 3.4.2 have comparable proportions of D- and S-subgenome 35S rDNA, as was shown by bioinformatic analysis, gCAPS and Southern hybridisation. These suggest no gradual elimination of the S-subgenome 35S rDNA in these genotypes.

The second scenario describing the elimination or conversion of the rDNA units of one ancestral species resulting in uniparental inheritance was observed in most of the

investigated genotypes (42 out of 50) and was characterised by D-subgenome chromosomes having more intense 25S rDNA hybridisation signals than S-subgenome ones. Interestingly, the hybridisation signals corresponding to S-subgenome 35S rDNA were barely visible in some studied accessions. This observation was further supported by the Southern blot hybridisation with the 25S rDNA as a probe, in which the S-subgenome 35S rDNA contribution accounted for less than half of the total rDNA in the genotypes representing this evolutionary scenario. Previous studies on different *B. hybridum* genotypes, including the reference line ABR113, also revealed the presence of substantially smaller FISH signals corresponding to 35S rDNA loci of the S-subgenome (Borowska-Zuchowska et al., 2016; Borowska-Zuchowska et al., 2020), suggesting a reduction in the copy number of the under-dominant *B. stacei*-inherited rRNA genes. The quantification of 35S rDNA homoeologues in different *B. hybridum* genotypes also showed that the contribution of the S-subgenome 35S rDNA units varied from 7% in genotype ABR100 to 39% in genotype ABR101 (Borowska-Zuchowska et al., 2020). Moreover, the fact that genotype 10.19.5 has almost all of the IGS reads from the D-subgenome could indicate that the 35S rDNA in this genotype is predominantly derived from the D-subgenome.

The removal of S-subgenome rDNA units may still be in progress in some *B. hybridum* genotypes, and the variability in 35S rDNA signal intensity among genotypes can be explained by the differences in the number of S-subgenome units presented in the *B. hybridum* genome (Borowska-Zuchowska et al., 2020). The gradual elimination of the under-dominant rDNA units is most likely related to the diploidisation of allotetraploid *B. hybridum* (Baduel et al., 2018). Such a difference in the ratio of D- and S-subgenome rDNA units may be explained by the polyphyletic origin of *B. hybridum*. It is assumed that *B. hybridum* arose at least two times as a result of crosses between two ancestral species that resemble modern *B. distachyon* and *B. stacei* that took place between ~1.4 and ~0.14 million years ago (Lopez-Alvarez et al., 2012; Díaz-Pérez et al., 2018; Gordon et al., 2020). The reduction of the under-dominant 35S rDNA loci was also shown in different allopolyploid species that belong to genera such as *Nicotiana* (Dadejova et al., 2007; Volkov et al., 2007; Kovarik et al., 2008), *Tragopogon* (Dobesova et al., 2015; Huska et al., 2016) and *Brassica* (Książczyk et al., 2011; Sochorova et al., 2017).

In one studied genotype (12.23.2 from Israel), the 25S rDNA FISH signal was observed in one pair of chromosomes from the D-subgenome, while the Bs6 chromosome

inherited from *B. stacei* did not exhibit any signal. Therefore, the FISH image of this genotype displayed a unique pattern, wherein only one pair of chromosomes carried the 35S rDNA loci. Distinct rDNA knobs were positioned at the ends of the D-subgenome secondary constrictions. gCAPS showed the presence of the S-subgenome rDNA remnants in this accession. Bioinformatic analysis of the Illumina raw reads allowed to estimate the approximate 35S rDNA homoeologue ratio in this *B. hybridum* genotype. According to the reads count, S-subgenome 35S rDNA comprised as little as 1.6 % of the total 35S rDNA reads. This result is in congruence with data provided by FISH and gCAPS experiments. At least one more *B. hybridum* genotype, ABR117, also showed a lack of S-subgenome rDNA FISH signal, as shown by Hasterok et al. (2004) and Borowska-Zuchowska et al. (2016). Further studies on ABR117 revealed the presence of some S-subgenome 35S rDNA units (one S-subgenome 35S rDNA family out of two that were present in other *B. hybridum* accessions) that accounted for as little as 8% of the total rDNA, which was probably below the resolution of the FISH method (Borowska-Zuchowska et al., 2020). Analysis of gCAPS data obtained from *B. hybridum* genotype ABR117 showed the presence of an S-subgenome ITS1, and Southern blot also demonstrated a signal corresponding to S-subgenome rDNA homoeologue (Borowska-Zuchowska et al., 2020).

Also, in the case of genotype 12.23.2, the Southern blot hybridisation demonstrated one rDNA family, meaning a single cut with *Bgl*II within the repeated unit. The contribution of this rDNA component accounted for 22% of the total rDNA, which did not corroborate the results obtained by FISH, gCAPS and bioinformatic analysis for the S-subgenome 35S rDNA. This can be explained through an intergenomic transfer of S-subgenome rDNA to the *B. distachyon*-derived 35S rDNA loci and structural alterations leading to the emergence of a new rDNA family. An analogous process was described by Kovarik et al. (2008) and Clarkson et al. (2005) in evolutionary old *Nicotiana* allopolyploids. Interestingly, the length of the new rDNA family revealed by Southern blot was comparable but not the same as the S-subgenome rDNA. It was further supported by the bioinformatic analysis of the Illumina reads, which showed low reads coverage in the S-subgenome IGS region in 12.23.2. It can be speculated that this new rDNA family is now located in this heterochromatic knob on chromosomes from the D-subgenome.

However, further experiments are required to investigate the structure of the 35S rDNA loci in genotype 12.23.2. For example, it may be necessary to design primers

specific to the NTS of the S-subgenome 35S rDNA to create a *B. stacei*-specific probe. Subsequent FISH experiments using this probe would then allow to detect the S-subgenome 35S rDNA signal located on chromosomes resembling those of *B. distachyon*. Such signal distribution may indicate the intergenomic transfer of rDNA loci between chromosomes belonging to different ancestors. To explore the structure of 35S rDNA loci in genotype 12.23.2, an alternative approach would be to perform PacBio long-read sequencing of the complete 35S rDNA units derived from both ancestral species.

Interestingly, the diploid *B. stacei* genotypes Bsta5 and ABR114 exhibited different restriction patterns. The observed variation in restriction patterns after *Bgl*II digestion between both genotypes can be attributed to distinct rDNA families. Since differences in the DNA sequence at the recognition sequence can lead to specific cleavage patterns, differences in restriction patterns between ABR114 and Bsta5 may suggest different evolution of 35S rDNA loci in these genotypes.

Overall, these findings demonstrate the utility of FISH, Southern blot, gCAPS and Illumina sequencing data in investigating the structure of rDNA units in *B. hybridum* and providing insights into the origin and evolution of 35S rDNA in this species. However, further studies, including long-read sequencing capable of covering the whole rDNA unit, are needed to fully understand the mechanisms underlying the observed differences in rDNA unit structure and elucidate their functional implications.

5.1.1. Homogeneity of ITS1 and 18S rDNA in *B. stacei* and *B. hybridum*.

The homogeneity analysis of ITS1 and 18S rDNA regions overall showed a higher level of similarity in the ITS1 region of *B. stacei* compared to the *B. stacei*-derived ITS1 in *B. hybridum*. In *B. hybridum* (at least in the genotypes analysed in this study), S-subgenome 35S rDNA was suppressed in most analysed tissues. However, in the diploid like *B. stacei,* the rRNA genes cannot be suppressed since they are housekeeping genes. Thus, the lower homogeneity level in the *B. stacei*-derived 35S rDNA in *B. hybridum* may be connected with the accumulation of mutations in the rDNA units that are not transcribed. Therefore, the ITS1 in *B. stacei* is somewhat more homogeneous. The 18S rDNA sequence was found to be more homogeneous in both species. Such distribution pattern of SNPs in the rDNA units, where the 18S rDNA region is significantly more conserved than the non-coding ITS1 sequence, has been observed in various plants, including *A. thaliana* (Rabanal et al., 2017) and *Nicotiana* species (Lunerová et al., 2017).

The presence of 11 SNPs in the coding region of 18S rDNA in one of the *B. stacei*-like clones of *B. hybridum* genotype 2.2.2 suggested that this rDNA unit accumulated mutations and became a pseudogene. Escape from concerted evolution was also observed in rDNA sequences of *Cycas revoluta* and transmembrane gene *CEACAM32* in cattle (*Bos taurus*) (Wang et al., 2016; Hänske et al., 2020).

It is essential to highlight that the distribution of SNPs was not consistent across the coding and non-coding subregions (Subramanian and Kumar, 2003). Specifically, the ITS1 sequence displayed a significantly higher number of SNPs, which is expected because this sequence evolves faster than coding regions. Interestingly, this finding contradicts the results of rDNA studies conducted on *C. revoluta*, where mutations impacting the numerous pseudogenes were observed at similar frequencies in both the coding and non-coding regions (Wang et al., 2016). However, the authors specify that the case of *C. revoluta* rDNA pseudogenisation is rather an exception among studied species. The pseudogene clone found in *B. hybridum* genotype 2.2.2 may represent an example of an rDNA pseudogene in plants, and further investigation is needed to determine its evolutionary origin and implications for the homogenisation of rDNA in this genotype. The low levels of SNPs observed in the 18S region of both species suggest that this region is highly conserved.

ITS1 and 18S region analysis provides insights into the homogeneity of rDNA regions in closely related plant species and highlights the need for further investigation into the evolutionary mechanisms underlying rDNA variability. The results have implications for using rDNA regions as molecular markers and provide a foundation for future studies investigating the evolution and diversity of these regions in related species (Delorme-Hinoux et al., 2023).

5.2. Developmental regulation of ND in *B. hybridum*

ND is a tissue-specific phenomenon likely to rely on the current tissue demands in ribosomal synthesis (Brombin et al., 2015). The expression of 35S rRNA genes is significantly higher in root and callus than in mature leaves in *Nicotiana* (Koukalova et al., 2005). The same expression imbalance was observed in *Tragopogon*: callus, root and flower bud showed higher levels of 35S rRNA expression than old and young leaves (Dobesova et al., 2015). Fluctuations in ND stability were observed in different organs of *B. napus* (AACC, where C genome derived from *B. oleracea* and A genome from

B. rapa), where usually absent *B. oleracea*-derived rRNA transcripts were detected in floral buds, sepals, petals, anthers and siliques (Chen and Pikaard, 1997b) and lack of ND in roots from 3-day-old seedlings (Hasterok and Maluszynska, 2000). Variations in the stability of ND were also noticed in *Solanum* allopolyploids with activation of under-dominant rDNA in anthers and calli (Komarova et al., 2004). Well-studied model dicot allopolyploid *Arabidopsis suecica* demonstrates that the ND is absent during embryogenesis but becomes well noticeable during early postembryonic development in shoot and root apical meristems (Pontes et al., 2007). However, the establishment of ND in monocotyledonous allopolyploids appears to follow a distinct developmental regulation of ND. In wheat × rye F1 hybrids, the 35S rRNA genes derived from rye undergo transcriptional repression between the fourth and fifth days after fertilisation, as observed in the study conducted by Castilho et al. (1995). Such establishment of ND takes place considerably earlier than in the case of the dicot *A. suecica*. Overall, due to the complexity of genomes harbouring numerous rDNA loci, ND investigation in monocots is incomplete and mainly limited to several works done on wheat (Guo and Han, 2014; Mirzaghaderi et al., 2017; Tulpová et al., 2022).

In *B. hybridum* reference genotype ABR113, the ND was detected in primary roots, leaves, the prophase I meiocytes, microspores, and at different stages of embryo development (Idziak and Hasterok, 2008; Borowska-Zuchowska et al., 2019; Borowska-Zuchowska et al., 2020). In genotype 3-7-2 from Turkey, the developmental regulation of ND was shown for the first time in this species – the transcriptional activity of the S-subgenome 35S rDNA loci occurred in the primary and adventitious roots. In this work, ND abolishment in the adventitious roots was also shown in about half of the genotypes analysed. It is worth noting that S-subgenome 35S rRNA gene activation appears to be independent of the S-subgenome rDNA contribution to the total rDNA. In a study conducted by Borowska-Zuchowska et al. (2020), genotypes ABR113 and ABR137 exhibited an equal amount of S-subgenome 35S rDNA homoeologues in the *B. hybridum* genome as shown by Southern blot hybridisation. RT-CAPS analysis of the leaves showed the presence of ND in both genotypes. However, this study has broadened this analysis and demonstrates a notable difference: the ABR113 genotype lacks observable (by RT-CAPS) *B. stacei*-derived 35S pre-rRNA transcripts, while ABR137 exhibits a prominent expression of S-subgenome 35S rRNA genes. Thus, the ND in this allotetraploid may be independent of the ancestral 35S rDNA contributions.

Although RT-CAPS analysis on the reference line ABR113 did not detect the S-subgenome 35S rDNA activity in the adventitious roots, research conducted on the same tissue using RT-qPCR revealed a detectable level of S-subgenome 35S rRNA gene expression, accounting for approximately 1.5% of the total pre-rRNA. It seems that RT-CAPS cannot detect such a low level of expression due to the sensitivity limitation of the technique. In contrast, the remaining tissues from genotype ABR113 demonstrated the absence of S-subgenome pre-rRNA transcripts even if the RT-qPCR was used, showing a strong ND in this genotype.

Interestingly, the RT-qPCR analysis of adventitious roots in genotypes 2.2.2 and 3-7-2 revealed a higher S-subgenome pre-rRNA level than all other tissues examined. Similar observations were made in the *Urochloa* H1863 hybrid, where the expression of the dominant *U. brizantha* 45S rRNA gene was detected in the leaves. However, the 45S rRNA genes from *U. brizantha* and *U. ruziziensis* were expressed in the roots, indicating a codominant expression pattern from both parental genomes (Santos et al., 2020). *B. hybridum* genotype 3-7-2 exhibited expression of *B. stacei*-derived 35S rRNA in both primary and adventitious roots. This finding aligns with the experimental data presented by Borowska-Zuchowska et al. (2021). However, in this study, the RT-CAPS technique failed to detect S-subgenome expression in leaf tissue. Nonetheless, RT-qPCR revealed minimal expression, constituting up to 2% of the total pre-rRNA transcripts, exclusively in the leaves from 6-week-old plants. The rest of the leaf and spike tissues showed the presence of strong ND in genotype 3-7-2.

A more interesting picture was observed in genotype 2.2.2, where the primary and adventitious roots demonstrated the prevalence of S-subgenome rRNA gene expression over D-subgenome ones. The leaf analysis showed a different picture of *B. stacei*-derived 35S rRNA gene expression in each individual analysed. These results show an interesting case of individual- and tissue-specific ancestral rRNA gene expression patterns. A similar difference in leaf expression patterns was also observed in the experiment conducted by Sochorova et al. (2017), where among 13 cultivars of *Brassica napus,* only in the leaf tissue of cultivar 'Norin 9' ND was abolished, and both *B. rapa*- and *B. oleracea*-derived rRNA genes were active.

35S rRNA genes can be silenced through repressive epigenetic modifications or irreversibly inactivated through the accumulation of mutations, which leads to pseudogenisation. A good illustration of this process can serve a gymnosperm *C. revoluta* where inactive rDNA units (~80% from all rRNA genes) were pseudogenised and

uniformly accumulated mutations in both non-coding and coding regions (Wang et al., 2016). Borowska-Zuchowska et al. (2020) investigated the potential occurrence of under-dominant S-subgenome 35S rDNA pseudogenisation in the *B. hybridum* genotype ABR113. Their findings revealed no evidence of pseudogenisation within this specific genotype. However, SNPs were distributed non-uniformly in the non-coding ITS1 sequence and coding part of 18S rDNA of both *B. hybridum* and *B. stacei*. It is common for plant rDNA that non-coding sequences are under weaker selection pressure and could accumulate a higher number of SNPs (Rosato et al., 2016). Wet-lab haplotypic analysis demonstrated that *B. stacei*-derived 18S rRNA genes are highly conserved and homogenous in the ABR113 genotype of *B. hybridum* but still capable of transcriptional activation only in adventitious roots and at a very low level. This data implies that pseudogenisation is probably not a mechanism of ND in *B. hybridum*. To confirm this conclusion, additional studies are required. For example, long-read sequencing of the entire 35S rDNA unit variants in different accessions of *B. hybridum* would allow verifying if the under-dominant S-subgenome rRNA genes are pseudogenised or not.

5.3. DNA methylation analysis of rDNA units in *B. hybridum* genotypes.

Previous studies indicated that DNA methylation has a significant function in the epigenetic mechanism that controls the rRNA gene dosage and ND (Lawrence et al., 2004; Pontes et al., 2007). Distinct DNA methylation patterns in the 35S rDNA homoeologues of *B. hybridum* were identified using a *Pst*I restriction enzyme capable of identifying methylated cytosine in the CHG context. All *B. hybridum* genotypes analysed demonstrated an observable band on the membrane representing the unmethylated fraction of rRNA genes from the D-subgenome. The presence of the band from the D-subgenome does not imply that all genes are in a demethylated state – only a fraction of 35S rRNA genes from the rDNA locus are expressed (Lawrence et al., 2004). In contrast, in most of the tested genotypes, the band from the S-subgenome was not visible, which proves that the *B. stacei*-inherited units were strongly methylated. The presence of demethylated S-subgenome 35S rDNA loci was positively correlated with their transcription, e.g., genotype 3.4.2 showed the presence of S-subgenome unmethylated 35S rDNA in leaves and genotype 3-7-3 in adventitious roots. The most interesting *B. hybridum* genotype 2.2.2 demonstrated a lack of S-subgenome 35S rDNA methylation in all tissues analysed. All methylation data is congruent with expression data obtained

by RT-CAPS and RT-qPCR techniques and showed that DNA methylation plays a vital role in ND regulation in *B. hybridum*. These findings align with previous studies on various plant hybrids and allopolyploids, which have demonstrated that the presence of DNA methylation often leads to the 35S rRNA gene repression (Vieira et al., 1990b; Komarova et al., 2004; Costa-Nunes et al., 2010; Guo and Han, 2014; Dobesova et al., 2015).

Using molecular cytogenetic methods, Borowska-Zuchowska and Hasterok (2017) showed DNA methylation patterns of the 35S rDNA loci in several *B. hybridum* genotypes, including reference ABR113. Intriguingly, it was also observed that the S-subgenome rDNA units did not undergo reactivation even after global hypomethylation induced by 5-azacytidine (Borowska-Zuchowska and Hasterok, 2017). This indicates that DNA hypomethylation is insufficient for ND abolishment in genotype ABR113. Differences between the DNA methylation patterns between the D- and S-subgenome 35S rDNA were also observed in this work. The repressed S-subgenome units exhibited significantly higher levels of DNA methylation than the D-subgenome ones. The same picture was observed in several different *B. hybridum* genotypes by Borowska-Zuchowska et al. (2020). A similar situation was reported by Lawrence et al. (2004) in *A. thaliana*, where coordinated alterations in the density of cytosine methylation within promoters and distinct modifications of histones play an essential role in the regulation of the 45S rRNA gene expression and, thus, ND establishment and maintenance.

The S-subgenome rRNA gene expression data in ten *B. hybridum* individuals belonging to genotype 2.2.2 showed a 10-fold variation in expression intensity. However, Southern blot results with methylation-sensitive enzymes on the same eight individuals showed S-subgenome bands corresponding to unmethylated units that were similar in size in all analysed plants. This implies that the S-subgenome rRNA gene expression level is probably not fully correlated with the methylation rate in this genotype; however, it still proves that methylation plays a vital role in ND in *B. hybridum*.

5.4. ND in *B. hybridum* is independent of the maternal effect.

Most angiosperm inheritance patterns of chloroplast genomes are non-Mendelian, with maternal inheritance being predominant (Park et al., 2021). Concerning ND research, ND seems independent of maternal effect as it was shown for many polyploids, e.g., *B. napus*, where Chen and Pikaard (1997b) investigated two lines derived from reciprocal crosses

and proved the lack of the maternal effect on ND. Similarly, in the *B. hybridum* chloroplast *trn*LF gene region, sequencing of different genotypes showed a *B. stacei*-derived chloroplast DNA in all genotypes analysed. This data implies a lack of maternal effect on ND in *B. hybridum* since, despite the same direction of the cross between ancestral species, the differential expression of 35S rDNA was shown in the analysed genotypes. The lack of maternal or paternal effect on ND in plants was already described in pioneer Navashin's work on *Crepis* hybrids (Navashin, 1934). In monocots, the lack of maternal or parental effects was also described in wheat × *Aegilops* hybrids (Mirzaghaderi et al., 2017). Chen and Pikaard revealed that ND is independent of maternal effect and genome dosage in *Brassica* species (Chen and Pikaard, 1997b). The lack of maternal effect in ND is also a feature of animal species. For example, ND establishment was independent of maternal effect in *Drosophila* and whiptail lizards *Cnemidophorus* (Reeder and Roan, 1984; Ward and Cole, 1986; Eickbush et al., 2008). However, one example of the influence of the maternal effect on ND establishment is described in the literature since Jupe and Zimmer (1993) findings provided molecular proof of ND in the maize hybrid B73 × Mo17. When inbred line B73 was employed as the maternal contributor in hybrid creation, roughly 80% of the pre-rRNA transcripts belonged to B73. However, when Mo17 was utilised as the maternal contributor, around 85% of the pre-rRNA transcripts exhibited similarity to Mo17 hybridisation probes. These findings prove that the ND in maize hybrids can be attributed to the maternal effect.

The findings of this study support the accepted view that the ND phenomenon is independent of the maternal or paternal effect; even though the process of rRNA gene expression in the newly formed hybrid cell takes place in environments exceptionally enriched with maternal proteins, rRNA and associated small RNAs (Michalak et al., 2015).

6. CONCLUSIONS

1. *B. hybridum* is a good model for ND studies because of its allopolyploid nature and the presence of single chromosomal pairs harbouring 35S rDNA from each ancestor in the majority of its genotypes.
2. ITS1 sequence demonstrates a higher level of homogeneity in *B. stacei* than the S-subgenome ITS1 in *B. hybridum*. 18S rDNA is more homogeneous than the ITS1 sequence in *B. hybridum* and *B. stacei*.
3. In most *B. hybridum* genotypes, the under-dominant S-subgenome 35S rDNA loci are gradually eliminated during evolution.
4. In genotype 12.23.2, the S-subgenome 35S rDNA is almost eliminated and most probably a new 35S rDNA family arose.
5. ND is a tissue-specific phenomenon in *B. hybridum*.
6. ND is more stable in leaves than in the roots of studied *B. hybridum* genotypes. Additionally, the S-subgenome rRNA gene expression level is higher in adventitious than in the primary roots.
7. In some *B. hybridum* genotypes, ND can be a generation- and even individual-specific phenomenon.
8. DNA methylation plays a vital role in ND regulation in *B. hybridum*.
9. ND in *B. hybridum* is not a maternal-dependent phenomenon.
10. Aridity level does not affect the ND in *B. hybridum*.

7. SUMMARY

Nucleolar dominance (ND) describes an epigenetic uniparental silencing of 35S rRNA genes in plant hybrids and allopolyploids. Despite many years of research on ND, the mechanisms of this phenomenon are still poorly understood. Thus, this study primarily focuses on the molecular mechanisms underlying the selection of 35S rRNA genes set for repression in *Brachypodium hybridum*. This allotetraploid grass with a genome composition DDSS (D-subgenome from *B. distachyon*; S-subgenome from *B. stacei*) presents a valuable model for ND studies due to its compact genome and low content of repetitive sequences. The research aimed at population-level analysis of 35S rDNA loci in different *B. hybridum* accessions.

By employing the FISH technique, it was shown that most of the studied *B. hybridum* genotypes possess the sum of 35S rDNA loci as expected based on their number in its putative progenitors. Using Southern hybridisation and bioinformatic analysis, the contributions of rDNA homoeologues across different *B. hybridum* genotypes were evaluated, and the gradual elimination of the S-subgenome rDNA loci was shown in most studied genotypes. The expression patterns of 35S rDNA homoeologues at different developmental stages were examined through RT-qPCR with genome-specific primers and RT-CAPS. Expression data demonstrated that ND is a genotype-, generation-, tissue- and individual-specific phenomenon. Furthermore, the methylation status of rRNA genes was assessed in selected *B. hybridum* genotypes using Southern hybridisation on gDNA subjected to restriction with methylation-sensitive enzyme, showing an essential role of DNA methylation in ND maintenance.

The findings underline that ND in *B. hybridum* is developmentally regulated in some but not all genotypes. Moreover, it was shown that ND is independent of maternal effect. In corroboration with previous ND studies on *B. hybridum*, this study expands our knowledge of ND mechanisms and advances our understanding of the intricate interactions among gene expression, epigenetics, and population diversity. It also demonstrates the significance of *B. hybridum* as a model for deciphering the enigmatic phenomenon of ND.

8. STRESZCZENIE

Dominacja jąderkowa (ang. *nucleolar dominance*; ND) jest zjawiskiem o podłożu epigenetycznym, występującym u wielu mieszańców międzygatunkowych i allopoliploidów i polegającym na selektywnym wyciszeniu transkrypcyjnym genów 35S rRNA wywodzących się od jednego z gatunków ancestralnych. Pomimo wielu lat badań nad ND, mechanizmy stojące za tym zjawiskiem są wciąż słabo poznane. Dlatego też zasadniczym celem niniejszej pracy było zbadanie mechanizmów molekularnych leżących u podstaw preferencyjnego wyciszenia genów 35S rRNA na drodze ND u allotetraploidalnej trawy, *Brachypodium hybridum*. Gatunek ten charakteryzuje się składem genomowym DDSS (subgenom D z *B. distachyon*; subgenom S z *B. stacei*) i z racji małego genomu o niskiej zawartości sekwencji powtarzalnych stanowi cenny model do badań nad ND. Analizom poddano loci 35S rDNA u różnych genotypów *B. hybridum*, a badania prowadzono na poziomie populacyjnym.

Stosując technikę FISH wykazano, że większość badanych genotypów *B. hybridum* posiada liczbę loci 35S rDNA odpowiadającą sumie loci występujących w genomach domniemanych przodków. Stosując hybrydyzację Southerna i analizy bioinformatyczne określono udział homeologów 35S rDNA u różnych genotypów *B. hybridum*. Wykazano, że u większości badanych genotypów loci 35S rDNA z subgenomu S były stopniowo eliminowane w toku ewolucji. Ekspresję homeologów 35S rDNA badano na różnych etapach ontogenezy *B. hybridum* z wykorzystaniem metody RT-qPCR ze starterami genomowo-specyficznymi i RT-CAPS. Wykazano, że ND jest zjawiskiem zależnym od genotypu, pokolenia, tkanki, jak również osobnika. Ponadto badano metylację DNA w loci 35S rDNA u wybranych genotypów *B. hybridum* z wykorzystaniem hybrydyzacji Southerna na gDNA poddanym restrykcji enzymem wrażliwym na metylację DNA. Wykazano ważną rolę metylacji DNA w kształtowaniu ND u *B. hybridum*.

ND u *B. hybridum* okazała się być zależna od konkretnego etapu rozwoju rośliny jedynie w odniesieniu do niektórych genotypów. Ponadto wykazano, że ND występuje niezależnie od kierunku krzyżówki. Wyniki badań przedstawione w niniejszej pracy poszerzają wiedzę na temat podstaw molekularnych ND oraz skomplikowanych interakcji między ekspresją genów a mechanizmami epigenetycznymi na poziomie populacyjnym. Pokazują również, że *B. hybridum* może stanowić cenny model w zaawansowanych badaniach nad ND.

9. REFERENCES

Amado, L., Abranches, R., Neves, N., and Viegas, W. (1997). Development-dependent inheritance of 5-azacytidine-induced epimutations in triticale: analysis of rDNA expression patterns. *Chromosome Research* 5**,** 445-450.

Baduel, P., Bray, S., Vallejo-Marin, M., Kolář, F., and Yant, L. (2018). The "Polyploid Hop": Shifting Challenges and Opportunities Over the Evolutionary Lifespan of Genome Duplications. *Frontiers in Ecology and Evolution* 6.

Borisjuk, N.V., Davidjuk, Y.M., Kostishin, S.S., Miroshnichenco, G.P., Velasco, R., Hemleben, V., and Volkov, R.A. (1997). Structural analysis of rDNA in the genus *Nicotiana*. *Plant Molecular Biology* 35**,** 655-660.

Borowska-Zuchowska, N., and Hasterok, R. (2017). Epigenetics of the preferential silencing of *Brachypodium stacei*-originated 35S rDNA loci in the allotetraploid grass *Brachypodium hybridum*. *Scientific Reports* 7**,** 5260.

Borowska-Zuchowska, N., Kovarik, A., Robaszkiewicz, E., Tuna, M., Savaş Tuna, G., Gordon, S., Vogel, J.P., and Hasterok, R. (2020). The fate of 35S rRNA genes in the allotetraploid grass *Brachypodium hybridum*. *The Plant Journal* 103.

Borowska-Zuchowska, N., Kwasniewski, M., and Hasterok, R. (2016). Cytomolecular Analysis of Ribosomal DNA Evolution in a Natural Allotetraploid *Brachypodium hybridum* and Its Putative Ancestors-Dissecting Complex Repetitive Structure of Intergenic Spacers. *Frontiers in Plant Science* 7**,** 1499.

Borowska-Zuchowska, N., Mykhailyk, S., Robaszkiewicz, E., Matysiak, N., Mielanczyk, L., Wojnicz, R., Kovarik, A., and Hasterok, R. (2023). Switch them off or not: selective rRNA gene repression in grasses. *Trends in Plant Science* 28**,** 661-672.

Borowska-Zuchowska, N., Robaszkiewicz, E., Mykhailyk, S., Wartini, J., Pinski, A., Kovarik, A., and Hasterok, R. (2021). To Be or Not to Be Expressed: The First Evidence of a Nucleolar Dominance Tissue-Specificity in *Brachypodium hybridum*. *Frontiers in Plant Science* 12**,** 768347.

Borowska-Zuchowska, N., Robaszkiewicz, E., Wolny, E., Betekhtin, A., and Hasterok, R. (2019). Ribosomal DNA loci derived from *Brachypodium stacei* are switched off for major parts of the life cycle of *Brachypodium hybridum*. *Journal of Experimental Botany* 70**,** 805-815.

Boval, M., and Dixon, R.M. (2012). The importance of grasslands for animal production and other functions: a review on management and methodological progress in the tropics. *Animal* 6**,** 748-762.

Brombin, A., Joly, J.S., and Jamen, F. (2015). New tricks for an old dog: ribosome biogenesis contributes to stem cell homeostasis. *Current Opinion in Genetics & Development* 34**,** 61-70.

Cabrera, A., and Martín, A. (1991). Cytology and morphology of the amphiploid *Hordeum chilense* (4x) × *Aegilops squarrosa* (4x). *Theoretical and Applied Genetics* 81**,** 758-760.

Carvalho, A., Polanco, C., Guedes-Pinto, H., and Lima-Brito, J. (2013). Differential rRNA genes expression in bread wheat and its inheritance. *Genetica* 141**,** 319-328.

Castilho, A., Neves, N., Rufini-Castiglione, M., Viegas, W., and Heslop-Harrison, J.S. (1999). 5-Methylcytosine distribution and genome organization in triticale before and after treatment with 5-azacytidine. *Journal of Cell Science* 112**,** 4397-4404.

Castilho, A., Queiroz, A., Neves, N., Barao, A., Silva, M., and Viegas, W. (1995). The developmental stage of inactivation of rye origin rRNA genes in the embryo and endosperm of wheat × rye F1 hybrids. *Chromosome Research* 3**,** 169-174.

Catalán, P., Müller, J., Hasterok, R., Jenkins, G., Mur, L.A., Langdon, T., Betekhtin, A., Siwinska, D., Pimentel, M., and López-Alvarez, D. (2012). Evolution and taxonomic split of the model grass *Brachypodium distachyon*. *Annals of Botany* 109**,** 385-405.

Catalán, P., and Olmstead, R.G. (2000). Phylogenetic reconstruction of the genus *Brachypodium* P. Beauv. (Poaceae) from combined sequences of chloroplast *ndhF* gene and nuclear ITS. *Plant Systematics and Evolution* 220**,** 1-19.

Catalán, P., Shi, Y., Armstrong, L., Draper, J., and Stace, C.A. (1995). Molecular phylogeny of the grass genus *Brachypodium* P. Beauv. based on RFLP and RAPD analysis. *Botanical Journal of the Linnean Society* 117**,** 263-280.

Catalán, P., and Vogel, J.P. (2020). Advances on genomics, biology, ecology and evolution of *Brachypodium*, a bridging model grass system for cereals and biofuel grasses. *New Phytologist* 227**,** 1587-1590.

Chen, Z.J., Comai, L., and Pikaard, C.S. (1998). Gene dosage and stochastic effects determine the severity and direction of uniparental ribosomal RNA gene silencing

(nucleolar dominance) in *Arabidopsis* allopolyploids. *Proceedings of the National Academy of Sciences of the United States of America* 95**,** 14891-14896.

Chen, Z.J., and Pikaard, C.S. (1997a). Epigenetic silencing of RNA polymerase I transcription: a role for DNA methylation and histone modification in nucleolar dominance. *Genes & Development* 11**,** 2124-2136.

Chen, Z.J., and Pikaard, C.S. (1997b). Transcriptional analysis of nucleolar dominance in polyploid plants: biased expression/silencing of progenitor rRNA genes is developmentally regulated in *Brassica*. *Proceedings of the National Academy of Sciences of the United States of America* 94**,** 3442-3447.

Clarkson, J.J., Lim, K.Y., Kovarik, A., Chase, M.W., Knapp, S., and Leitch, A.R. (2005). Long-term genome diploidization in allopolyploid *Nicotiana* section *Repandae* (Solanaceae). *New Phytologist* 168**,** 241-252.

Consortium, T.I.W.G.S., Appels, R., Eversole, K., Stein, N., Feuillet, C., Keller, B., Rogers, J., Pozniak, C.J., Choulet, F., Distelfeld, A., Poland, J., Ronen, G., Sharpe, A.G., Barad, O., Baruch, K., Keeble-Gagnère, G., Mascher, M., Ben-Zvi, G., Josselin, A.-A., Himmelbach, A., Balfourier, F., Gutierrez-Gonzalez, J., Hayden, M., Koh, C., Muehlbauer, G., Pasam, R.K., Paux, E., Rigault, P., Tibbits, J., Tiwari, V., Spannagl, M., Lang, D., Gundlach, H., Haberer, G., Mayer, K.F.X., Ormanbekova, D., Prade, V., Šimková, H., Wicker, T., Swarbreck, D., Rimbert, H., Felder, M., Guilhot, N., Kaithakottil, G., Keilwagen, J., Leroy, P., Lux, T., Twardziok, S., Venturini, L., Juhász, A., Abrouk, M., Fischer, I., Uauy, C., Borrill, P., Ramirez-Gonzalez, R.H., Arnaud, D., Chalabi, S., Chalhoub, B., Cory, A., Datla, R., Davey, M.W., Jacobs, J., Robinson, S.J., Steuernagel, B., Van Ex, F., Wulff, B.B.H., Benhamed, M., Bendahmane, A., Concia, L., Latrasse, D., Bartoš, J., Bellec, A., Berges, H., Doležel, J., Frenkel, Z., Gill, B., Korol, A., Letellier, T., Olsen, O.-A., Singh, K., Valárik, M., Van Der Vossen, E., Vautrin, S., Weining, S., Fahima, T., Glikson, V., Raats, D., Číhalíková, J., Toegelová, H., Vrána, J., Sourdille, P., Darrier, B., Barabaschi, D., Cattivelli, L., Hernandez, P., Galvez, S., Budak, H., Jones, J.D.G., Witek, K., Yu, G., et al. (2018). Shifting the limits in wheat research and breeding using a fully annotated reference genome. *Science* 361**,** eaar7191.

Consortium, T.I.W.G.S., Mayer, K.F.X., Rogers, J., Doležel, J., Pozniak, C., Eversole, K., Feuillet, C., Gill, B., Friebe, B., Lukaszewski, A.J., Sourdille, P., Endo, T.R., Kubaláková, M., Číhalíková, J., Dubská, Z., Vrána, J., Šperková, R., Šimková,

H., Febrer, M., Clissold, L., Mclay, K., Singh, K., Chhuneja, P., Singh, N.K., Khurana, J., Akhunov, E., Choulet, F., Alberti, A., Barbe, V., Wincker, P., Kanamori, H., Kobayashi, F., Itoh, T., Matsumoto, T., Sakai, H., Tanaka, T., Wu, J., Ogihara, Y., Handa, H., Maclachlan, P.R., Sharpe, A., Klassen, D., Edwards, D., Batley, J., Olsen, O.-A., Sandve, S.R., Lien, S., Steuernagel, B., Wulff, B., Caccamo, M., Ayling, S., Ramirez-Gonzalez, R.H., Clavijo, B.J., Wright, J., Pfeifer, M., Spannagl, M., Martis, M.M., Mascher, M., Chapman, J., Poland, J.A., Scholz, U., Barry, K., Waugh, R., Rokhsar, D.S., Muehlbauer, G.J., Stein, N., Gundlach, H., Zytnicki, M., Jamilloux, V., Quesneville, H., Wicker, T., Faccioli, P., Colaiacovo, M., Stanca, A.M., Budak, H., Cattivelli, L., Glover, N., Pingault, L., Paux, E., Sharma, S., Appels, R., Bellgard, M., Chapman, B., Nussbaumer, T., Bader, K.C., Rimbert, H., Wang, S., Knox, R., Kilian, A., Alaux, M., Alfama, F., Couderc, L., Guilhot, N., Viseux, C., Loaec, M., Keller, B., and Praud, S. (2014). A chromosome-based draft sequence of the hexaploid bread wheat (*Triticum aestivum*) genome. *Science* 345**,** 1251788.

Copenhaver, G.P., and Pikaard, C.S. (1996). Two-dimensional RFLP analyses reveal megabase-sized clusters of rRNA gene variants in *Arabidopsis thaliana*, suggesting local spreading of variants as the mode for gene homogenization during concerted evolution. *The Plant Journal* 9**,** 273-282.

Costa-Nunes, P., Pontes, O., Preuss, S.B., and Pikaard, C.S. (2010). Extra views on RNA-dependent DNA methylation and MBD6-dependent heterochromatin formation in nucleolar dominance. *Nucleus* 1**,** 254-259.

Cuellar, T., Belhassen, E., Fernández-Calvín, B., Orellana, J., and Bella, J.L. (1996). Chromosomal differentiation in *Helianthus annuus* var. *macrocarpus*: heterochromatin characterization and rDNA location. *Heredity* 76**,** 586-591.

Dadejova, M., Lim, K.Y., Souckova-Skalicka, K., Matyasek, R., Grandbastien, M.A., Leitch, A., and Kovarik, A. (2007). Transcription activity of rRNA genes correlates with a tendency towards intergenomic homogenization in *Nicotiana* allotetraploids. *New Phytologist* 174**,** 658-668.

Delorme-Hinoux, V., Mbodj, A., Brando, S., De Bures, A., Llauro, C., Covato, F., Garrigue, J., Guisset, C., Borrut, J., Mirouze, M., Reichheld, J.-P., and Sáez-Vásquez, J. (2023). 45S rDNA Diversity In Natura as One Step towards Ribosomal Heterogeneity in *Arabidopsis thaliana*. *Plants* 12**,** 2722.

Díaz-Pérez, A., López-Álvarez, D., Sancho, R., and Catalán, P. (2018). Reconstructing the origins and the biogeography of species' genomes in the highly reticulate allopolyploid-rich model grass genus *Brachypodium* using minimum evolution, coalescence and maximum likelihood approaches. *Molecular Phylogenetics and Evolution* 127**,** 256-271.

Dobesova, E., Malinska, H., Matyasek, R., Leitch, A.R., Soltis, D.E., Soltis, P.S., and Kovarik, A. (2015). Silenced rRNA genes are activated and substitute for partially eliminated active homeologs in the recently formed allotetraploid, *Tragopogon mirus* (Asteraceae). *Heredity* 114**,** 356-365.

Dover, G. (1982). Molecular drive: a cohesive mode of species evolution. *Nature* 299**,** 111-117.

Doyle, J. (1991). "DNA Protocols for Plants," in *Molecular Techniques in Taxonomy,* eds. G.M. Hewitt, A.W.B. Johnston & J.P.W. Young. (Berlin, Heidelberg: Springer Berlin Heidelberg), 283-293.

Draper, J., Mur, L.a.J., Jenkins, G., Ghosh-Biswas, G.C., Bablak, P., Hasterok, R., and Routledge, A.P.M. (2001). *Brachypodium distachyon*. A New Model System for Functional Genomics in Grasses. *Plant Physiology* 127**,** 1539-1555.

Dydak, M., Kolano, B., Nowak, T., Siwinska, D., and Maluszynska, J. (2009). Cytogenetic studies of three European species of *Centaurea* L. (Asteraceae). *Hereditas* 146**,** 152-161.

Earley, K., Lawrence, R.J., Pontes, O., Reuther, R., Enciso, A.J., Silva, M., Neves, N., Gross, M., Viegas, W., and Pikaard, C.S. (2006). Erasure of histone acetylation by *Arabidopsis* HDA6 mediates large-scale gene silencing in nucleolar dominance. *Genes & Development* 20**,** 1283-1293.

Eickbush, D.G., Ye, J., Zhang, X., Burke, W.D., and Eickbush, T.H. (2008). Epigenetic Regulation of Retrotransposons within the Nucleolus of Drosophila. *Molecular and Cellular Biology* 28**,** 6452-6461.

Feldman, M., Galili, G., and Levy, A.A. (1986). "Genetic and Evolutionary Aspects of Allopolyploidy in Wheat," in *Developments in Agricultural and Managed Forest Ecology,* ed. C. Barigozzi. Elsevier, 83-100.

Flavell, R.B., and O'dell, M. (1976). Ribosomal RNA genes on homoeologous chromosomes of groups 5 and 6 in hexaploid wheat. *Heredity* 37**,** 377-385.

Frankel, O.H., Gerlach, W.L., and Peacock, W.J. (1987). The ribosomal RNA genes in synthetic tetraploids of wheat. *Theoretical and Applied Genetics* 75**,** 138-143.

French, S.L., Osheim, Y.N., Cioci, F., Nomura, M., and Beyer, A.L. (2003). In exponentially growing *Saccharomyces cerevisiae* cells, rRNA synthesis is determined by the summed RNA polymerase I loading rate rather than by the number of active genes. *Molecular and Cellular Biology* 23**,** 1558-1568.

Garcia, S., Cortés, P., Fernàndez, X., Garnatje, T., and Kovarik, A. (2016). Organisation, expression and evolution of rRNA genes in plant genomes. *Recent Advances in Pharmaceutical Sciences* VI**,** 49-75.

Garcia, S., Crhák Khaitová, L., and Kovařík, A. (2012). Expression of 5 S rRNA genes linked to 35 S rDNA in plants, their epigenetic modification and regulatory element divergence. *BMC Plant Biology* 12**,** 95.

Garcia, S., and Kovařík, A. (2013). Dancing together and separate again: gymnosperms exhibit frequent changes of fundamental 5S and 35S rRNA gene (rDNA) organisation. *Heredity* 111**,** 23-33.

Garcia, S., Panero, J.L., Siroky, J., and Kovarik, A. (2010). Repeated reunions and splits feature the highly dynamic evolution of 5S and 35S ribosomal RNA genes (rDNA) in the Asteraceae family. *BMC Plant Biology* 10**,** 176.

Gatti, M., Choulet, F., Macadré, C., Guérard, F., Seng, J.M., Langin, T., and Dufresne, M. (2018). Identification, Molecular Cloning, and Functional Characterization of a Wheat UDP-Glucosyltransferase Involved in Resistance to Fusarium Head Blight and to Mycotoxin Accumulation. *Frontiers in Plant Science* 9**,** 1853.

Gerlach, W.L., and Dyer, T.A. (1980). Sequence organization of the repeating units in the nucleus of wheat which contain 5S rRNA genes. *Nucleic acids research* 8**,** 4851-4865.

Gilbert, W. (1986). Origin of life: The RNA world. *Nature* 319**,** 618-618.

Glombik, M., Bačovský, V., Hobza, R., and Kopecký, D. (2020). Competition of Parental Genomes in Plant Hybrids. *Frontiers in Plant Science* 11.

Gordon, S.P., Contreras-Moreira, B., Levy, J.J., Djamei, A., Czedik-Eysenberg, A., Tartaglio, V.S., Session, A., Martin, J., Cartwright, A., Katz, A., Singan, V.R., Goltsman, E., Barry, K., Dinh-Thi, V.H., Chalhoub, B., Diaz-Perez, A., Sancho, R., Lusinska, J., Wolny, E., Nibau, C., Doonan, J.H., Mur, L.a.J., Plott, C., Jenkins, J., Hazen, S.P., Lee, S.J., Shu, S., Goodstein, D., Rokhsar, D., Schmutz, J., Hasterok, R., Catalan, P., and Vogel, J.P. (2020). Gradual polyploid genome evolution revealed by pan-genomic analysis of *Brachypodium hybridum* and its diploid progenitors. *Nature Communications* 11**,** 3670.

Groszmann, M., Greaves, I.K., Fujimoto, R., James Peacock, W., and Dennis, E.S. (2013). The role of epigenetics in hybrid vigour. *Trends in Genetics* 29**,** 684-690.

Grover, C.E., Gallagher, J.P., Szadkowski, E.P., Yoo, M.J., Flagel, L.E., and Wendel, J.F. (2012). Homoeolog expression bias and expression level dominance in allopolyploids. *New Phytologist* 196**,** 966-971.

Guo, X., and Han, F. (2014). Asymmetric Epigenetic Modification and Elimination of rDNA Sequences by Polyploidization in Wheat. *The Plant Cell* 26**,** 4311-4327.

Handa, H., Kanamori, H., Tanaka, T., Murata, K., Kobayashi, F., Robinson, S.J., Koh, C.S., Pozniak, C.J., Sharpe, A.G., Paux, E., Consortium, I.W.G.S., Wu, J., and Nasuda, S. (2018). Structural features of two major nucleolar organizer regions (NORs), Nor-B1 and Nor-B2, and chromosome-specific rRNA gene expression in wheat. *The Plant Journal* 96**,** 1148-1159.

Hänske, J., Hammacher, T., Grenkowitz, F., Mansfeld, M., Dau, T.H., Maksimov, P., Friedrich, C., Zimmermann, W., and Kammerer, R. (2020). Natural selection supports escape from concerted evolution of a recently duplicated CEACAM1 paralog in the ruminant CEA gene family. *Scientific Reports* 10**,** 3404.

Hasterok, R., Catalan, P., Hazen, S.P., Roulin, A.C., Vogel, J.P., Wang, K., and Mur, L.a.J. (2022). *Brachypodium*: 20 years as a grass biology model system; the way forward? *Trends in Plant Science* 27**,** 1002-1016.

Hasterok, R., Draper, J., and Jenkins, G. (2004). Laying the Cytotaxonomic Foundations of a New Model Grass, *Brachypodium distachyon* (L.) Beauv. *Chromosome Research* 12**,** 397-403.

Hasterok, R., and Maluszynska, J. (2000). Nucleolar dominance does not occur in root tip cells of allotetraploid *Brassica* species. *Genome* 43**,** 574-579.

Hasterok, R., Marasek, A., Donnison, I.S., Armstead, I., Thomas, A., King, I.P., Wolny, E., Idziak, D., Draper, J., and Jenkins, G. (2006). Alignment of the genomes of *Brachypodium distachyon* and temperate cereals and grasses using bacterial artificial chromosome landing with fluorescence *in situ* hybridization. *Genetics* 173**,** 349-362.

Hemleben, V., Volkov, R.A., Zentgraf, U., and Medina, F.J. (2004). "Molecular Cell Biology: Organization and Molecular Evolution of rDNA, Nucleolar Dominance, and Nucleolus Structure," in *Progress in Botany: Genetics Physiology Systematics Ecology,* eds. K. Esser, U. Lüttge, W. Beyschlag & J. Murata. (Berlin, Heidelberg: Springer Berlin Heidelberg), 106-146.

Heneen, W.K. (1962). Karyotype studies in *Agropyron junceum*, *A. repens* and their spontaneous hybrids. *Hereditas* 48**,** 471-502.

Hirsch, C.D., and Springer, N.M. (2017). Transposable element influences on gene expression in plants. *Biochimica et Biophysica Acta - Gene Regulatory Mechanisms* 1860**,** 157-165.

Hodkinson, T.R. (2018). "Evolution and Taxonomy of the Grasses (Poaceae): A Model Family for the Study of Species-Rich Groups," in *Annual Plant Reviews online*., 255-294.

Hodkinson, T.R., Klaas, M., Jones, M.B., Prickett, R., and Barth, S. (2015). *Miscanthus*: a case study for the utilization of natural genetic variation. *Plant Genetic Resources* 13**,** 219-237.

Hodkinson, T.R., and Parnell, J.A.N. (2006). *Reconstructing the Tree of Life: Taxonomy and Systematics of Species Rich Taxa.* CRC Press., 72, 251-270.

Hori, Y., Engel, C., and Kobayashi, T. (2023). Regulation of ribosomal RNA gene copy number, transcription and nucleolus organization in eukaryotes. *Nature Reviews Molecular Cell Biology* 24**,** 414–429.

Hus, K., Betekhtin, A., Pinski, A., Rojek-Jelonek, M., Grzebelus, E., Nibau, C., Gao, M., Jaeger, K.E., Jenkins, G., Doonan, J.H., and Hasterok, R. (2020). A CRISPR/Cas9-Based Mutagenesis Protocol for *Brachypodium distachyon* and Its Allopolyploid Relative, *Brachypodium hybridum*. *Frontiers in plant science* 11**,** 614-614.

Huska, D., Leitch, I.J., De Carvalho, J.F., Leitch, A.R., Salmon, A., Ainouche, M., and Kovarik, A. (2016). Persistence, dispersal and genetic evolution of recently formed *Spartina* homoploid hybrids and allopolyploids in Southern England. 18**,** 2137-2151.

Hutchinson, J., and Miller, T.E. (1982). The nucleolar organisers of tetraploid and hexaploid wheats revealed by *in situ* hybridisation. *Theoretical and Applied Genetics* 61**,** 285-288.

Ibi (2010). Genome sequencing and analysis of the model grass *Brachypodium distachyon*. *Nature* 463**,** 763-768.

Ichino, L., Boone, B.A., Strauskulage, L., Harris, C.J., Kaur, G., Gladstone, M.A., Tan, M., Feng, S., Jami-Alahmadi, Y., Duttke, S.H., Wohlschlegel, J.A., Cheng, X., Redding, S., and Jacobsen, S.E. (2021). MBD5 and MBD6 couple DNA

methylation to gene silencing through the J-domain protein SILENZIO. *Science* 372**,** 1434-1439.

Idziak, D., and Hasterok, R. (2008). Cytogenetic evidence of nucleolar dominance in allotetraploid species of *Brachypodium*. *Genome* 51**,** 387-391.

Ironside, J.E. (2013). Diversity and Recombination of Dispersed Ribosomal DNA and Protein Coding Genes in Microsporidia. *PLoS One* 8**,** e55878.

Jenkins, G., and Hasterok, R. (2007). BAC 'landing' on chromosomes of *Brachypodium distachyon* for comparative genome alignment. *Nature Protocols* 2**,** 88-98.

Jiao, Y., Wickett, N.J., Ayyampalayam, S., Chanderbali, A.S., Landherr, L., Ralph, P.E., Tomsho, L.P., Hu, Y., Liang, H., Soltis, P.S., Soltis, D.E., Clifton, S.W., Schlarbaum, S.E., Schuster, S.C., Ma, H., Leebens-Mack, J., and Depamphilis, C.W. (2011). Ancestral polyploidy in seed plants and angiosperms. *Nature* 473**,** 97-100.

Jones, M.B., Finnan, J., and Hodkinson, T.R. (2015). Morphological and physiological traits for higher biomass production in perennial rhizomatous grasses grown on marginal land. *GCB Bioenergy* 7**,** 375-385.

Jupe, E.R., and Zimmer, E.A. (1993). DNaseI-sensitive and undermethylated rDNA is preferentially expressed in a maize hybrid. *Plant Molecular Biology* 21**,** 805-821.

Keep, E. (1962). Satellite and nucleolar number in hybrids between Ribes nigrum and R. grossularia and in their backcrosses. *Canadian Journal of Genetics and Cytology* 4**,** 206-218.

Komarova, N.Y., Grabe, T., Huigen, D.J., Hemleben, V., and Volkov, R.A. (2004). Organization, differential expression and methylation of rDNA in artificial *Solanum* allopolyploids. *Plant Molecular Biology* 56**,** 439-463.

Kotseruba, V., Gernand, D., Meister, A., and Houben, A. (2003). Uniparental loss of ribosomal DNA in the allotetraploid grass *Zingeria trichopoda* (2n = 8). *Genome* 46**,** 156-163.

Koukalova, B., Fojtova, M., Lim, K.Y., Fulnecek, J., Leitch, A.R., and Kovarik, A. (2005). Dedifferentiation of tobacco cells is associated with ribosomal RNA gene hypomethylation, increased transcription, and chromatin alterations. *Plant Physiology* 139**,** 275-286.

Kovarik, A., Dadejova, M., Lim, Y.K., Chase, M.W., Clarkson, J.J., Knapp, S., and Leitch, A.R. (2008). Evolution of rDNA in *Nicotiana* allopolyploids: a potential

link between rDNA homogenization and epigenetics. *Annals of Botany* 101**,** 815-823.

Kovarik, A., Pires, J.C., Leitch, A.R., Lim, K.Y., Sherwood, A.M., Matyasek, R., Rocca, J., Soltis, D.E., and Soltis, P.S. (2005). Rapid concerted evolution of nuclear ribosomal DNA in two *Tragopogon* allopolyploids of recent and recurrent origin. *Genetics* 169**,** 931-944.

Krawczyk, K., Nobis, M., Nowak, A., Szczecińska, M., and Sawicki, J. (2017). Phylogenetic implications of nuclear rRNA IGS variation in *Stipa* L. (Poaceae). *Scientific Reports* 7**,** 11506.

Książczyk, T., Kovarik, A., Eber, F., Huteau, V., Khaitova, L., Tesarikova, Z., Coriton, O., and Chèvre, A.-M. (2011). Immediate unidirectional epigenetic reprogramming of NORs occurs independently of rDNA rearrangements in synthetic and natural forms of a polyploid species *Brassica napus*. *Chromosoma* 120**,** 557-571.

Lawrence, R.J., Earley, K., Pontes, O., Silva, M., Chen, Z.J., Neves, N., Viegas, W., and Pikaard, C.S. (2004). A Concerted DNA Methylation/Histone Methylation Switch Regulates rRNA Gene Dosage Control and Nucleolar Dominance. *Molecular Cell* 13**,** 599-609.

Le Vay, K., and Mutschler, H. (2019). The difficult case of an RNA-only origin of life. *Emerging Topics in Life Sciences* 3**,** 469-475.

Levy, A.A., and Feldman, M. (2002). The impact of polyploidy on grass genome evolution. *Plant Physiology* 130**,** 1587-1593.

Levy, A.A., and Feldman, M. (2022). Evolution and origin of bread wheat. *The Plant Cell* 34**,** 2549-2567.

Lima-Brito, J., Guedes-Pinto, H., and Heslop-Harrison, J.S. (1998). The activity of nucleolar organizing chromosomes in multigeneric F1 hybrids involving wheat, triticale, and tritordeum. *Genome* 41**,** 763-768.

Linde-Laursen, I., and Bothmer, R. (1989). Allocycly and nucleolar dominance in *Hordeum* × *Secale* amphiploid somatic metaphases. *Hereditas* 111**,** 85-86.

Linde-Laursen, I., Schrader, O., and Zerneke, F. (1993). Chromosomal Constitution of Rye (*Secale Cereale*) – *Hordeum Chilense* Addition Lines. *Hereditas* 119**,** 21-29.

Ling, H.-Q., Ma, B., Shi, X., Liu, H., Dong, L., Sun, H., Cao, Y., Gao, Q., Zheng, S., Li, Y., Yu, Y., Du, H., Qi, M., Li, Y., Lu, H., Yu, H., Cui, Y., Wang, N., Chen, C., Wu, H., Zhao, Y., Zhang, J., Li, Y., Zhou, W., Zhang, B., Hu, W., Van Eijk,

M.J.T., Tang, J., Witsenboer, H.M.A., Zhao, S., Li, Z., Zhang, A., Wang, D., and Liang, C. (2018). Genome sequence of the progenitor of wheat A subgenome *Triticum urartu*. *Nature* 557**,** 424-428.

Lopez-Alvarez, D., Lopez-Herranz, M.L., Betekhtin, A., and Catalan, P. (2012). A DNA barcoding method to discriminate between the model plant *Brachypodium distachyon* and its close relatives *B. stacei* and *B. hybridum* (Poaceae). *PLoS One* 7**,** e51058.

Lopez, F.B., Fort, A., Tadini, L., Probst, A.V., Mchale, M., Friel, J., Ryder, P., Pontvianne, F.D.R., Pesaresi, P., Sulpice, R., Mckeown, P., Brychkova, G., and Spillane, C. (2021). Gene dosage compensation of rRNA transcript levels in *Arabidopsis thaliana* lines with reduced ribosomal gene copy number. *Plant Cell* 33**,** 1135-1150.

Lu, F.H., Mckenzie, N., Gardiner, L.J., Luo, M.C., Hall, A., and Bevan, M.W. (2020). Reduced chromatin accessibility underlies gene expression differences in homologous chromosome arms of diploid *Aegilops tauschii* and hexaploid wheat. *GigaScience* 9.

Lunerová, J., Renny-Byfield, S., Matyášek, R., Leitch, A., and Kovařík, A. (2017). Concerted evolution rapidly eliminates sequence variation in rDNA coding regions but not in intergenic spacers in *Nicotiana tabacum* allotetraploid. *Plant Systematics and Evolution* 303**,** 1043-1060.

Luo, M.-C., Gu, Y.Q., Puiu, D., Wang, H., Twardziok, S.O., Deal, K.R., Huo, N., Zhu, T., Wang, L., Wang, Y., Mcguire, P.E., Liu, S., Long, H., Ramasamy, R.K., Rodriguez, J.C., Van, S.L., Yuan, L., Wang, Z., Xia, Z., Xiao, L., Anderson, O.D., Ouyang, S., Liang, Y., Zimin, A.V., Pertea, G., Qi, P., Bennetzen, J.L., Dai, X., Dawson, M.W., Müller, H.-G., Kugler, K., Rivarola-Duarte, L., Spannagl, M., Mayer, K.F.X., Lu, F.-H., Bevan, M.W., Leroy, P., Li, P., You, F.M., Sun, Q., Liu, Z., Lyons, E., Wicker, T., Salzberg, S.L., Devos, K.M., and Dvořák, J. (2017). Genome sequence of the progenitor of the wheat D genome *Aegilops tauschii*. *Nature* 551**,** 498-502.

Lusinska, J., Majka, J., Betekhtin, A., Susek, K., Wolny, E., and Hasterok, R. (2018). Chromosome identification and reconstruction of evolutionary rearrangements in *Brachypodium distachyon*, *B. stacei* and *B. hybridum*. *Annals of Botany* 122**,** 445-459.

Ma, G., Zhang, W., Liu, L., Chao, W.S., Gu, Y.Q., Qi, L., Xu, S.S., and Cai, X. (2018). Cloning and characterization of the homoeologous genes for the Rec8-like meiotic cohesin in polyploid wheat. *BMC Plant Biology* 18**,** 224.

Ma, X.F., and Gustafson, J.P. (2005). Genome evolution of allopolyploids: a process of cytological and genetic diploidization. *Cytogenetic and Genome Research* 109**,** 236-249.

Maccaferri, M., Harris, N.S., Twardziok, S.O., Pasam, R.K., Gundlach, H., Spannagl, M., Ormanbekova, D., Lux, T., Prade, V.M., Milner, S.G., Himmelbach, A., Mascher, M., Bagnaresi, P., Faccioli, P., Cozzi, P., Lauria, M., Lazzari, B., Stella, A., Manconi, A., Gnocchi, M., Moscatelli, M., Avni, R., Deek, J., Biyiklioglu, S., Frascaroli, E., Corneti, S., Salvi, S., Sonnante, G., Desiderio, F., Marè, C., Crosatti, C., Mica, E., Özkan, H., Kilian, B., De Vita, P., Marone, D., Joukhadar, R., Mazzucotelli, E., Nigro, D., Gadaleta, A., Chao, S., Faris, J.D., Melo, A.T.O., Pumphrey, M., Pecchioni, N., Milanesi, L., Wiebe, K., Ens, J., Maclachlan, R.P., Clarke, J.M., Sharpe, A.G., Koh, C.S., Liang, K.Y.H., Taylor, G.J., Knox, R., Budak, H., Mastrangelo, A.M., Xu, S.S., Stein, N., Hale, I., Distelfeld, A., Hayden, M.J., Tuberosa, R., Walkowiak, S., Mayer, K.F.X., Ceriotti, A., Pozniak, C.J., and Cattivelli, L. (2019). Durum wheat genome highlights past domestication signatures and future improvement targets. *Nature Genetics* 51**,** 885-895.

Maddison, W., and Maddison, D. (2009). MESQUITE: a modular system for evolutionary analysis. 3.81.

Matzke, M.A., and Mosher, R.A. (2014). RNA-directed DNA methylation: an epigenetic pathway of increasing complexity. *Nature Reviews Genetics* 15**,** 394-408.

Mayer, K.F.X., Waugh, R., Langridge, P., Close, T.J., Wise, R.P., Graner, A., Matsumoto, T., Sato, K., Schulman, A., Muehlbauer, G.J., Stein, N., Ariyadasa, R., Schulte, D., Poursarebani, N., Zhou, R., Steuernagel, B., Mascher, M., Scholz, U., Shi, B., Langridge, P., Madishetty, K., Svensson, J.T., Bhat, P., Moscou, M., Resnik, J., Close, T.J., Muehlbauer, G.J., Hedley, P., Liu, H., Morris, J., Waugh, R., Frenkel, Z., Korol, A., Bergès, H., Graner, A., Stein, N., Steuernagel, B., Scholz, U., Taudien, S., Felder, M., Groth, M., Platzer, M., Stein, N., Steuernagel, B., Scholz, U., Himmelbach, A., Taudien, S., Felder, M., Platzer, M., Lonardi, S., Duma, D., Alpert, M., Cordero, F., Beccuti, M., Ciardo, G., Ma, Y., Wanamaker, S., Close, T.J., Stein, N., Cattonaro, F., Vendramin, V., Scalabrin, S., Radovic, S.,

Wing, R., Schulte, D., Steuernagel, B., Morgante, M., Stein, N., Waugh, R., Nussbaumer, T., Gundlach, H., Martis, M., Ariyadasa, R., Poursarebani, N., Steuernagel, B., Scholz, U., Wise, R.P., Poland, J., Stein, N., Mayer, K.F.X., Spannagl, M., Pfeifer, M., Gundlach, H., Mayer, K.F.X., Gundlach, H., Moisy, C., Tanskanen, J., Scalabrin, S., Zuccolo, A., Vendramin, V., Morgante, M., Mayer, K.F.X., Schulman, A., Pfeifer, M., Spannagl, M., Hedley, P., Morris, J., Russell, J., Druka, A., Marshall, D., et al. (2012). A physical, genetic and functional sequence assembly of the barley genome. *Nature* 491**,** 711-716.

Michalak, K., Maciak, S., Kim, Y.B., Santopietro, G., Oh, J.H., Kang, L., Garner, H.R., and Michalak, P. (2015). Nucleolar dominance and maternal control of 45S rDNA expression. *Proceedings of the Royal Society B: Biological Sciences* 282**,** 20152201.

Mirzaghaderi, G., Abdolmalaki, Z., Zohouri, M., Moradi, Z., and Mason, A.S. (2017). Dynamic nucleolar activity in wheat × *Aegilops* hybrids: evidence of C-genome dominance. *Plant Cell Reports* 36**,** 1277-1285.

Mohannath, G., Pontvianne, F., and Pikaard, C.S. (2016). Selective nucleolus organizer inactivation in *Arabidopsis* is a chromosome position-effect phenomenon. *Proceedings of the National Academy of Sciences* 113**,** 13426-13431.

Mohapatra, S., Mishra, S.S., Bhalla, P., and Thatoi, H. (2019). Engineering grass biomass for sustainable and enhanced bioethanol production. *Planta* 250**,** 395-412.

Muoki, R.C., Paul, A., Kumari, A., Singh, K., and Kumar, S. (2012). An Improved Protocol for the Isolation of RNA from Roots of Tea (*Camellia sinensis* (L.) O. Kuntze). *Molecular Biotechnology* 52**,** 82-88.

Navashin, M. (1934). Chromosome Alterations Caused by Hybridization and Their Bearing upon Certain General Genetic Problems. *CYTOLOGIA* 5**,** 169-203.

Nelson, J.W., and Breaker, R.R. (2017). The lost language of the RNA World. *Science Signaling* 10.

Neves, N., Heslop-Harrison, J.S., and Viegas, W. (1995). rRNA gene activity and control of expression mediated by methylation and imprinting during embryo development in wheat x rye hybrids. *Theoretical and Applied Genetics* 91**,** 529-533.

Nicoloff, H., Anastassova-Kristeva, M., Rieger, R., and Künzel, G. (1979). 'Nucleolar dominance' as observed in barley translocation lines with specifically reconstructed SAT chromosomes. *Theoretical and Applied Genetics* 55**,** 247-251.

Odintsova, T.I., Slezina, M.P., and Istomina, E.A. (2020). Defensins of Grasses: A Systematic Review. *Biomolecules* 10**,** 1029.

Park, H.-S., Lee, W.K., Lee, S.-C., Lee, H.O., Joh, H.J., Park, J.Y., Kim, S., Song, K., and Yang, T.-J. (2021). Inheritance of chloroplast and mitochondrial genomes in cucumber revealed by four reciprocal F1 hybrid combinations. *Scientific Reports* 11**,** 2506.

Penner, S., Dror, B., Aviezer, I., Bar-Lev, Y., Salman-Minkov, A., Mandakova, T., Šmarda, P., Mayrose, I., and Sapir, Y. (2020). Phenology and polyploidy in annual *Brachypodium* species (Poaceae) along the aridity gradient in Israel. *Journal of Systematics and Evolution* 58**,** 189-199.

Pikaard, C.S. (2000). Nucleolar dominance: uniparental gene silencing on a multi-megabase scale in genetic hybrids. *Plant Molecular Biology* 43**,** 163-177.

Pontes, O., Lawrence, R.J., Silva, M., Preuss, S., Costa-Nunes, P., Earley, K., Neves, N., Viegas, W., and Pikaard, C.S. (2007). Postembryonic establishment of megabase-scale gene silencing in nucleolar dominance. *PLoS One* 2**,** e1157.

Pontvianne, F., Blevins, T., Chandrasekhara, C., Feng, W., Stroud, H., Jacobsen, S.E., Michaels, S.D., and Pikaard, C.S. (2012). Histone methyltransferases regulating rRNA gene dose and dosage control in *Arabidopsis*. *Genes & Development* 26**,** 945-957.

Preuss, S.B., Costa-Nunes, P., Tucker, S., Pontes, O., Lawrence, R.J., Mosher, R., Kasschau, K.D., Carrington, J.C., Baulcombe, D.C., Viegas, W., and Pikaard, C.S. (2008). Multimegabase silencing in nucleolar dominance involves siRNA-directed DNA methylation and specific methylcytosine-binding proteins. *Molecular Cell* 32**,** 673-684.

Rabanal, F.A., Mandáková, T., Soto-Jiménez, L.M., Greenhalgh, R., Parrott, D.L., Lutzmayer, S., Steffen, J.G., Nizhynska, V., Mott, R., Lysak, M.A., Clark, R.M., and Nordborg, M. (2017). Epistatic and allelic interactions control expression of ribosomal RNA gene clusters in *Arabidopsis thaliana*. *Genome Biology* 18**,** 75.

Rapp, R.A., Udall, J.A., and Wendel, J.F. (2009). Genomic expression dominance in allopolyploids. *BMC Biology* 7**,** 18.

Reeder, R.H., and Roan, J.G. (1984). The mechanism of nucleolar dominance in *Xenopus* hybrids. *Cell* 38**,** 39-44.

Ritossa, F.M., and Spiegelman, S. (1965). Localization Of DNA Complementary To Ribosomal RNA In The Nucleolus Organizer Region Of Drosophila

Melanogaster. *Proceedings of the National Academy of Sciences of the United States of America* 53**,** 737-745.

Robertson, I.H. (1981). Chromosome numbers in *Brachypodium* Beauv. (Gramineae). *Genetica* 56**,** 55-60.

Robertson, M.P., and Joyce, G.F. (2012). The origins of the RNA world. *Cold Spring Harbor Perspectives in Biology* 4.

Rosato, M., Kovařík, A., Garilleti, R., and Rosselló, J.A. (2016). Conserved Organisation of 45S rDNA Sites and rDNA Gene Copy Number among Major Clades of Early Land Plants. *PLoS One* 11**,** e0162544.

Ruas, C.D.F., Vanzela, A.L., Santos, M.O., Fregonezi, J.N., Ruas, P.M., Matzenbacher, N.I., and De Aguiar-Perecin, M.L. (2005). Chromosomal organization and phylogenetic relationships in *Hypochaeris* species (Asteraceae) from Brazil. *Genetics and Molecular Biology* 28**,** 129-139.

Sancho, R., Inda, L.A., Díaz-Pérez, A., Des Marais, D.L., Gordon, S., Vogel, J.P., Lusinska, J., Hasterok, R., Contreras-Moreira, B., and Catalán, P. (2022). Tracking the ancestry of known and 'ghost' homeologous subgenomes in model grass *Brachypodium* polyploids. *The Plant Journal* 109**,** 1535-1558.

Santos, J.L., Lacadena, J.R., Cermeño, M.C., and Orellana, J. (1984). Nucleolar organiser activity in wheat-barley chromosome addition lines. *Heredity* 52**,** 425-429.

Santos, Y.D., Pereira, W.A., De Paula, C.M.P., De Campos Rume, G., Lima, A.A., Chalfun-Junior, A., Souza Sobrinho, F., and Techio, V.H. (2020). Epigenetic Marks Associated to the Study of Nucleolar Dominance in *Urochloa* P. Beauv. *Plant Molecular Biology Reporter* 38**,** 380-393.

Sato, K., Abe, F., Mascher, M., Haberer, G., Gundlach, H., Spannagl, M., Shirasawa, K., and Isobe, S. (2021). Chromosome-scale genome assembly of the transformation-amenable common wheat cultivar 'Fielder'. *DNA Research* 28.

Scholthof, K.-B.G., Irigoyen, S., Catalan, P., and Mandadi, K.K. (2018). *Brachypodium*: A Monocot Grass Model Genus for Plant Biology. *The Plant Cell* 30**,** 1673-1694.

Schubert, I., and Künzel, G. (1990). Position-dependent NOR activity in barley. *Chromosoma* 99**,** 352-359.

Schwarzacher-Robinson, T., Finch, R., Smith, J.B., and Bennett, M. (1987). Genotypic control of centromere positions of parental genomes in *Hordeum* × *Secale* hybrid metaphases. *Journal of Cell Science* 87**,** 291-304.

Shi, Y., Draper, J., and Stace, C. (1993). Ribosomal DNA variation and its phylogenetic implication in the genus *Brachypodium* (Poaceae). *Plant Systematics and Evolution* 188**,** 125-138.

Shkutina, F.M., and Khvostova, V.V. (1971). Cytological investigation of Triticale. *Theoretical and Applied Genetics* 41**,** 109-119.

Singh, J., Mishra, V., Wang, F., Huang, H.Y., and Pikaard, C.S. (2019). Reaction Mechanisms of Pol IV, RDR2, and DCL3 Drive RNA Channeling in the siRNA-Directed DNA Methylation Pathway. *Molecular Cell* 75**,** 576-589.e575.

Sochorova, J., Coriton, O., Kuderova, A., Lunerova, J., Chevre, A.M., and Kovarik, A. (2017). Gene conversion events and variable degree of homogenization of rDNA loci in cultivars of *Brassica napus*. *Annals of Botany* 119**,** 13-26.

Sone, T., Fujisawa, M., Takenaka, M., Nakagawa, S., Yamaoka, S., Sakaida, M., Nishiyama, R., Yamato, K.T., Ohmido, N., Fukui, K., Fukuzawa, H., and Ohyama, K. (1999). Bryophyte 5S rDNA was inserted into 45S rDNA repeat units after the divergence from higher land plants. *Plant Molecular Biology* 41**,** 679-685.

Subramanian, S., and Kumar, S. (2003). Neutral substitutions occur at a faster rate in exons than in noncoding DNA in primate genomes. *Genome Research* 13**,** 838-844.

Svačina, R., Sourdille, P., Kopecký, D., and Bartoš, J. (2020). Chromosome Pairing in Polyploid Grasses. *Frontiers in Plant Science* 11.

Talbert, P.B., Masuelli, R., Tyagi, A.P., Comai, L., and Henikoff, S. (2002). Centromeric localization and adaptive evolution of an *Arabidopsis* histone H3 variant. *Plant Cell* 14**,** 1053-1066.

Taylor, S., Wakem, M., Dijkman, G., Alsarraj, M., and Nguyen, M. (2010). A practical approach to RT-qPCR - Publishing data that conform to the MIQE guidelines. *Methods* 50**,** S1-S5.

Thomas, B.C., Pedersen, B., and Freeling, M. (2006). Following tetraploidy in an *Arabidopsis* ancestor, genes were removed preferentially from one homeolog leaving clusters enriched in dose-sensitive genes. *Genome Research* 16**,** 934-946.

Thomas, H.M., and Pickering, R.A. (1983). Chromosome elimination in *Hordeum vulgare* x *H. bulbosum* hybrids. *Theoretical and Applied Genetics* 66**,** 141-146.

Thomas, H.M., and Pickering, R.A. (1985). Comparisons of the hybrids *Hordeum chilense* x *H. vulgare*, *H. chilense* x *H. bulbosum*, *H. chilense* x *Secale cereale*

and the amphidiploid of *H. chilense* x *H. vulgare*. *Theoretical and Applied Genetics* 69**,** 519-522.

Thomas, J.B., and Kaltsikes, P.J. (1983). Effect of chromosomes 1B and 6B on nucleolus formation in hexaploid triticale. *Canadian Journal of Genetics and Cytology* 25**,** 292-297.

Trifinopoulos, J., Nguyen, L.T., Von Haeseler, A., and Minh, B.Q. (2016). W-IQ-TREE: a fast online phylogenetic tool for maximum likelihood analysis. *Nucleic Acids Research* 44**,** 232-235.

Tulpová, Z., Kovařík, A., Toegelová, H., Navrátilová, P., Kapustová, V., Hřibová, E., Vrána, J., Macas, J., Doležel, J., and Šimková, H. (2022). Fine structure and transcription dynamics of bread wheat ribosomal DNA loci deciphered by a multi-omics approach. *The Plant Genome* 15**,** e20191.

Unfried, I., and Gruendler, P. (1990). Nucleotide sequence of the 5.8S and 25S rRNA genes and of the internal transcribed spacers from *Arabidopsis thaliana*. *Nucleic acids research* 18**,** 4011-4011.

Vieira, R., Queiroz, Á., Morais, L., Barão, A., Mello-Sampayo, T., and Viegas, W. (1990a). Genetic control of 1R nucleolus organizer region expression in the presence of wheat genomes. *Genome* 33**,** 713-718.

Vieira, R., Queiroz, Á., Morais, L., Barão, A., Mello-Sampayo, T., and Viegas, W.S. (1990b). 1R chromosome nucleolus organizer region activation by 5-azacytidine in wheat × rye hybrids. *Genome* 33**,** 707-712.

Volkov, R.A., Komarova, N.Y., and Hemleben, V. (2007). Ribosomal DNA in plant hybrids: Inheritance, rearrangement, expression. *Systematics and Biodiversity* 5**,** 261-276.

Volkov, R.A., Komarova, N.Y., Panchuk, I.I., and Hemleben, V. (2003). Molecular evolution of rDNA external transcribed spacer and phylogeny of sect. *Petota* (genus *Solanum*). *Molecular Phylogenetics and Evolution* 29**,** 187-202.

Wang, H.L., and Chekanova, J.A. (2016). Small RNAs: essential regulators of gene expression and defenses against environmental stresses in plants. *Wiley Interdisciplinary Reviews: RNA* 7**,** 356-381.

Wang, W., Ma, L., Becher, H., Garcia, S., Kovarikova, A., Leitch, I.J., Leitch, A.R., and Kovarik, A. (2016). Astonishing 35S rDNA diversity in the gymnosperm species *Cycas revoluta* Thunb. *Chromosoma* 125**,** 683-699.

Ward, O.G., and Cole, C.J. (1986). Nucleolar dominance in diploid and triploid parthogenetic lizards of hybrid origin. *Cytogenetic and Genome Research* 42**,** 177-182.

Weiss-Schneeweiss, H., Stuessy, T.F., Siljak-Yakovlev, S., Baeza, C.M., and Parker, J. (2003). Karyotype evolution in South American species of *Hypochaeris* (Asteraceae, Lactuceae). *Plant Systematics and Evolution* 241**,** 171-184.

Wendel, J.F., Schnabel, A., and Seelanan, T. (1995). Bidirectional interlocus concerted evolution following allopolyploid speciation in cotton (*Gossypium*). *Proceedings of the National Academy of Sciences of the United States of America* 92**,** 280-284.

Wilkinson, J. (1944). The Cytology of Salix in Relation to its Taxonomy. *Annals of Botany* 8**,** 269-284.

Woodhouse, M.R., Cheng, F., Pires, J.C., Lisch, D., Freeling, M., and Wang, X. (2014). Origin, inheritance, and gene regulatory consequences of genome dominance in polyploids. *Proceedings of the National Academy of Sciences of the United States of America* 111**,** 5283-5288.

Zhu, W., Hu, B., Becker, C., Doğan, E.S., Berendzen, K.W., Weigel, D., and Liu, C. (2017). Altered chromatin compaction and histone methylation drive non-additive gene expression in an interspecific *Arabidopsis* hybrid. *Genome Biology* 18**,** 157.